AB INITIO QUANTUM CHEMICAL PREDICTIONS OF STRUCTURES, ENERGETICS AND PHYSICAL PROPERTIES: FROM ENVIRONMENTALLY ACTIVE MOLECULES TO SMALL CLUSTERS TO DNA BASE PAIRS.

by

PARTHA PRATIM BERA

(Under the direction of H. F. Schaefer III)

ABSTRACT: *Ab initio* quantum chemistry (AIQC) methods have been employed in order to investigate small environmentally active triatomic NO_2 to large DNA base pairs in this thesis. The reliablity of predicting structures, energetics and physical properties of molecular systems are discussed with an eye on the applicability of density functional theory and highly correlated methods. Structures and spectroscopic parameters are predicted for several excited electronic states of NO_2. An unbiased stochastic method to search for minima on the potential energy surfaces of molecules or clusters is developed and applied to variety of molecules. Biologically important topic of DNA damage by radiation is also addressed by predicting the gas phase radicals and ions and their molecular properties.

INDEX WORDS: ab initio, quantum chemistry, DFT, small molecule, NO_2, electronic structure, electronic states, quartet, atomic cluster, small cluster, stochastic, mindless chemistry, mindless, kick, potential search, PES, DNA, DNA damage, lesions, radiation damage, radicals, ions.

AB INITIO QUANTUM CHEMICAL PREDICTIONS OF STRUCTURES, ENERGETICS AND PHYSICAL PROPERTIES: FROM ENVIRONMENTALLY ACTIVE MOLECULES TO SMALL CLUSTERS TO DNA BASE PAIRS.

by

PARTHA PRATIM BERA

B. Sc. Presidency College, Calcutta, India 1998

M. Sc., The University of Calcutta, Calcutta, India 2000

A Dissertation Submitted to the Graduate Faculty

of The University of Georgia in the Partial Fulfillment

of the

Requirements for the Degree

DOCTOR OF PHILOSOPHY

ATHENS, GEORGIA

2006

AB INITIO QUANTUM CHEMICAL PREDICTIONS OF STRUCTURES, ENERGETICS AND PHYSICAL PROPERTIES: FROM ENVIRONMENTALLY ACTIVE MOLECULES TO SMALL CLUSTERS TO DNA BASE PAIRS.

by

Partha Pratim Bera

Approved:

Major Professor: Henry F. Schaefer III

Committee: Nigel Adams

Lucia Babcock

Electronic Version Approved:

Maureen Grasso
Dean of Graduate School
The University of Georgia
December 2006

To

My teachers

ACKNOWLEDGEMENTS

Any amount of thanks will be insufficient to the people I owe my appreciation. I have always considered myself blessed to have born to my parents. I am thankful to them for the education, discipline and rich culture they have cultivated in me. They have raised me and my two sisters with a real sense of security, sensibility, ethics and principle. Those values will always be with me and help me choose between good and bad in this lifelong journey. Growing up with two loving and caring sisters made me experience every human emotions of a child and the values of a large family educated me of the rich Bengali culture and traditions.

I have to mention those who had a profound impact on the way my life has shaped so far. From the school days I was very much influenced by some of my teachers. Kalyan K. Jana, my biology teacher (more of a friend, philosopher and guide) in high school who was a constant source of encouragement and guidance; Sourendra Nath Jana, my chemistry teacher, from whom I have learned most of the chemistry I know. Ms. Moonmoon Jana gave me a lot of inspiration. Five years in Presidency College, Calcutta, first as an undergraduate and then as a post-graduate student was the golden days and the days of radical transformations in my life. There I have met some of the best teachers of chemistry and some of the best minds, amity or challenge of whose have only made me better and stronger.

I tender my special gratitude to Professor Henry F. Schaefer III, the most bright and most positive being I have ever met, and a pioneer of the field, for this chance of a lifetime to be trained by and work with him. This last four years have been a fruitful and worthwhile scientific experience by his support, generosity and guidance. Here at CCQC I have enjoyed the facilitation, collaboration and friendship of many. Mrs. Linda Rowe, being such motherly figure

and the administrative staff has cocooned us from all the professional hazards. I offer my special thanks to two dedicated scientists: Dr. Yukio Yamaguchi, a true man of science, for his patience, intense hands on teaching of state of the art *ab initio* techniques and above all scientific values; Dr. Yaoming Xie, for late night (china time!) research chats. I have met some of the most diverse and talented set of people here. Some of them are: my good mentor Dr. Lubos Horný who guided me about everything from science to sports; intellectual Dr. Kurt Sattelmeyer; Dr. Chaitanya S. Wannere, my proof reader and reference of Indian classical music; Sunguan Kim, my true CCQC buddy; Dr. Justin Turney, always had a quick fix for my stupid computer related questions; Dr. Veronika Kasalova, enjoyed sharing the 1211 lab with her and lots of CCQC small talks; Prof. Alexei Timoskn from St. Petersburg, Russia, miss the badminton, pool and CCQC late night work/chat; Francesco Evangelista, a truly scientific mind and my special research critic; Andrew Simmonett, hard hitting Manchester United basher, shared good cricket talks; Maria C. Lind, my good mentoree; and my buddy Monica S. Choi for all the advises.

Coming to U. S. from a third world country, I was scared at the beginning. However, the calm environment in Athens has grown on me over the years. I have many good memories associated with the life, the music, the book stores, the coffee shops of Athens. I call it my home away from home. Friends are like stars; although the brightness will fade away, they will always be remembered for the light they tendered. I bid my personal appreciation and thanks to all my friends in Athens, without whom life would have been difficult. I thank you from my heart for the moments shared. Time will take friends away from each other, but they will have a everlasting place in my mind. Last but not the least I express my deepest pleasure and admiration to my childhood friend and now wife, Monalisa, for being there with me always, in good or bad; and for understanding me. All I want is to see you happy.

TABLE OF CONTENTS

CHAPTER 1

INTRODUCTION AND LITERATURE REVIEW

1.1 INTRODUCTION

The accurate prediction of the evolution of a chemical reaction, and the physical and chemical properties of molecular systems, are the drive to pursue the quest of knowledge in the field of computational quantum chemistry. The last three words of the previous sentence combine the three worlds: 'Computers', 'Quantum theory' and 'Chemistry' in one. Computational quantum chemistry opened up a whole new dimension of fundamental research that has seen dramatic transformations in the last two decades. So much so, that the field of Computational Quantum Chemistry is challenging experimental chemistry for equality, if not superiority in the accuracy of results, reliability, speed and cost effectiveness in some cases. The advancement of technology has made the field of *ab initio* quantum chemistry an extremely useful tool to perform high accuracy predictions using computers.

The two fundamental observables of interest in chemistry are the structural parameters and energies (or energy differences) of the molecular species involved in a chemical reaction. Most of the relevant properties of matter are the manifestation of the energy differences between states or between species. Therefore, the prediction of the structures and energies with extreme precision plays an important role. However, achieving a sufficient of accuracy and precision in the prediction of the physical properties requires a certain computational power. The degree of accuracy achieved in predicting the energies and physical properties of small molecules containing a handful of atoms is very hard to achieve with molecules of larger size. This chapter is intended to introduce the most accurate theoretical methods used to address chemical problems. In the following chapters I will be discussing the specific projects I have undertaken in the last four years and chemical problems solved using the theoretical methodologies introduced in this chapter.

To understand and predict chemistry using reliable quantum chemical methods, it is necessary to concentrate on two key aspects of the electronic problem.[1] First, an accurate description of orbitals. The allowed regions an electron can reside in in a molecule is represented by a linear combination of a set of ortho-normal functions. The more complete the set of functions is, the better is the description of electrons in a molecule. In a real computation, this is done by basis sets containing the co-efficient and exponents of functions of s, p, d etc. type orbitals. This is the major source of error in a quantum chemical calculation and one for which no defined recipe of improvement exists. The second key aspect is the way electronic interactions are addressed; i.e., the estimation of interaction energies. Hartree-Fock (HF) and Post-Hartree-Fock theories take into account the electronic interaction in various ways and find the best wave function by minimizing energy. Density Functional Theory (DFT) on the other hand, treats the electron as density smeared over the space surrounding the nucleus. While the HF and Post-HF correlated methods can achieve chemical accuracy easily for small molecules, these methods become too expensive for larger systems and therefore DFT methods have to be employed. For larger molecules, DFT methods maintain the quantum chemical nature of the prediction bringing in a small number of adjustable parameters. In the following sections these methods will be briefly discussed in the context of the calculations performed on small and large molecules.

1.2 SMALL MOLECULES AND CORRELATED METHODS

The main premise is that solving the non-relativistic Schrödinger equation would produce the exact electronic energy for a given electronic configuration of a molecule in a particular

electronic state. Under the Born-Oppenheimer approximation with nuclei position clamped, the non-relativistic Schrödinger equation looks like

$$\hat{H}\varphi_{el} = E\varphi_{el}$$

Where, φ_{el} is the electronic wave function and $\hat{H}_{el}$ is the non-relativistic electronic Hamiltonian.

$$\hat{H} = (\hat{H}_{el} + V_{NN})$$

$$\hat{H}_{el} = -\frac{\hbar^2}{2m_e}\sum_i \Delta_i^2 - \sum_\alpha \sum_i \frac{Z_\alpha e'^2}{r_{i\alpha}} + \sum_j \sum_{i>j} \frac{e'^2}{r_{ij}}$$

$$V_{NN} = \sum_\alpha \sum_{\beta>\alpha} \frac{Z_\alpha Z_\beta}{r_{\alpha\beta}}$$

The electronic Hamiltonian ($\hat{H}$) consists of three terms: the kinetic energy of the electrons, the nucleus-electron attraction and the electron-electron repulsion. The solution of the Schrödinger equation gives the energy of the system. Total energies, relative energies, dipole moments, quadruple moments, force constants and harmonic vibrational frequencies are calculated by taking energy differences or energy derivatives of some sort. However conceptually robust this idea might be, actually solving the Schrödinger equation, explicitely, becomes extremely complicated, even for simple systems because of the presence of the inter-electronic distance term in the Hamiltonian. So the entire field of quantum chemistry is built upon various levels of approximations.[2]

The simplest of all the quantum chemical approximation methods is the Hartree-Fock method. In Hartree-Fock approximation, the ground state of an N-electron system is described a single Slater determinant.

$$|\varphi\rangle = |\phi^{HF}\rangle = |\chi_1\chi_2\chi_3\cdots\chi_n\rangle$$

The energy is minimized with respect to the choice of spin orbitals in the Slater determinant.

$$E^{HF} = \langle\phi^{HF}|\hat{H}|\phi^{HF}\rangle$$
$$E^0 < E^{HF}$$

By the variational principle, the HF energy is a strict upper bound to the exact electronic energy. By minimizing E^0 one can reach the following Hartree-Fock equations.

$$F_i\chi_i = \varepsilon\chi_i$$
$$F_i = -\frac{1}{2}\nabla_i^2 - \sum_{N=1}^{M}\frac{Z}{r_{iN}} + v_i^{HF}$$

where, v_i^{HF} is the average potential experienced by the ith electron due to the presence of all the other electrons and F_i is the one electron Fock operator. The HF equations are solved by making an initial guess for the spin orbitals and solving them iteratively until self-consistency is reached. HF theory treats the complicated many electron problem as a one electron problem. Thus, HF theory takes no account of the notorious electron correlation problem.[3]

Electron Correlation energy is expressed as the energy difference between the exact non-relativistic energy of a system and the HF energy of the same for a given basis set.

$$E_{Corr} = \varepsilon_{Total} - E_{HF}$$

In real systems electron correlation makes a big difference for both the ground state and excited states, when many electron systems are considered. Most of the times, electron correlation changes the "chemistry", not only quantitatively but also qualitatively. There exits various techniques to model the electron correlation problem are discussed in the following paragraphs.

Configuration Interaction (CI) is conceptually the simplest of the approximations, to improve upon the deficiencies of the HF methods, available to get the correlation energy of a multi-electron system. In a CI scheme, the HF determinant consisting of optimal spin orbitals, (assume it adequately represents the HF wave function of the ground state of the system) is improved by adding excited determinants which differ from the HF determinant ($|\varphi_0\rangle$) by one or more spin orbitals.

$$|\phi_0\rangle = c_0|\varphi_0\rangle + \sum_{ar} c_a^r |\varphi_a^r\rangle + \sum_{\substack{a<b \\ r<s}} c_{ab}^{rs} |\varphi_{ab}^{rs}\rangle + \sum_{\substack{a<b<c \\ r<s<t}} c_{abc}^{rst} |\varphi_{abc}^{rst}\rangle + \cdots$$

The equation above shows the full CI wave function. It is a better approximation to the exact form of the wave function than the HF reference wave function according to variational principle. The full CI wave function provides an exact recipe for the many electron problem. However, in practice one needs to truncate this expansion for the sake of simplicity and cost. So, the CI energy, which is obtained by diagonalizing the above wave function on the many electron Hamiltonian matrix, is a rigorously upper bound to the exact energy of the system. Although CI is a very good approximation to estimate correlation effects and extracts more than 80 per cent of the total correlation energy, in most cases it is not enough.

In a single determinant wave function description, the Coupled Cluster (CC) theories perform much better and extract out more than 90 per cent of the correlation effects in most cases. CC theories generalize and incorporate the excited determinants by an exponential wave function ansatz. Unlike the CI scheme, the CC scheme takes care of the excitation from the single reference determinant by an exponential excitation operator T.[4-7]

$$|\phi_{CC}\rangle = \exp(\hat{T})|\phi_0\rangle = (1 + \hat{T}_1 + \frac{1}{2}\hat{T}_2 + \frac{1}{3!}\hat{T}_3 + \cdots)|\phi_0\rangle$$
$$where, T = T_1 + \hat{T}_2 + T_3 + \cdots + \hat{T}_n$$

Depending upon the length of the expansion and the truncation, various CC schemes are formulated. Coupled Cluster Singles and Doubles (CCSD), and perturbative triples (CCSD(T) – the contributions of the triple excitations are incorporated perturbatively to the iterative CCSD procedure) theories are used in estimating the energies and the physical properties.

NO_2 is an environmentally active molecule. It takes part in the formation of NO_x gases and also contributes to the green house effect and global warming. The exploration of ground and the excited electronic states of NO_2 is extremely important. NO_2, being an open shell neutral molecule, poses interesting challenges to the theoretical exploration of the excited states. It serves both as a practical chemical problem as well as a model for open shell species. Multiple excitations of the inner shell electrons lead to the quartet electronic states which are closely spaced. This brings in the possibility of multi-reference character and interactions between states of same spin. Necessity arises for the treatment of multiple reference states using multi-reference methods like Complete Active Space Self Consistent Field (CASSCF) and State Averaged CASSCF (SA-CASSCF) methods. In chapter 6 the theoretical journey through the quartet excited states of NO_2 is documented. All the methods discussed above are used in the electronic structures calculation of the excited states of NO_2.

1.3 SMALL CLUSTERS

Comprehensively predicting the structures of the small atomic clusters, newly found molecules and novel interstellar molecules is a challenging task. Molecules with unconventional connectivities are produced in the gas phase in the atmosphere, the interstellar medium and also in combustion processes. These non-conventional structures

represent local minimum in the potential energy surface of a molecule. Unfortunately, very little experimental data is available for these types of molecules with a handful of atoms. For small atomic clusters especially, the experimental data are hard to come by. Theoretically, the problem of finding out all the possible isomers, both local and global, on the potential energy surface of a molecule has been addressed with partial success.

An automated stochastic procedure to search for all local and the global minima on the potential energy surface (PES) of a molecule or a cluster of atoms has been developed and coded, as will be discussed thoroughly in chapter 5. The conceptually simple idea of random kicking is implemented in an automated computer program and demonstrated with illustrative examples. The procedure developed here has the unique feature of being unbiased by human chemical intuition and automated to reduce human intervention and computational expense.

1.4 LARGE MOLECULES AND DENSITY FUNCTIONAL THEORY

In a truly astounding development, density functional theory (DFT)[8-11] has captured the attention of this generation of quantum chemists. Although the formulation of DFT is far from simple, its ability to perform large calculations has attracted many of theoretical as well as experimental chemists to try their hands. Full geometry optimizations of molecules consisting of as many as one hundred second row atoms with modest sized diffuse basis sets (e.g. a thousand basis functions) are now being done on a regular basis on desktop pc. Modeling reactions theoretically will also be feasible in near future with reasonable accuracy.

DFT takes a special approach to the quantum chemical problem. At the root of this approach is the finding made by Walter Kohn, that all the ground state molecular properties

can be predicted exactly for fixed nuclear positions by using density only. Unlike ab initio quantum chemical methods, DFT moves away from the wave function formalism and deals with density, thus decreasing the 3n co-ordinate dependence of wave function based methods. Hohenberg and Kohn[11] proved that there exists a unique relationship between the electronic Hamiltonian and the electron density. All the molecular properties could be calculated if the functional form of the electron density is known exactly. Alas! No such 'exact functional form' exists in reality. The most successful development towards the formulation of an exact functional form of the density came in the form of Kohn-Sham DFT.[10] Using the iterative concept of the HF-self consistent field theory, the explicit construction of electronic kinetic energy terms was bypassed. In the Kohn-Sham formalism of DFT, the exchange correlation functionals were introduced to extract the non-classical exchange effects and correlation energy. Thus the construction of exchange-correlation functional is of paramount interest in KS-DFT. The effects of correlation are included in an exchange correlation functional, so its efficiency compares with the post-HF correlated levels of theory at a cost of HF.

Early success for DFT was obtained from the Thomas-Fermi model and the first generation DFT, the local density approximations (LDA) which is a variant of Slater's Xα theory. Periodic boundary conditions were set to emulate the molecular environment from a uniform electron gas. However, the biggest breakthrough of the KS-DFT came in the form of generalized gradient approximation (GGA) exchange-correlation functionals which are generally considered as the second generation the of DFT functionals and shown to perform much better than before. Numerous functionals were proposed over the years. Among them, Becke's 1988 exchange functional and Lee, Yang and Parr's correlation functional and

Perdew-86 correlation functionals are the most popular. Combinations of these functionals [e.g. BLYP, BP86] are called the pure functionals and produce accurate structure and thermo-chemical results for variety of chemical systems for much lower computational costs than the wave function based correlated ab initio methods. The hybrid DFT functionals followed soon after to correct for some of the deficiencies of the pure functionals. Becke's three parameter hybrid density functional (B3) is the most common of this type and the hybrid exchange-correlation functional B3LYP is the most widely used DFT functional in the quantum chemical computations. The accuracy in the energy calculations and structural and vibrational frequency analysis of the DFT methods is close to the acceptable limits of chemical accuracy. Very recently the third generation of DFT, the optimized potential methods (OPM) started taking shape.

The ground state properties of large molecules like purine and pyrimidine bases, base pairs, radicals, and anions formed by variety of chemical reactions are predicted by the DFT functionals discussed above. This research is a creation of our conviction that the comprehensive understanding of biochemistry will stem from the understanding of structures, energetics and the intermolecular interactions of biomolecules in an isolated condition followed by, first, micro-solvation and then total solvation. I chose to work on the DNA damage caused by radiation and oxidation at the molecular level because of its importance in unraveling the mysteries of cancer-like diseases. Radiation starts a sequence of events in biological systems, which are mainly categorized into two main types: primary events and secondary events. Primary events include the radiation itself which produces Compton and photoelectrons, charged particles, excited molecules, radicals, anions and most importantly the low energy secondary electrons (SE). The secondary events are the events

caused by the products, manly SE, of primary events. The SEs retain most of the energies of the primary electrons. Although the energy of the SE's vary from 0.1 – 30 eV, they are produced in large numbers (~ 10^5/MeV). Recently it was shown experimentally by Sanche et al. and theoretically by several groups, that these low energy electrons can break bonds and create radicals. Radicals are extremely reactive species which in turn undergoe various types of chemicals reactions. Chemical reactions in the double stranded DNA can lead to strand breaks. I am interested in following the processes that occur in the gas phase after the radiation damage and also in predicting valuable physical properties of these very important transient species. In chapters three and four I have explored and elaborated on the structural and physical observables[12, 13] of these radical and anionic species of purine and pyrimidine bases and base pairs.

1.5 BIBLIOGRAPHY

1. Schaefer, H. F., *The Electronic Structure of Atoms and Molecules: A Survey of Rigourous Quantum Mechanical Results*. Addison-Wesly: Readng, MA, 1972.

2. Szabo, A.; Ostlund, N., Dover Publications, Inc.: New York, 1989.

3. Bartlett, R. J.; Stanton, J. F., *Reviews in Compuational Chemistry*. 1994; Vol. 5, p 65.

4. Paldus, J.; Piecuch, P., *International Journal of Quantum Chemistry* **1992,** *42*, 135.

5. Paldus, J., *Relativistic and Electron Correlation Effects in Molecules and Solids* **1994,** *318*, 207.

6. Paldus, J., *Methods in Computational Molecular Physics* **1992,** *293*, 99.

7. Cizek, J., *Journal of Chemical Physics* **1966,** *45*, 4256.

8. Parr, R. G.; Yang, W., *DFT*. OXford University Press: New York, 1989.

9. Labanowski, J. K.; Andzelm, J. W., *DFT Methods*. Springer-Verlag: New York, 1991.

10. Kohn, W.; Sham, L. J., *Phys. Rev.* **1965,** *140*, A1133.

11. Hohenberg, P.; Kohn, W., *Phys. Rev. B* **1964,** *136*, 864.

12. Simons, J.; Jordan, K. D., *Chemical Reviews* **1987,** *87*, 535.

13. Rienstra-Kiracofe, J. C.; Tschumper, G. S.; Schaefer, H. F.; Nandi, S.; Ellison, G. B., *Chemical Reviews* **2002,** *102*, 231.

CHAPTER 2

CYCLIC PERFLUOROCARBON RADICALS AND ANIONS HAVING HIGH GLOBAL WARMING POTENTIALS (GWPS): STRUCTURES, ELECTRON AFFINITIES AND VIBRATIONAL FREQUENCIES.

Bera, Partha P. and Ľ. Horný, and H. F. Schaefer III. 2004. Journal of American Chemical Society. 126: 6692-6702. Reprinted by permission of the American Chemical Society.

2.1 ABSTRACT

Adiabatic electron affinities, optimized molecular geometries, and IR-active vibrational frequencies have been predicted for small cyclic hydrocarbon radicals C_nH_{2n-1} (n=3-6) and their perfluoro counterparts C_nF_{2n-1} (n=3-6). Total energies and optimized geometries of the radicals and corresponding anions have been obtained using carefully calibrated (Chem. Rev. **2002**, *102*, 231) density functional methods, namely the B3LYP, BLYP, and BP86 functionals in conjunction with the DZP++ basis set. The predicted electron affinities show that only the cyclopropyl radical tends to bind electron among the hydrocarbon radicals studied. The trend for the perfluorocarbon (PFC) radicals is quite different. The electron affinities increase with expanding ring size until n=5 and then slightly decrease at n=6. Predicted electron affinities of the hydrocarbon radicals using B3LYP hybrid functional are: 0.24 eV ($C_3H_5/C_3H_5^-$), -0.19 eV ($C_4H_7/C_4H_7^-$), -0.15 eV ($C_5H_9/C_5H_9^-$) and -0.11 eV ($C_6H_{11}/C_6H_{11}^-$). Analogous electron affinities of the perfluorocarbon radicals are: 2.81 eV ($C_3F_5/C_3F_5^-$), 3.18 eV ($C_4F_7/C_4F_7^-$), 3.34 eV ($C_5F_9/C_5F_9^-$), 3.21 eV ($C_6F_{11}/C_6F_{11}^-$).

2.2 INTRODUCTION

Cyclic hydrocarbons and perfluorocarbons (PFC) have drawn attention due to their effects on the environment, very high atmospheric stability and lack of proper systematic study. Smaller (three to six C-atom rings) cyclic hydrocarbons and especially perfluorocarbons are exceptionally stable in the atmosphere (>3000 Yrs).[1,2] This exceptional high stability has earned them (cyclic perfluorocarbons) the dubious name "immortal molecules". Along with their very high atmospheric stability these PFCs are very potent greenhouse gases. The PFCs Global Warming Potentials (GWPs) are 10^3-10^4 times as high as

that of carbon dioxide. Although, the present amount of PFCs in the atmosphere is not high enough to cause any immediate threat to the environment, concern over these molecules is serious because, unlike other PFCs (CF_4 and C_2F_6, controlled substances considered by the Kyoto Protocol[3], United Nations, 1997), they are not controlled substances. However, cyclic PFCs due to their non-toxic nature, oxygen and carbon dioxide dissolving power, and high stability make them usable as blood plasma substitutes[4] (cyclic seven and eight membered rings). Also they are extensively used in rapidly developing high-density plasma (HDP) processes and atmospheric tracer studies.[5-7] All these factors and the lack of sufficient experimental data for the hydrocarbon and perfluorocarbon radicals and anions make these types of molecules important and interesting for further study.

The cyclopropyl radical has been studied over the years both theoretically[8-16] and experimentally. Fessenden and Schuler[11] deduced the out-of-plane angle of the alpha-hydrogen to be 41^o from ESR spectra. Ellinger. *et al.*[12] in the 1970's carried out *ab* initio studies of the cyclopropyl radical and reported the hyperfine coupling properties. Dupuis and Pacansky[13] in early 1980's had predicted the equilibrium structure and the vibrational properties of the cyclopropyl radical at the ab initio Hartree-Fock level, using the standard Pople "split valence" 4-31G basis. They estimated the total energy to be -116.2394 a. u. and the out of plane angle to be 39.3^o at the equilibrium geometry which has C_s symmetry. However no comprehensive study has been reported on the structure and energetics of the larger hydrocarbon radicals and anions. Schleyer, Spitznagel and Chandrashekhar[17] in 1986 predicted the existence of cyclopropyl anion in the gas phase. They even predicted that the cyclopropyl anion should be more stable than other secondary carbanions. For example, Schleyer considered the cyclobutyl anion and concluded that C_4H_9 should have a negative

electron affinitiy. The electron affinities estimated by them, at the MP2/6-31+G* level of theory, were 5.1 kcal/mol (0.22 eV) for C_3H_5 and -11.4 kcal/mol (-0.49 eV) for C_4H_7. Subsequently, Squires *et al* [18] in the same year demonstrated the existence of the cyclopropyl anion produced by collision induced decarboxylation in the gas phase. Seburg and Squires[19] in 1997 determined the electron affinity of C_3H_5 to be 0.397+/- 0.069 eV using gas phase kinetic methods. Recent studies[20-21] by our group have shown that DFT methods generally reproduce the experimental electron affinities of the radicals and neutral molecules well, on average within 0.15 eV of definitive experimental values. Despite the controversies involving the HOMO energies of the anions and electron self interaction, DFT functionals have been proved to predict the structures and electron affinities well.[22-35] Although the cyclopropyl radical and anion have been investigated over the years, very little research has been done on the corresponding c-butyl, c-pentyl and c-hexyl counterparts, suggested by Schleyer, Spitznagel and Chandrashekhar[17] to have negative (unfavourable) electron affinities. Although a lot of work has been done on the straight chain perfluorocarbons, the cyclic perfluorocarbons were neglected for a long time. In this work are presented optimized equilibrium geometries, total energies, and vibrational frequencies of the cyclic hydrocarbon as well as cyclic perfluorocarbon radicals and anions.

2.3 THEORETICAL METHODS

Density Functional Theory (DFT) studies were performed on the cyclic hydrocarbon C_nH_{2n-1} (n=3-6) radicals and corresponding anions, as well as the cyclic perfluorocarbon C_nF_{2n-1}(n=3-6) radicals and the corresponding anions. We report optimized equillibrium molecular geometries, harmonic vibrational frequencies, and electron affinities of the radicals

using three well known DFT functionals[19] B3LYP, BLYP and BP86. The radicals were initially simulated (theoretically) by homolytically cleaving (pedagogically) a C-H bond for hydrocarbons or C-F bond in case of perfluorocarbons. The anions were examined by adding an electron to the radicals. All radical and anion molecular structures were fully optimized. Adiabatic electron affinities have been evaluated by subtracting the total energy of the anion from the total energy of the neutral radical. The optimized geometries of the molecules and anions and their harmonic vibrational frequencies are also reported.

Throughout this study, DZP++,[36-39] a standard[19] basis set of contracted double-zeta Gaussian functions was used. This basis set is constructed by augmenting the Huzinaga-Dunning set of contracted double-zeta Gaussian functions with one set of p polarization functions (H) and one set of five d polarization functions (C, F). The basis set is completed by adding one even-tempered s diffuse function to each H atom and a set of even-tempered s and p diffuse functions to all the heavier atoms. The even-tempered orbital exponents were determined according to the recommendations made by Lee and Schaefer.[39] The s-type or p-type diffuse function exponent for a given atom is given by

$$\alpha_{diffuse} = \frac{1}{2}\left(\frac{\alpha_1}{\alpha_2} + \frac{\alpha_2}{\alpha_3}\right)\alpha_1$$

where α_1, α_2, α_3 are, respectively, the first, second, and third smallest Gaussion orbital exponent of the s-type or p-type primitive functions of that atom.

Three different exchange–correlation density functionals were used in this study, namely B3LYP, BLYP and BP86. B3LYP is a hybrid Hartree-Fock/DFT functional which employs Becke's 3-parameter HF/DFT hybrid exchange functional[40] (B3) coupled with the dynamical correlation functional of Lee, Yang, Parr[41] (LYP). BLYP, a pure DFT functional, employs Becke's 1988[42] exchange functional (B) in conjunction with correlation functional

of Lee, Yang and Parr (LYP). BP86 uses Perdew's[43] correlation fuctional with Becke's exchange functional.

All the quantum chemical computations were conducted using the GAUSSIAN 94[44] set of DFT programs. Both radical and the anion geometries were fully optimized by the analytic gradient method. The harmonic vibrational frequencies were obtained analytically from the mass-weighted Hessian matrix.

2.4 RESULTS AND DISCUSSION

HYDROCARBONS

The optimized molecular geometries of the ground state cyclic hydrocarbon radicals and the corresponding anions are given in Figures 2.1-2.8. The hydrocarbon radicals were initially obtained by breaking one of the C-H bonds homolytically. The optimized C_s symmetry ground state structures of the C_3H_5 (Fig. 2.1) and C_4H_7 (Fig. 2.3) radicals have $^2A'$ electronic ground states. The anions were obtained conceptually by adding one electron in the singly occupied radical HOMO orbitals. The ground electronic state of the anions $C_3H_5^-$, $C_4H_7^-$ and $C_6H_{11}^-$ thus are of $^1A'$ symmetry, as expected. Interestingly, the C_5H_9 (Fig. 2.5) radical is puckered and is most stable in C_2 symmetry whereas the corresponding anion $C_5H_9^-$ (Fig. 2.6) has C_s symmetry in the ground state. The C_5H_9 radical in C_s geometry is found to represent a transition state with a single, but significant (144 i cm^{-1}) imaginary vibrational frequency.

The adiabatic electron affinity (AEA) is obtained by subtracting the energy of the optimized anion in the $^1A'$ state from the energy of the optimized radical in the $^2A'$ state. The total energies and adiabatic electron affinities (AEA) of the radicals and anions at their respective optimized ground state geometries are listed in Table 2.1. Addition of one electron

to the radical lowers the total energy of the anion $C_3H_5^-$ compared to the C_3H_5 radical. The positive (favorable) adiabatic electron affinity indicates that the C_3H_5 radical successfully binds an electron. On the contrary, addition of one electron to the other hydrocarbon radicals studied does not stabilize the radical energetically. The total energies of the anions are thus higher than the energies of the respective radicals. Indeed, as predicted by Schleyer, Spitznagel and Chandrashekhar[17], the cyclobutyl and higher member cyclic hydrocarbon anions are not bound with respect to loss of an electron. This finding can be explained in two ways. It is clear from the HOMO of the cyclopropyl anion (Picture 2.1) that the anionic charge is delocalized to an extent which is not visible in the HOMO of the cyclobutyl (Picture 2.1), cyclopentyl and cyclohexyl anions. Secondly, due to the very small C-C-C bond angle (62.9˚) in the cyclopropyl radicals (Figure 2.1) the C-C bonds have a high degree of p-character, and the orbital which the radical electron occupies has very high degree of s-character. The extra electron in the anion goes to an s-rich orbital. In general s orbitals are compact and hold the electrons tighter. However, in larger cyclic hydrocarbon radicals, angle strain is relieved and the degree of p-character increases gradually on the orbital which "holds" the radical electron. Clearly the extra stability of the cyclopropyl anion accounts for the positive electron affinity of the cyclopropyl radical. For all three radicals, the AEA predicted by BP86 DFT functional is higher than that predicted by the B3LYP and BLYP functionals. In the case of C_3H_5 the theoretically obtained electron affinities generally agree with the experimental electron affinity obtained using the kinetic method by Seburg and Squires[19]. The electron affinity predicted by BP86 (0.38 eV) DFT functional is in very good agreement with the experimentally reported electron affinity (0.40 ± 0.07 eV). Electron affinities predicted by B3LYP and BLYP methods are 0.24 eV and 0.23 eV, respectively.

The optimized ground state geometries for both the radicals and the anions are given in Figures 2.1-2.8. As predicted previously by Ellinger *et al*[12] and by Dupuis and Pacanski,[13] the three C atoms and the H at the radical center of the cyclopropyl radical, are not in plane. Due to the very small C-C-C bond angles, the orbitals used for C-C bonding have a large degree of p-character. The orbital used for holding the radical's single electron has high s-character. This s-rich orbital pushes the C-H bonding orbital by an angle of ~39º from the C-C-C plane. The high electron density at the carbanion center (Picture 2.1) also makes the C-C-C bond angle smaller than 60º (deviation of 3.2º from the radical, Figure 2.2) on the anion. Table 2.4 summarizes the IR active harmonic vibrational frequencies along with their symmetries of the three hydrocarbon radicals and anions.

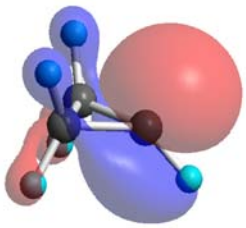

Picture 2.1. HOMO of $C_3H_5^-$ anion

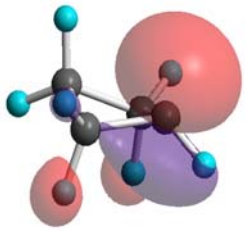

Picture 2.2. HOMO of $C_4H_7^-$ anion

PERFLUOROCARBONS

A similar approach has been taken for the study of geometries, total energies and IR active harmonic vibrational frequencies of the four (n=3-6) cyclic perfluorocarbon radicals (C_nF_{2n-1}) and the corresponding anions ($C_nF_{2n-1}^-$). Conceptually, the perfluorocarbon radicals are obtained by breaking one C-F bond homolytically. All the radicals have C_s symmetry and the HOMOs have a′ symmetry resulting in $^2A'$ electronic ground states. Anions are obtained by

adding one electron to the half filled HOMO of the radicals and therefore have $^1A'$ electronic ground states. Adiabatic electron affinities (AEA) were evaluated by subtracting the total energy of the anion, in the $^1A'$ state, from the total energy of the radical in the $^2A'$ state.

Table 1. Ground State Total Energies (Hartrees) and Adiabatic Electron Affinities (eV) of Hydrocarbon Radicals (C_nH_{2n-1}) and Anions (C_nH_{2n-1}-) [$^1A'$] , n=3-6, using the DFT functionals B3LYP, BLYP, BP86.

Molecule/Method	**B3LYP**	**BLYP**	**BP86**	**Experiment**
C_3H_5	-117.23306	-117.15972	-117.22738	
$C_3H_5^-$	-117.24199	-117.16822	-117.24127	
AEA(C_3H_5/ $C_3H_5^-$)	0.24	0.23	0.38	0.397 +/- 0.069[a]
C_4H_7	-156.57168	-156.46954	-156.563667	
$C_4H_7^-$	-156.56455	-156.46376	-156.563677	
AEA (C_4H_7/ $C_4H_7^-$)	-0.19	-0.16	0.00	
C_5H_9	-195.92735	-195.79505	-195.91574	
$C_5H_9^-$	-195.91766	-195.78809	-195.91380	
AEA(C_5H_9/ $C_5H_9^-$)	-0.26	-0.19	-0.05	
C_6H_{11}	-235.251815	-235.090917	-235.236120	
$C_6H_{11}^-$	-235.247951	-235.089898	-235.240896	
AEA (C_6H_{11}/ C_6H_{11})	-0.11	-0.03	0.13	

The total energies of the perfluorocarbon radicals and anions and the adiabatic electron affinities are shown in Table 2.2. The electron affinities of the radicals are in general gradually increasing with ring size (n=3-6) in the case of perfluorocarbons. Fluorine, due to its high electronegativity and powerful electron withdrawing inductive effect, pulls the bonding electron towards itself from the C-F single bond, rendering the already electron

deficient radical carbon even more electron deficient. Thus the electron binding ability of the perfluorocarbon radicals is much greater than that of analogous hydrocarbon radicals. With the increasing ring size (n=3-6) more fluorine atoms are attached to the ring, which makes the ring and the radical center more electron deficient. The anions are stabilized due to delocalization of anionic charge by the negative hyperconjugative effect of F. Thus the electron affinities of the perfluorocarbons increase gradually with ring size. The adiabatic electron affinity reaches a maximum for C_5F_9. Fluorine atoms that are far away from the radical carbon atom do not have much influence on the electron affinity of the radical. The changes in electron affinity with increasing atomic number are shown in Chart 2.1.

Table 2.2 Total Energies (Hartrees) and Adiabatic Electron Affinities (in eV) of the cyclic Perfluorocarbon Radicals (C_nF_{2n-1}), and anions ($C_nF_{2n-1}^-$), n=3-6 using the B3LYP, BLYP, and BP86 DFT methods with the DZP++ basis set.

Molecule/Method	**B3LYP**	**BLYP**	**BP86**
C3F5	-613.541566	-613.480233	-613.548986
$C3F5^-$	-613.644657	-613.582968	-613.654864
AEA(in eV)	2.81	2.80	2.88
C4F7	-851.441657	-851.351393	-851.447499
$C4F7^-$	-851.558364	-851.467774	-851.566922
AEA(in eV)	3.18	3.17	3.25
C5F9	-1089.315798	-1089.198057	-1089.319689
$C5F9^-$	-1089.438622	-1089.32103	-1089.445400
AEA(in eV)	3.34	3.35	3.42
C6F11	-1327.171135	-1327.025864	-1327.173528
$C6F11^-$	-1327.288979	-1327.144246	-1327.294084
AEA(in eV)	3.21	3.22	3.28

The optimized ground state structures of the radicals and anions are shown in Figures 2.9-2.16. The C-C single bond distances increase in all PFC species when compared with the C-C distance on hydrocarbons. The fluorine atoms pull electron density towards themselves by negative hyperconjugative and inductive effects, making the C-C bonds weaker. Most of the structural features are the same as in the analogous hydrocarbons. The C_5F_9 radical has C_s symmetry in its ground state, unlike C_5H_9 which is of C_2 symmetry.

Table 2.3. Comparative study of IR intensities (in km/mole) of CO_2 and perfluorocarbons using B3LYP/DZP++.

	Cumulative IR intensity of all the vibrational modes(in km/mole)	Cumulative IR intensity in the atmospheric IR "window"(in km/mole)	Percent of IR intensity falling in the atmospheric IR "window".
CO_2	734		
C_3F_5	1149	979	85.2 %
$C_3F_5^-$	2073	1502	72.5 %
C_4F_7	1579	1116	70.6 %
$C_4F_7^-$	2328	1900	81.6 %
C_5F_9	1721	1295	75.2 %
$C_5F_9^-$	3077	2091	67.9 %
C_6F_{11}	1951	1466	75.1 %
$C_6F_{11}^-$	2991	2252	75.3 %

Predicted IR active harmonic vibrational frequencies along with their intensities are also listed for all the radicals and anions in Table 2.5. The total infrared intensities of the perfluorocarbons show a growing trend on going from radicals to anions. The typical IR intensities of the perfluorocarbons are also higher than those of hydrocarbons for the same ring size. The radiation spectrum of earth spans almost the entire IR and near IR range of the

electromagnetic spectra. However, molecules having high absorption intensities in the atmospheric IR "window"[45] (~800 to ~1200 cm^{-1}) are likely have high GWPs. Molecules that were once rare but are now being introduced in the atmosphere can occupy new regions of the radiation spectrum emitted from the earth. From Table 5 it is evident that there are several vibrational modes available for each of the perfluorocarbons in this region. The total IR intensities (of CO_2) and the IR intensities in the atmospheric IR "window" are tabulated in Table 2.3. The predicted IR absorption lines are strong and 70-85 percent of the total IR intensities fall on the atmospheric IR "window" of the electromagnetic spectrum. Chart 2.2 depicts the cumulative intensities of all the vibrational modes, for each perfluorocarbon radical and anion, in the same region (~ 800 cm^{-1} to ~1200 cm^{-1}).

2.5 CONCLUSIONS

Since not a great deal of experimental data is available for the molecules studied, we are convinced that this work on the cyclic hydrocarbon and perfluorocarbon radicals should be very helpful in the future in providing valuable information about the vibrational frequencies and electron affinities of these small perfluorocarbon radicals. However, there is no way of knowing with absolute certainty which DFT functional performs best in predicting the structures, energetics and vibrational frequencies for a particular molecular system. Taken more positively, the scatter of the results from the three DFT methods gives us a good idea of the reliability of these methods. Using same DZP++ basis set for all three DFT functionals we see that BP86 predicts the electron affinities (AEA) for all the radicals higher than those predicted by the other two DFT functionals, which are close to each other. BP86 performs very well in predicting the electron affinity of the C_3H_5 radical. Absolute error from

experimentally known electron affinity of C_3H_5, reported by Seburg et al, are : 0.16 eV (B3LYP), 0.17 eV (BLYP), and 0.02 eV (BP86).

We conclude that the ground electronic states of all the radicals are $^2A'$ except for C_5H_9 (which is ^2A) and that all the anions have $^1A'$ symmetry. The ground state geometries of the radicals are C_s except for C_5H_9 which is C_2. The C_s structure of the C_3H_5 radical is a transition state. The unsubstituted cyclopropyl radical binds an electron while the cyclobutyl and cyclopentyl radicals do not. This observation is explained by the presence of "extended anionic charge delocalization" in C_3H_5 and absence of the same in C_4H_7, C_5H_9 and C_6H_{11}. The lack of a positive (favorable) electron affinity indicates that the cyclobutyl and cyclopentyl radicals can exist in the atmosphere independently without fear of electron attachment. In the case of perfluorocarbons however, all the radicals strongly bind an electron because of the stabilization obtained from the delocalization of excess charge by the electron withdrawing inductive and negative hyperconjugative effects of fluorine. The high electron affinities of radicals suggest that anions may have substantial lifetimes as independent species under atmospheric conditions. Cyclic perfluorocarbon radicals are likely to be short lived in the atmosphere. However, the fact that the anions are very stable in the atmosphere and they absorb, with very high intensities, in the atmospheric IR "window" region makes them potentially very potent greenhouse gases.

2.6 ACKNOWLEDGEMENTS

Partha P. Bera thanks Prof. P. v. R. Schleyer for usefull comments, Dr. Alexey Timoskin, Chaitanya Wannere and Ankan Paul for helpful discussions. This research was supported by National Science Foundation under Grant CHE-0136184.

2.7 REFERENCES

1. Simmonds, P.G.; Greally, B.R.; Olivier, S.; Nickless, G.; Cook, K.M.; Dietz, R.N. *Atmospheric Environment*, **2002**, *36*, 2147.

2. World Meteorological Organization (WMO), Scientific Assessment of Ozone Depletion, **1988**. Albritton, D. (Ed) *Report 44*. 650 pp,Global Ozone Res. and Monit. Project, Geneva **1999**.

3. United Nations Framework Convention on Climate Change. **1997**, The Kyoto Protocol to the *UNFCC* , *FCCC-CP*-**1997**-1.,7-Add 1.

4. Dagani, R. *Synthetic Blood Research Progressing*, *Chemical and Engineering News* **1982,** *60*, 31.

5. Zyron® 8020. *DuPont, Zyron Electronic Gases for Plasma Process Applications*.

6. De Bertoli, M.; Pecchio, E.J. *High Resolution Chromatographic Communications* **1985**, *8*, 422-425.

7. Dietz, R.N. **1987**. *Perfluorocarbon Tracer Technology*, BNL, 38847. In: Sndroni, S.; (Ed), *Regional and Long Range Transport of Air Pollution*, Elsevier, Amsterdam, pp. 215.

8. Wong, M.W.; Radom, L. *J. Am. Chem. Soc*. **1993**, *115*, 1507; Rogers. D.W.; McLafferty, F. *J. Phys. Chem*. **1995,** *99,* 1375.

9. Smith, B.J.; Radom, L. *J. Phys. Chem*. **1991**, *95*, 10549.

10. Glukhovtsev, M.N.; Lalter, S.; Pross, A. *J. Phys. Chem*. **1996**, *100*, 17801.

11. Fessenden, R. W.; Schuler, R. H. *J. Chem. Phys.* **1963,** *39*, 2147.

12. Ellinger, Y.; Subra, R.; Levy, B.; Millie, P.; Berthier, G. *J. Chem. Phys*. **1975,** *62*, 10.

13. Dupuis, M.; Pacansky, J. *J. Chem. Phys*. **1982,** *76*, 2511.

14. Cremer, D.; Kraka, E. *J. Am. Chem. Soc*. **1985**, *107*, 3800.

15. Dyke, J.; Ellis, A.; Jonathon, N.; Morris, A. *J. Chem. Soc. Faraday Trans. 2* **1985**, *81*, 1573.

16. Cremer, D.; Gauss, J. *J. Am. Chem. Soc*. **1986**, *108,* 7467.

17. Schleyer, P. v. R.; Spitznagel, G. W.; Chandrashekhar, J. *Tetrahedron Letters* **1986**, *27*, 4411.

18. Frolicher, S. W.; Freiser, B. S.; Squires, R. R. *J. Am. Chem. Soc*. **1986,** *108*, 2853.

19. Seburg, R. A.; Squires, R. A. *Int. J. of Mass Spec. and Ion Processes* **1997,** *167/168,* 541.

20. Rienstra-Kiracofe, J. C.; Tschumper, G. S.; Schaefer, H. F.; Nandi, S.; Ellison, G. B. *Chem. Rev*. **2002**, *102,* 231.

21. King, R.A.; Pettigrew, N.D.; Schaefer, H.F. *J. Chem. Phys*, **1997**, *107,* 8536.

22. Tschumper, G. S.; Fermann, J. T.; Schaefer, H.F. *J. Chem. Phys*. **1995,** *14*, 3676.

23. Tschumper, G. S.; Schaefer, H.F. *J. Chem. Phys*. **1997,** *107*, 2529.

24. Curtiss, L. A.; Redfern, P. C.; Raghavachari, K.; Pople, J. A. *J. Chem. Phys*. **1998,** *109*, 42.

25. Ziegler, T.; Gutsev, G. L. *J. Comput. Chem*. **1991,** *13*, 70.

26. King, R.A.; Mastryukov, V. S.; Tschumper, G. S.; Schaefer, H. F. *J. Chem. Phys*. **1996**, 105, 6880.

27. Van Huis, T. J.; Galbraith, J. M.; Schaefer, H. F. *Mol. Phys.* **1996**, *89*, 607.

28. Chong, G. P.; Ng, C. Y. *J. Chem. Phys.* **1993**, *98*, 759.

29. King, R.A.; Galbraith, J. M.; Schaefer, H. F. *J. Phys. Chem.* **1996**, *100*, 6061.

30. Cole, L. A.; Perdew, J. P. *Phys. Rev. A* **1982**, *25*, 1265.

31. Grafton, A. K.; Wheeler, R. A. *J. Phys. Chem.* **1997**, *101*, 7154.

32. Boesch, S. E.; Grafton, A. K.; Wheeler, R. A. *J. Phys. Chem.* **1996**, *100*, 10083.

33. Rienstra-Kiracofe, J. C.; Graham, D. E.; Schaefer, H. F. *Mol. Phys*. **1998**, *94*, 767.

34. Galbraith, J. M.; Schaefer, H. F. *J. Chem. Phys*. **1996**, *105*, 862.

35. Roesch, N.; Tricky, S. B. *J. Chem. Phys*. **1997**, *106*, 8941.

36. Dunning, T. H. *J. Chem. Phys.* **1971**, *55*, 3958.

37. Huzinaga, S. *J. Chem. Phys*. **1962,** *42*, 1293.

38. Dunning, T. H. *J. Chem. Phys*. **1970**, *53*, 2823.

39. Lee, T. J.; Schaefer, H. F. *J. Chem. Phys*. **1985**, *83*, 1784.

40. Becke, A. D. *J. Chem. Phys*. **1993**, *98*, 5648.

41. Lee, C.; Yang. W.; Parr, R. G. *Phys. Rev*. **1988**, *B 37*, 785.

42. Becke, A. D. *Phys. Rev*. **1988**, *A 38*, 3098.

43. Perdew, J. P. *Phys. Rev*. **1986**, *B 33*, 8822.

44. Frisch, M. J.; Trucks, G. W.; Schlegel, H. B.; Gill, P. M. W.; Johnson, B. G.; Robb, M. A.; Cheeseman, J. R.; Keith, T.; Peterson, G. A.; Montgomery, J. A.; Raghavachari, K.; Al-Laham, M. A.; Zakrzewski, V. G.; Oritz, J. V.; Foresman, J. B.; Cioslowski, J.; Stefanov, B. B.; Nanayakkara, A.; Challacombe, M.; Peng, C. Y.; Ayala, P. Y.; Chen, W.; Wong, M. W.; Andres, J. S.; Defrees, D. J.; Baker, J.; Stewart, J. P.; Head-Gordon, M.; Gonzalez, C.; Pople, J. A. ***Gaussian 94***; Gaussian, Inc: Pittsburgh, PA, **1995**.

45. Sturges, W. T.; Wallington, T. J.; Hurley, M. D.; Shine, K. P.; Sihra, K.; Angel, A.; Oram, D. E.; Penkett, S. A.; Mulvaney, R.; Brenninkmeijer, C. A. M. *Science* **2000**, *289*, 611.

2.8 FIGURES

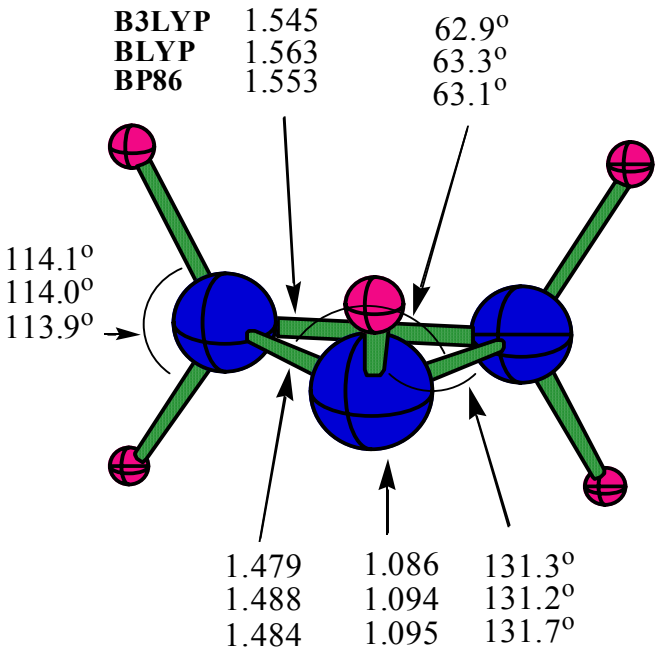

Figure 2.1. Optimized geometry of the C_3H_5 radical (C_s) in the $^2A'$ ground state. Bond lengths are in Å.

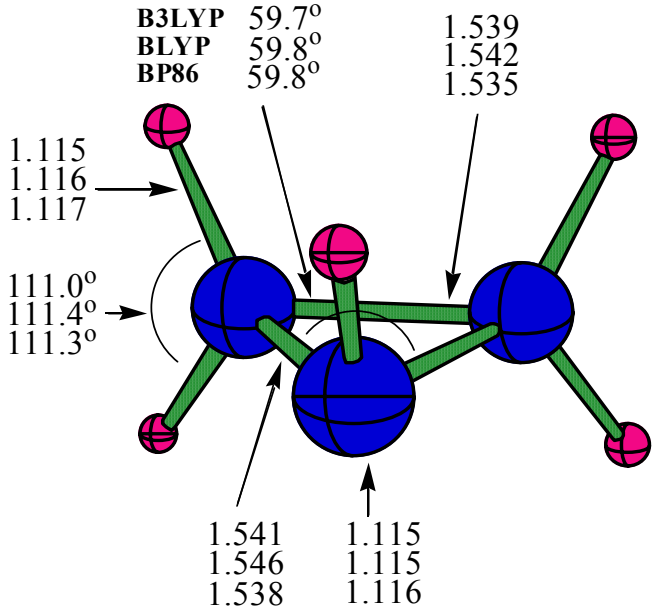

Figure 2.2. Optimized molecular geometry of the $C_3H_5^-$ anion in its $^1A'$ ground state. Bond lengths are in Å.

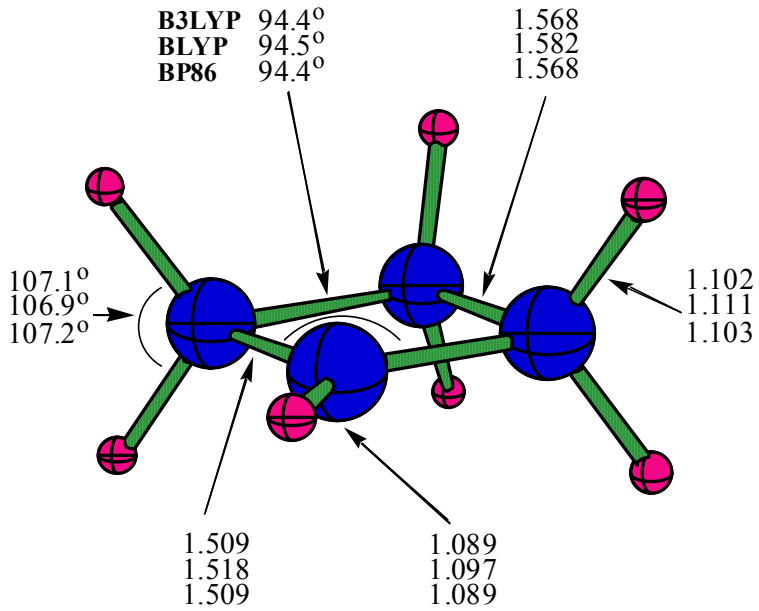

Figure 2.3. Optimized geometry of the C_4H_7 radical (C_s) in its $^2A'$ ground state. Bond lengths are expressed in Å.

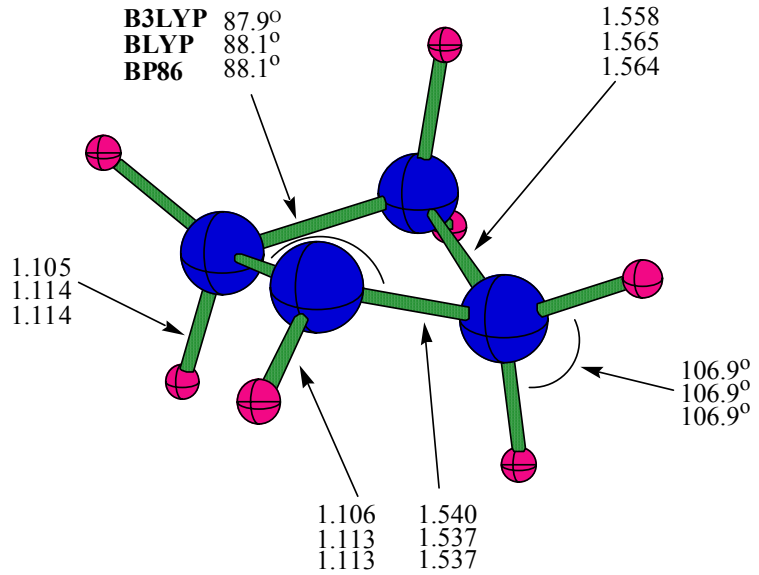

Figure 2.4. Optimized geometry of the $C_4H_7^-$ anion (C_s) in its $^1A'$ ground state. Bond angles are expressed in Å.

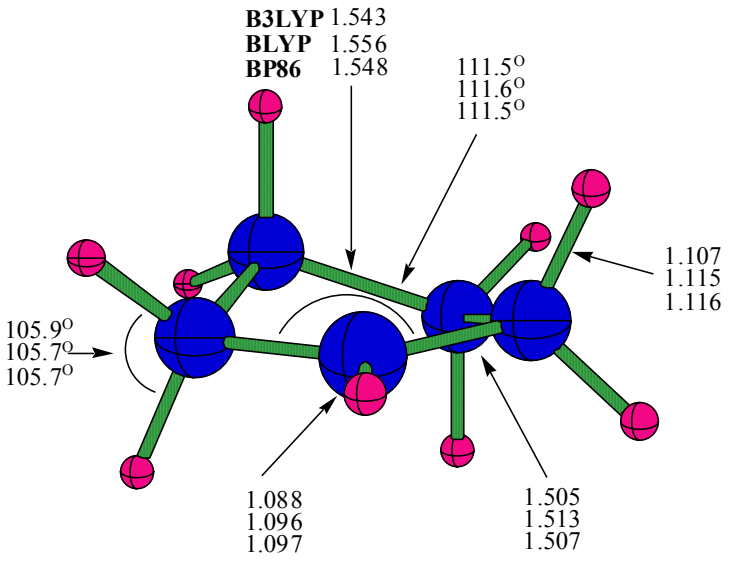

Figure 2.5. Optimized geometry of the C_5H_9 radical (C_2) in its ^2A ground state. Bond lengths are expressed in Å.

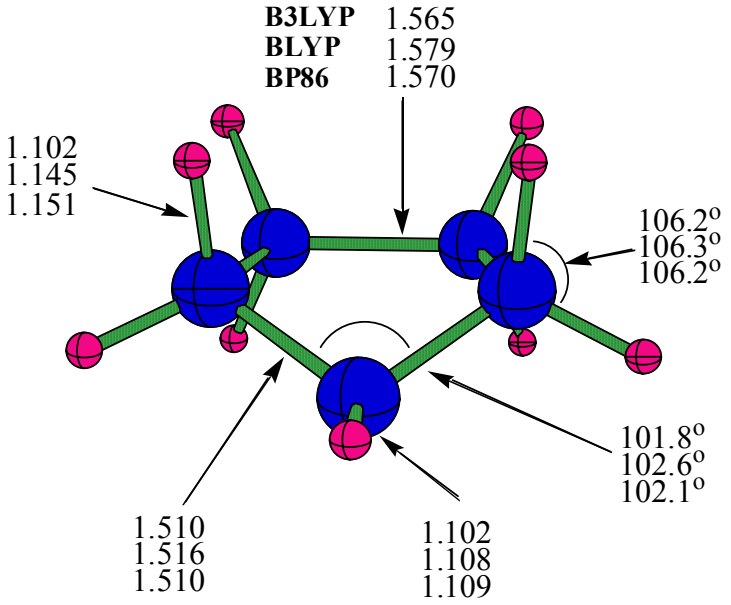

Figure 2.6. Optimized geometry of the $C_5H_9^-$ anion (C_s) in its $^1A'$ ground state. Bond lengths are in Å.

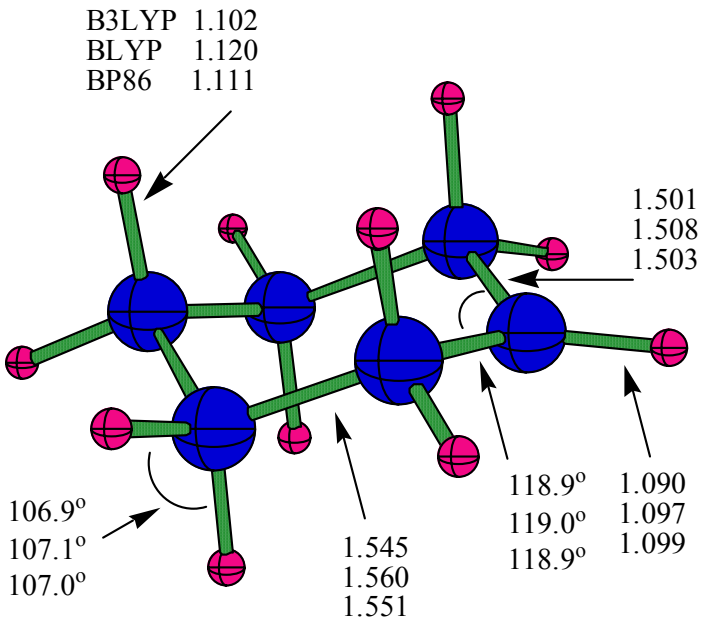

Figure 2.7. Optimized geometry of the C_6H_{11} radical (C_s) in its $^2A'$ ground state. Bond lengths are expressed in Å.

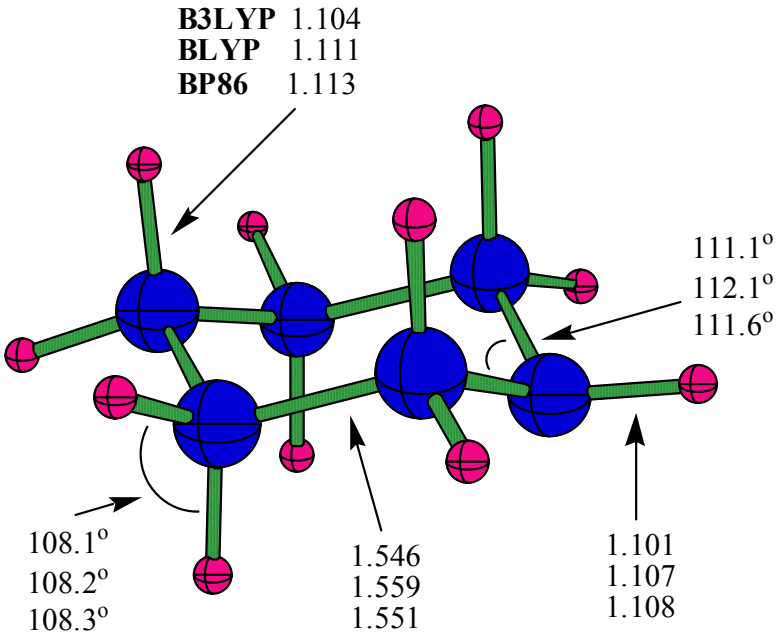

Figure 2.8. Optimized geometry of the $C_6H_{11}^-$ anion (C_s) in its $^1A'$ ground state. Bond lengths are expressed in Å.

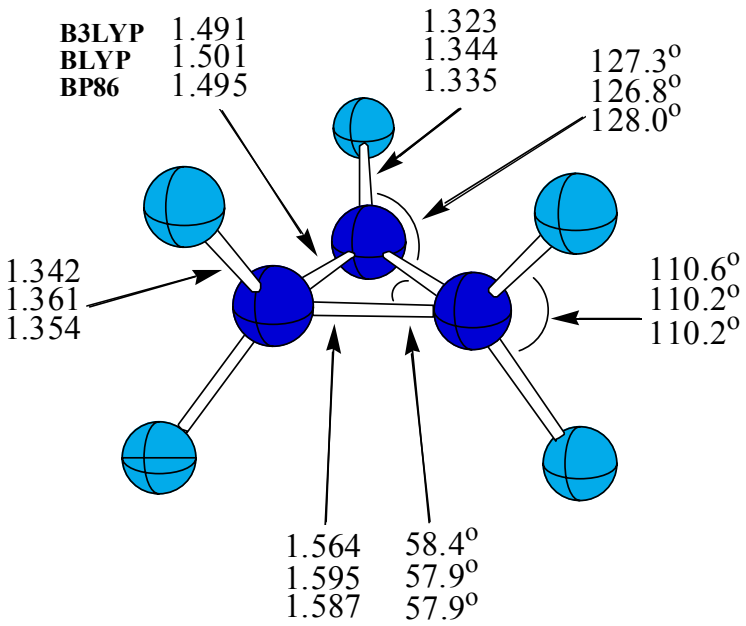

Figure 2.9. Optimized geometry of the C_3F_5 radical (C_s) in its $^2A'$ ground state. Bond lengths are in Å.

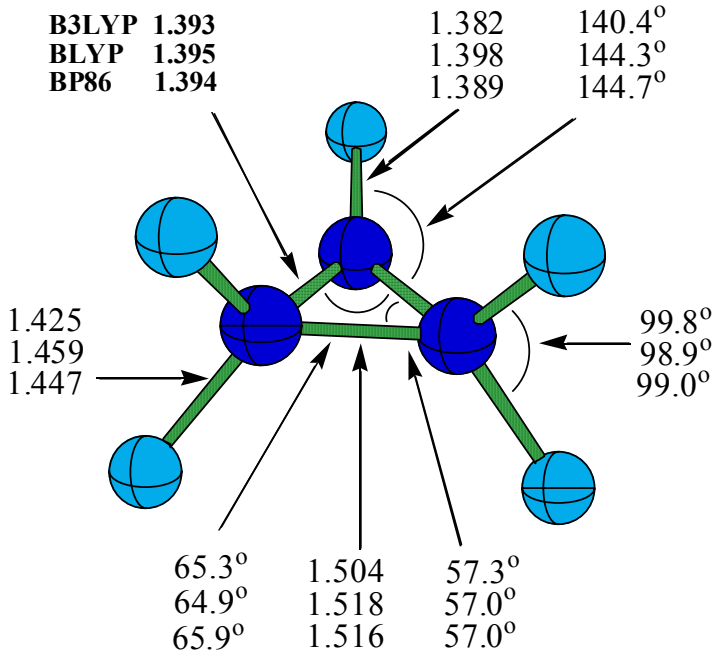

Figure 2.10. Optimized geometry of the $C_3F_5^-$ anion (C_s) in its $^1A'$ ground state. Bond lengths are in Å.

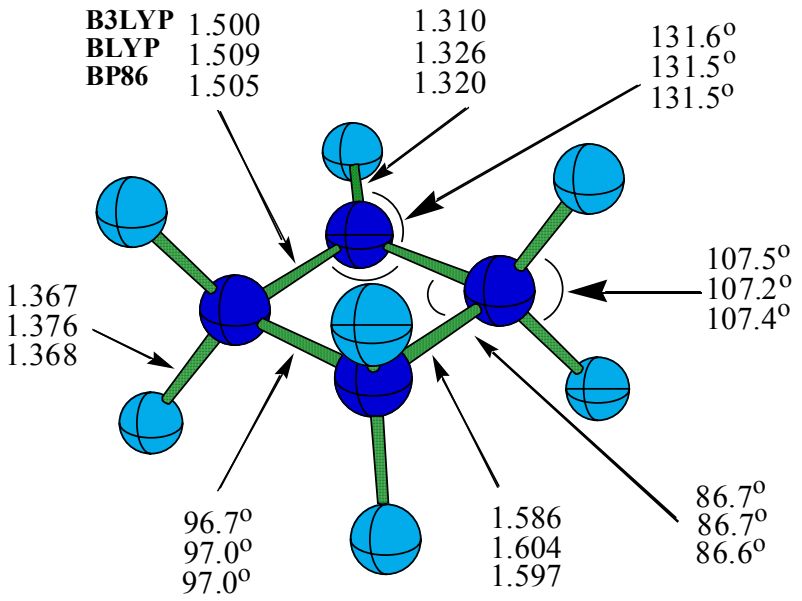

Figure 2.11. Optimized geometry of the C_4F_7 radical (C_s) in its $^2A'$ ground state. Bond lengths are in Å.

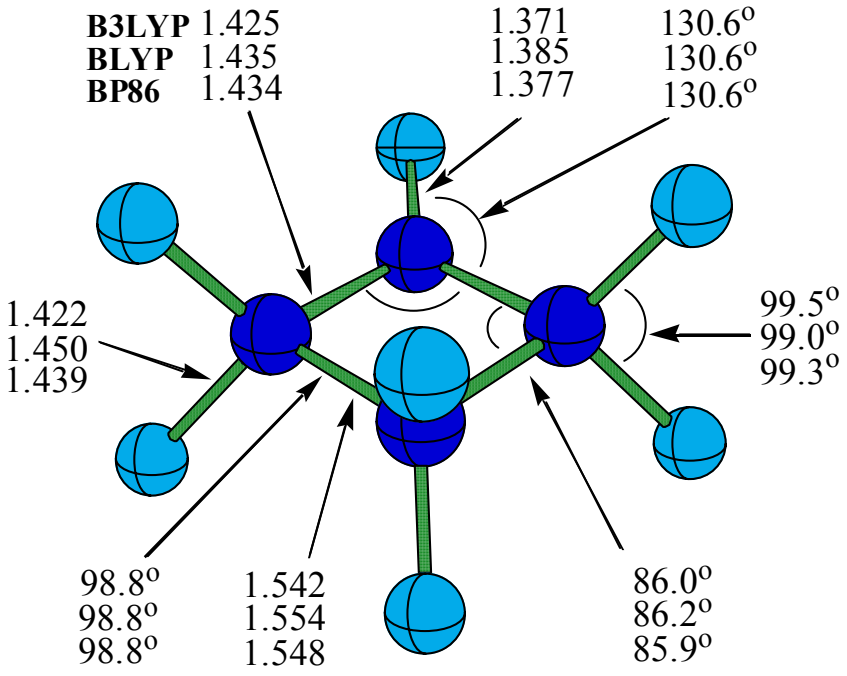

Figure 2.12. Optimized geometry of the $C_4F_7^-$ anion (C_s) in its $^1A'$ ground state. Bond lengths are in Å.

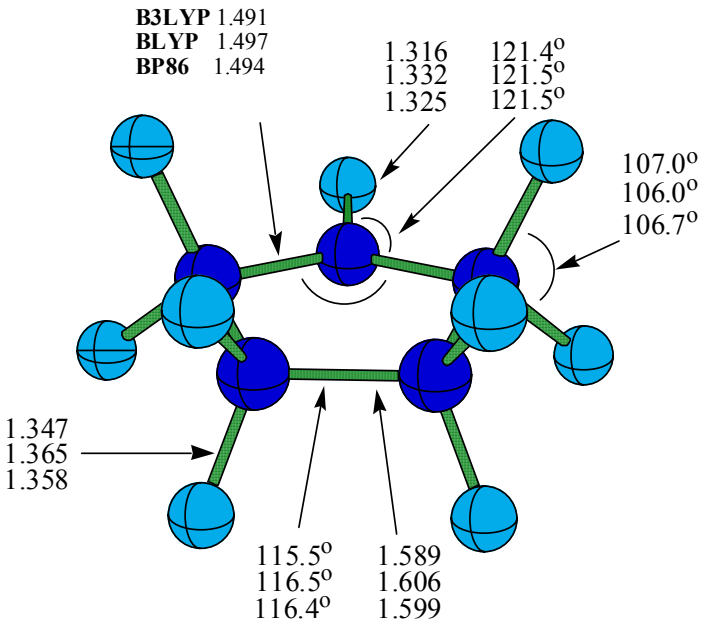

Figure 2.13. Optimized geometry of the C_5F_9 radical (C_s) in its $^2A'$ ground state. Bond lengths are in Å.

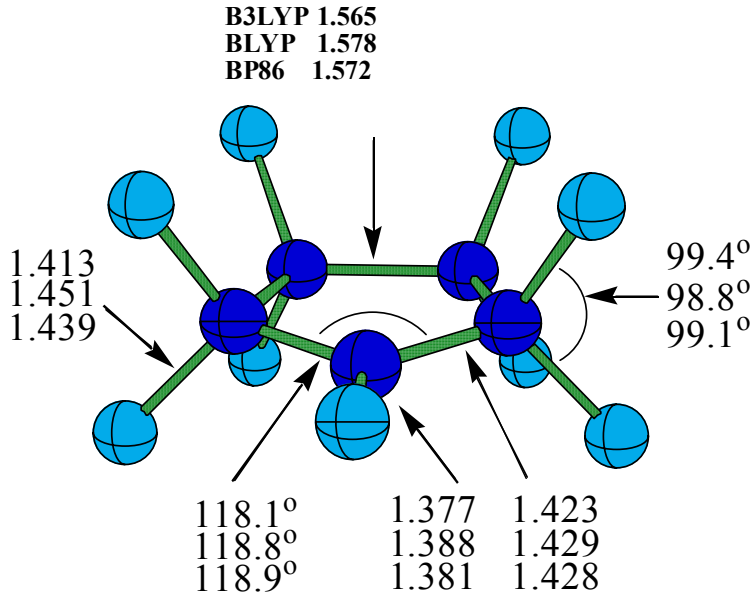

Figure 2.14. Optimized geometry of the $C_5F_9^-$ anion (C_s) in its $^1A'$ ground state. Bond lengths are in Å.

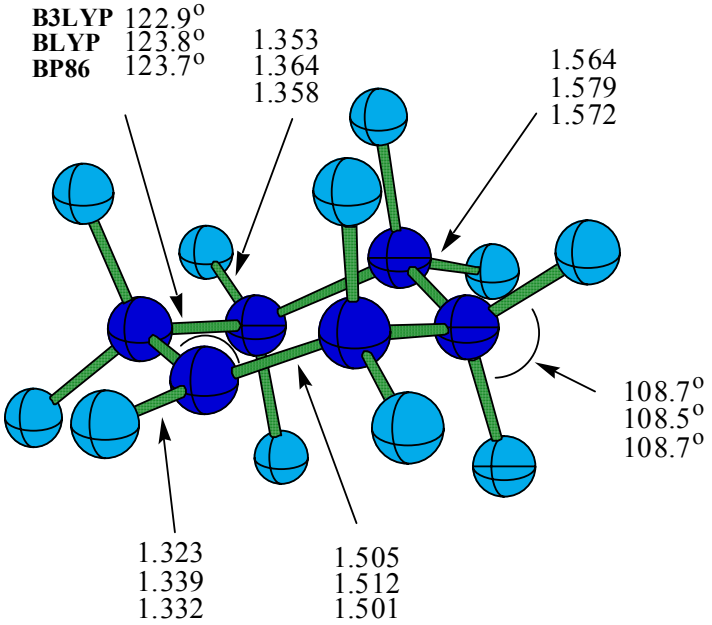

Figure 2.15. Optimized geometry of the C_6F_{11} radical (C_s) in its $^2A'$ ground state. Bond lengths are in Å.

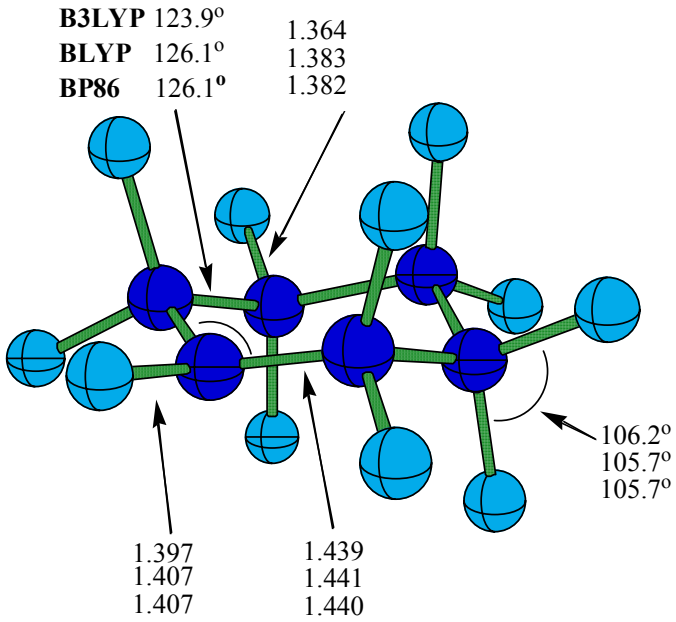

Figure 2.16. Optimized geometry of the $C_6F_{11}^-$ anion (C_s) in its $^1A'$ ground state. Bond lengths are in Å.

CHAPTER 3

LESIONS IN DNA SUBUNITS: RADICALS DERIVED FROM THE GUANINE-CYTOSINE BASE PAIR, (G-H)·-C AND G-(C-H)·

Bera, Partha P. and Henry F. Schaefer III 2005 Proceedings of the National Academy of Sciences of U. S. A. 102,6698-6703. Reprinted by permission of the National Academy of Science.

3.1 ABSTRACT

The radicals generated by the homolytic cleavage of an X-H bond from the guanine-cytosine base pair were studied using carefully calibrated theoretical methods. The gradient corrected density functional B3LYP was applied in conjunction with double-ζ plus polarization and diffuse function basis sets, as described in *Chem. Rev*. **2002**, *102*, 231. Optimized geometries, energies and vibrational frequencies were obtained for all the radicals considered. Structural perturbations along with energy relaxation due to radical formation were investigated. Dissociation energies of the guanine-cytosine base pair and all the radicals are predicted and compared with the dissociation energy of neutral G-C. The three lowest energy base pair radicals all involve removal of an H atom from one of the N atoms in G-C. The lowest energy base pair radical has the hydrogen atom removed from the guanine nitrogen atom used for the sugar phosphate linkage in DNA. This (G-H)·-C radical has a dissociation energy (to G-H· + C) of 30 kcal/mol, compared to 27 kcal/mol for G-C. All the radicals, which are possible outcomes of direct ionizing radiation or oxidizing species, were investigated for the presence of local minima with significant structural changes. Major structural deformations cause strain in the interstrand hydrogen bonding in the DNA double helix. Severe geometry changes were observed when the hydrogen was abstracted from interstrand hydrogen bonding sites, along with sizeable energy changes, indicating the potentially serious consequences to the guanine-cytosine base pair.

3.2 INTRODUCTION

The purines and pyrimidines are foundational constituents of DNA and RNA, which are the translators of genetic information from generation to generation. The causes of

damage to purine and pyrimidine bases have received significant attention from the scientific community. Both theoretical and experimental research on this important subject have been directed to understanding the underlying chemistry during and after damage to DNA[1]. Yet little is known about the possible outcome of damage to the base pairs in terms of energetics and possible structural changes that can lead to strand breakage and therefore loss of genetic information. Sophisticated experimental techniques have been used to investigate the causes and effects of DNA damage and also to determine structural features, as well as delving into the electron binding ability of the bases and base pairs [1-4]. Some of the more advanced experimental and theoretical methods have also been applied to model systems in both the gas and liquid phases to estimate and predict the physical properties and to study hydrogen bonding in purine and pyrimidine base pairs [5-19]. Over the years experimental crystallographic data and theoretical work on the isolated bases and base pairs seemed to disagree on the hydrogen bond lengths and interaction energies of the base pairs. Guerra, Bickelhaupt, Snijders and Baerends [5] assign this apparent discrepancy to the effects of molecular environment. They report that solvating the base pairs by H_2O and metal ions allows them to achieve agreement between experiment and theory with the BP86/TZ2P method [5]. Nevertheless, highly complex double stranded DNA helical patterns pose strong barriers to acquiring valuable experimental data from the DNA.

Damage to DNA and RNA base pairs can occur in at least two elementary ways, one through direct radiation and the other through oxidative cleavage of bonds. There are numerous experimental reports available in this respect, documenting the mechanisms involved in the various channels [20, 21]. Formation of the radicals from the neutral base pairs is possible due to direct exposure to radiation. Involvement of electronically excited triplet

states is also indicated in the formation of radicals from closed-shell neutrals [22]. The stacked nature of base pairs in DNA is also well suited for fast electron transfer by classes of mutagens, causing damage to DNA [23-25]. Radicals can bring about significant changes in the geometry of the base pair and overall shape of the DNA strand. Any significant structural change in the base pair can lead to strand breaking, possible mismatches in the pairing, and mutation. Investigations into the cause and effect of radical generation due to radiation and oxidative cleavage are necessary in terms of structural and energetic considerations.

Experiments done by several groups prove that even very low energy electrons can break DNA by various mechanisms [1]. Electron attachment followed by single strand break is one of the processes described [2]. The purpose of the present research is to explore the possibility of formation of stable radicals with significant structural changes and also to understand the energy changes associated with such processes. This is an important subject not only because attachment of electron to DNA base pairs or radical formation (due to high energy electron impact and/or ionizing radiation) would lead to strand breaks and therefore deter the information flow. Conversely, to the advantage of living things, such processes may break up mutant and potentially dangerous tumor cells. Rearrangement of the radicals to a deformed structure will incorporate increased strain in the rigid DNA strand. The resultant H and base pair radicals may be quenched by thiols in biological systems [20]. If not repaired quickly, the damaged DNA mutates, and may ultimately cause cell death.

The neutral single bases have been studied theoretically for their structures and energetic stability and predicted to be nonplanar in the gas phase. Complexation energies upon base pair formation have also been computed for both the DNA base pairs [26-31] and electron affinities of the single bases [32] and base pairs have been evaluated [27, 33].

Due to direct radiation damage and oxidation, hydrogen atoms present in the base pair can be removed, resulting in various neutral as well as cationic radicals. Hutter and Clark predicted a facile proton shift in the GC^+ radical cation along its central hydrogen bond and also reported the ionization potential of the isolated bases [26]. A recent study by Sponer, Jurecka, and Hobza investigated all possible combinations of base pairs in terms of their interaction energies and hydrogen bond lengths at the MP2 and CCSD(T) levels of theory using a cc-pVTZ basis set [34]. Radicals generated from guanine were also studied by Steenken et al [35], Cullis et al [36], and Melvin et al [37] for their thermodynamic stability and role in strand breaking in DNA.

The present research concentrates on the neutral radicals generated by removing one hydrogen atom from the guanine-cytosine base pair, depicted in Figure 3.1. Extracting a hydrogen bonded H atom from the GC base pair ruptures interstrand hydrogen bonds that hold the two strands together. Removing a hydrogen atom also leads to a radical at the 8 position (see Scheme 3.2) of the guanine. It is known that 8-oxo-guanine is a very important lesion that can change the conformational properties of the strand [3, 36, 38]. Radicals are formed by reactions with reactive oxygen species in the liquid phase, generated by ionizing radiation and by direct radiation damage in the gas phase [20]. A radical at the 8 position can be a possible intermediate for the formation of the 8-oxo species. Radicals at position 8 both in the isolated guanine and Watson-Crick base paired models are thus important species to investigate.

The present research is a contribution to the chemical physics of biomolecules in the gas phase. The decision to study the isolated base pair radicals is based on two considerations. The first is that any treatment of solvent effects for systems of the size of G-C

radicals would degrade the reliability of the theoretical predictions. The second consideration is our conviction that the deepest understanding of biochemistry can only result when the full range of conditions is studied: namely (a) the isolated molecules; (b) the same molecules in a microsolvated environment (e.g., a finite number of water molecules); and (c) the fully solvated molecular species. Clearly, from this perspective, the first step is to have definite theoretical predictions for the isolated molecular systems of interest.

3.3 METHODS

Optimized geometries, absolute energies and vibrational frequencies were determined a using Generalized Gradient Approximation (GGA) exchange-correlation density functional on the Watson-Crick guanine-cytosine base pair. The three parameter hybrid HF/DFT exchange functional, B3 [39] was used in conjunction with 1988 dynamical correlation functional of Lee, Yang and Parr (LYP) [40]. The dissociation energies of the guanine-cytosine base pair systems were evaluated as follows:

Dissociation Energy of Guanine-Cytosine

$D_e = E(G\text{-}C) - E(G) - E(C)$

Dissociation Energies of the Radicals

(i) $D_e = E[(G\text{-}H)\cdot\text{-}C] - E[(G\text{-}H)\cdot] - E(C)$

(ii) $D_e = E[G\text{-}(C\text{-}H)\cdot] - E(G) - E[(C\text{-}H)\cdot]$

The prediction of dissociation energies from theory for systems of the size of the G-C radicals necessarily requires a delicate cancellation of errors. This inevitably brings up the issue of basis set superposition error (BSSE). The use of diffuse basis functions lessens the

importance of BSSE. Typically, convergent quantum mechanical levels of theory without BSSE corrections tend to approach the true dissociation energy from above, while the opposite trend is seen with BSSE corrections. However, density functional theory, as it is usually carried out in practice, is not a part of a series of convergent quantum mechanical procedures. Thus it is important that the use of BSSE corrections be adressed with an eye to pragmatic concerns. As will be seen bellow, the true dissociation energy of the closed shell G-C system is reproduced without the use of BSSE corrections. Thus we choose not to apply BSSE corrections to the G-C radical dissociation energies.

A double-ζ quality basis set, DZP++, with polarization and diffuse functions was used throughout the optimization and vibrational frequency computations [41-44]. This DZP++ set was constructed by augmenting the Huzinaga-Dunning set of contracted double zeta Gaussian functions with one set of p polarization functions on the H atoms and also one set of five d polarization functions on each of the C, N and O atoms. An even-tempered s diffuse function was added to each H atom and one s and one set of p type even- tempered diffuse function was added to the each of the heavy atoms. The orbital exponents for even tempering were determined using the directive of Lee and Schaefer [41]:

$$\alpha_{diffuse} = \frac{1}{2}\left(\frac{\alpha_1}{\alpha_2} + \frac{\alpha_2}{\alpha_3}\right)\alpha_1$$

where, α_1, α_2 and α_3 are the three smallest Gaussian orbital exponents of the s or p-type primitive functions for an atom ($\alpha_3 > \alpha_2 > \alpha_1$). Therefore the final DZP++ basis set includes six functions per H atom (5s1p/3s/1p) and 19 functions per C, N or O atom (10s6p1d/5s3p/1d) giving a total of 421 basis functions for the GC base pair and 415 basis functions for the GC radicals.

Previous research has demonstrated that this level of theory is reliable for molecules for which higher level ab initio calculations are still too expensive, despite the improving speeds of computers [45]. All our computations were done using the Q-Chem 2.1 suite of density functional programs [46]. Stationary points were obtained via analytic gradient methods.

3.4 RESULTS

The crystallographic data [6, 8] available for the base pairs within DNA were compared with results predicted here (Table 3.1). However the structures of the possible radicals that can be generated from primary radiation damage, have never been explored experimentally. Although the radical cations and other lesions have been investigated using density functional levels of theory [26], neutral radicals have not previously been investigated.

Scheme 3.1. Above: guanine-cytosine base pair.

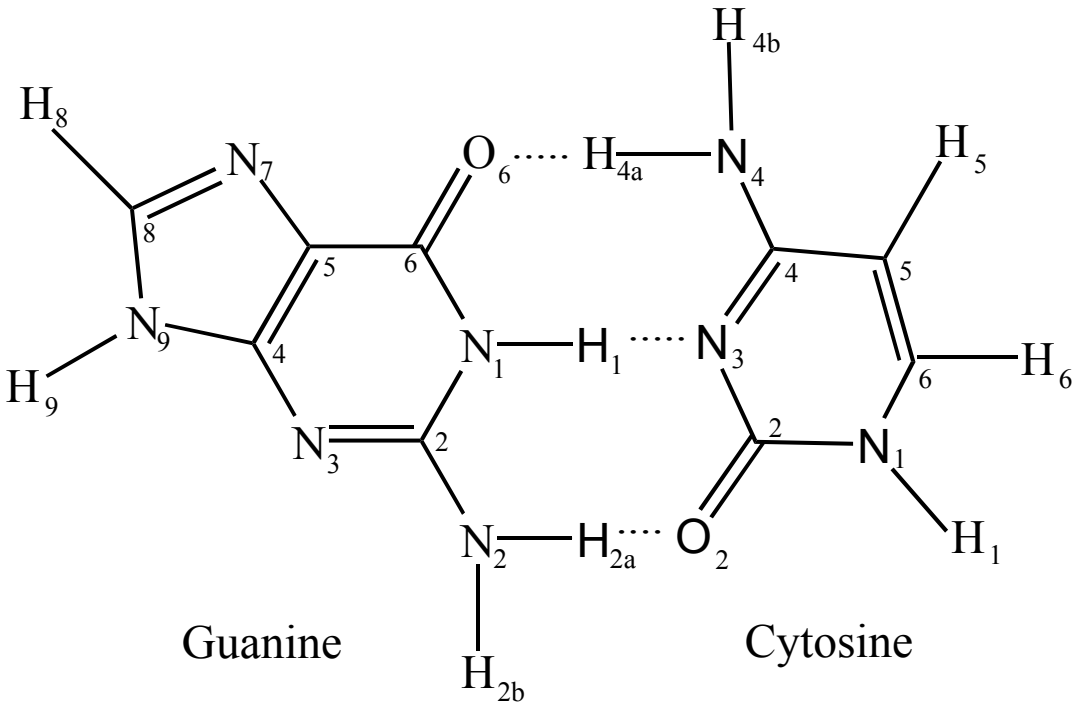

GUANINE-CYTOSINE

In the Watson-Crick model, the DNA double helices are formed from the coiling of two strands of purine and pyrimidine bases. Guanine pairs with cytosine, and adenine pairs with thymine in DNA. Interstrand hydrogen bonds are responsible for this pairing. The interatomic distances obtained in this work at C_1 symmetry using the B3LYP/DZP++ level of theory do not compare well with the crystallographic conclusions [6, 8]. We do find agreement with the theoretical structures reported by Guerra and Richardson [5, 27]. All previous G-C computations have been in poor agreement with the experimental crystal structure. Guerra and coworkers [5] have discussed possible reasons for the discrepancies. Hydrogen bonding distances in the base pair obtained from various techniques are tabulated in Table 1 [5, 6, 27, 47-49]. Figure 1 shows the optimized geometry of the guanine-cytosine base pair with the B3LYP/DZP++ method. All the density functional methods predict the hydrogen bonding distance between oxygen of guanine (O6) and nitrogen of cytosine (N4) to be 2.73-2.79 Å. However, the experimental X-ray crystallographic measurements by Rosenberg et al. [6] report this distance to be 2.91 Å. The theoretically obtained distance, between the nitrogen of guanine (N1) and the nitrogen of cytosine (N3), lies close to the experimentally reported value of 2.95 Å. Finally, the B3LYP distance (2.91 Å) between nitrogen of guanine (N2) and the oxygen of cytosine (O2) is larger than the experimental value of 2.86 Å. This apparent lack of agreement between theory and experiment for the hydrogen bond lengths has been analysed by Guerra *et al.* [5]. They conclude that the gas-phase geometry of G-C is inherently different from the observed crystal structure. The dissociation energies of the guanine-cytosine base pair and the radicals under consideration are reported in Table 3.4.

The dissociation energies of G-C, (G-H)·-C, and G-(C-H)· are reported in Table 3.4. Our predicted G-C dissociation energy D_e(G-C) = 27.2 kcal/mol is the same as that of Richardson [27]. The only experimental dissociation energy is the 1979 value D_0(G-C) = 21.0 kcal/mol, of Yanson, Tiplitsky, and Sukhodub [31]. The reliability of this experiment is in doubt. The most satisfactory value of D_e(G-C) is that provided by Sponer, Leszczynski, and Hobza [30]. These authors estimate the Hrtree-Fock limit to be 24.6 kcal/mol, the basis set limit for MP2 to be 25.8 kcal/mol and the final estimated D_e to be 26.3 kcal/mol. In the most recent paper on this subject, Sponer, Jurecka, and Hobza [34] conclude that the true value of D_e(G-C) may be slightly higher. The agreement with the present DFT prediction of 27.2 kcal/mol is sufficiently encouraging to repose a degree of confidence in our radical dissociation energies, for no previous results exist.

Table 3.1. Table of bond lengths for the neutral guanine-cytosine base pair in Å.

	O6-N4	N1-N3	N2-O2
Experiment – Crystal Structure[a]	2.91	2.95	2.86
HF/6-31G*[b]	2.93	3.05	3.01
HF/cc-pVTZ[c]	2.83	2.95	2.92
B3LYP/6-31G**[d]	2.79	2.93	2.92
BP86/TZ2P[e]	2.73	2.88	2.87
BHLYP/DZP++[f]	2.78	2.93	2.91
B3LYP/DZP++[this work]	2.76	2.92	2.91

a. Rosenberg, Seeman, Day, and Rich [6].
b. Gould and Kollman [48].
c. Brameld, Dasgupta, and Goddard [49].
d. Bertran, Oliva, Rodriguez-Santiago, and Sodupe [47].
e. Guerra, Bickelhaupt, Snijders, and Baerends [5].
f. Richardson, Weslowski, and Schaefer [27].

RADICALS

G(N1)-C – A generic label is used for each of the radicals investigated in this work. Radical G(N1)-C is generated by homolytically breaking the N1-H bond of guanine. GC

atoms are most conveniently labeled in Scheme 3.2. The energy of each base-pair radical is first obtained without any change in the closed-shell neutral equilibrium geometry. However, upon optimization the energy relaxes by 20.7 kcal/mol and the hydrogen bonding pattern drastically changes to give the structure shown in Figure 3.2. The entire backbone shifts by approximately 2.3 Å. Nevertheless, the hydrogen bond lengths do not change much due to optimization to the planar new structure with C_s symmetry. This new radical structure is a true minimum in which two NH···N hydrogen bonds are favored over the two NH···O hydrogen bonds that occur for G-C. This major structural change is found despite the fact that O···H hydrogen bonds appear to be stronger than N···H hydrogen bonds. This surprising result may be due to extended conjugation of the rings.

Table 2. Total energies of the radicals at the B3LYP/DZP++ level of theory.

Radicals	Absolute Energies (in hartrees)		Relative Energies (in kcal/mol)	
	Frozen Geometry	Optimized Geometry	Energy Relaxation upon Structural Optimization of the Radicals.	Energies of Optimized Geometries of the Radicals
G(N9)-C	-937.04675	-937.06740	12.95	0.00
G(N2b)-C	-937.04099	-937.05049	5.96	10.61
G(N1)-C	-937.01575	-937.04878	20.73	11.68
G-C(N1)	-937.03822	-937.04656	5.23	13.08
G(N2a)-C	-937.03066	-937.04331	7.94	15.49
G-C(N4b)	-937.02644	-937.03130	3.05	22.65
G-C(C6)	-937.02789	-937.03041	1.58	23.21
G(C8)-C	-937.02414	-937.02625	1.32	25.82
G-C(C5)	-937.02251	-937.02464	1.34	26.83
G-C(N4a)	-937.00219	-937.01560	8.41	32.15

Both the N-C bonds adjacent to the radical center are shortened due to the radical formation. The resulting radical minimum is predicted to lie 11.7 kcal/mol above the lowest energy radical G(N9)-C (Figure 3.6), produced by the hemolytic cleavage of the N9-H bond. The structure G(N1)-C is energetically the third most favorable radical found in this study, as reported in Table 3.2. An energy of 20.0 kcal/mol (Table 3.4) is necessary to dissociate the G(N1)-C radical into the G(N1) radical plus the cytosine molecule. The presence of two hydrogen bonds instead of three makes it easier to dissociate the guanine radical and cytosine fragments, compared to the energy (27.2 kcal/mol) required to dissociate the neutral guanine-cytosine base pair.

G(N2a)-C— This radical, shown in Figure 3, is generated from G-C by removing one of the hydrogen atoms bound to atom N2 of guanine. Removing the hydrogen from this nitrogen results in the loss of a hydrogen bond. The resulting radical relaxes by about 7.9 kcal/mol when optimized at the B3LYP/DZP++ level of theory. The resulting minimum (Figure 3) is predicted to lie 15.5 kcal/mol above the lowest energy G(N9)-C (Figure 3.5) radical at the same level of theory (see Table 3.2). The geometrical perturbations seen in Figure 3 are large compared to G-C because the three hydrogen bonds keep the backbone together in a plane. Once the H2a-O2 hydrogen bond is gone, the planarity is lost. The out-of-plane angle is about 38 degrees, as seen in Figure 3a. An out-of-plane angle so large will put significant strain on the closely stacked base pairs. The other two hydrogen bonds are slightly elongated (by 0.109 and 0.045 Å, respectively) compared to G-C. The dissociation energy of structure G(N2a)-C is reported in Table 3.4. The G(N2a)-C radical lies only 11.7 kcal/mol below the isolated G(N2a) radical plus cytosine molecule combined. A dissociation

energy this small is indicative of the high strain, resulting from the 38 degrees bond angle opening in this radical, in addition to the loss of the third hydrogen bond.

G(N2b)-C— Removing the guanine N2 hydrogen atom not used for making a hydrogen bond with cytosine gives the G(N2b)-C radical. Since this hydrogen atom is not involved in hydrogen bonding, removing it has little effect on the structure of the base pair. The hydrogen bond lengths are not expected to change in a major way. However, as depicted in Figure 3.4, all three hydrogen bonds are lengthened (compared to closed shell G-C) due to the radical generation. The energy change is only 6.0 kcal/mol upon optimization (relative to the closed shell G-C structure), and the optimized radical is only 10.6 kcal/mol higher in energy than the lowest energy radical, namely G(N9)-C. The binding energy (see Table 3.4) of the G(N2b)-C radical is -21.2 kcal/mol, which means that 21.2 kcal/mol energy is needed to dissociate the G(N2b)-C radical into the G(N2b) radical plus cytosine.

G(N9)-C — The lowest energy radical in this series is the radical generated by the abstraction of a hydrogen from atom N9 of guanine. The resulting G-C radical relaxes by 13.0 kcal/mol under geometry optimization and goes to a structure which is 10.6 kcal/mol lower in energy than the next higher energy radical G(N2b)-C. Table 3.3 reports the absolute and relative energies of the radicals. Radical G(N9)-C is generated from a position that is used for the sugar phosphate linkage in the single strand formation. Structural perturbations (relative to closed shell G-C) are modest in this case, as shown in Figure 3.5. Two of the three hydrogen bonds are shortened (by 0.033 and 0.066 Å, respectively, compared to G-C) in this case despite being away from the radical center. In both of these cases the N-H sigma bond distances (not the hydrogen bonds) responsible for hydrogen bonding lengthen,

although the elongation is not significant enough for a hydrogen shift towards cytosine. The dissociation energy (30.0 kcal/mol) of G(N9)-C is reported in Table 3.4.

Table 3.3. Table of hydrogen bond lengths (in Å) of the G-C radicals. Distances are reported both for the frozen geometry of the neutral G-C base pair (Figure 1) and for the optimized G-C radical geometries (Figure 3.2-3.11).

	Geometry Frozen (in Å)		Geometry Optimized (in Å)	
Radicals	Bonds	Bond Lengths	Bonds	Bond Lengths
G-C			O---HN	1.717
			NH---N	1.883
			NH---O	1.886
G(N1)-C	O---HN	1.717	N---HN	1.883
			NH---N	1.865
	NH---O	1.886		
G(N2a)-C	O---HN	1.717	O---HN	1.826
	NH---N	1.883	NH---N	1.928
G(N2b)-C	O---HN	1.717	O---HN	1.764
	NH---N	1.883	NH---N	1.915
	NH---O	1.886	NH---O	2.050
G(N9)-C	O---HN	1.717	O---HN	1.780
	NH---N	1.883	NH---N	1.850
	NH---O	1.886	NH---O	1.819
G(C8)-C	O---HN	1.717	O---HN	1.723
	NH---N	1.883	NH---N	1.877
	NH---O	1.886	NH---O	1.875
G-C(N4a)				
	NH---N	1.883	NH---N	1.829
	NH---O	1.886	NH---O	1.817
G-C(N4b)	O---HN	1.717	O---HN	1.867
	NH---N	1.883	NH---N	1.947
	NH---O	1.886	NH---O	1.935
G-C(C5)	O---HN	1.717	O---HN	1.708
	NH---N	1.883	NH---N	1.909
	NH---O	1.886	NH---O	1.889
G-C(C6)	O---HN	1.717	O---HN	1.706
	NH---N	1.883	NH---N	1.897
	NH---O	1.886	NH---O	1.916
G-C(N1)	O---HN	1.717	O---HN	1.724
	NH---N	1.883	NH---N	1.836
	NH---O	1.886	NH---O	1.817

G(C8)-C— The radical (Figure 6) generated by breaking the C-H bond at the C8 position of guanine is particularly important. The 8-oxo guanine molecule has been found to resemble adenine and identified as a lesion generator [50]. It is very important to investigate the properties of the radical G(C8)-C, as it may be an intermediate in the formation of 8-oxo guanine. The radical generated this way lies 25.8 kcal/mol above the lowest energy radical G(N9)-C. The structure relaxes by only 1.3 kcal/mol compared to the frozen G-C geometry; when the geometry of the radical is optimized, it is confirmed to be true minimum. Figure 3.6 describes the structural features of the radical at the B3LYP/DZP++ level of theory. As seen before, radical formation causes the hydrogen bonds to shorten, as is evident from Figure 3.6. Bond length shortening is most significant for the O···HN bond, where it changes by 0.043 Å. The dissociation energy for the G(C8)-C radical into G(C8) radical plus cytosine is 27.8 kcal/mol, comparable to that of G-C base pair (27.2 kcal/mol).

G-C(N4a)— Removing hydrogen atom H4a from the NH_2 group of cytosine results (Figure 3.7) in the elimination of a hydrogen bond. This brings about a change in the geometry of the base pair along with loss of planarity. This minimum hinders the other cytosine N4 hydrogen from collapsing to bridge the C=O group of guanine and producing the G-C(N4b) structure (Figure 3.8), which lies 9.5 kcal/mol lower in energy. It will be interesting to know the activation barrier for the interconversion of the G-C(N4a) and G-C(N4b) radicals. The G-C(N4a) radical is predicted to lie 32.2 kcal/mol above the lowest energy G(N9)-C radical at the B3LYP/DZP++ level of theory. The G-C constrained hydrogen abstracted radical releases 8.4 kcal/mol of energy as it is optimized to the G-C(N4a) structure shown in Figure 3.7. The structural perturbations associated with this relaxation are quite significant. Planarity is lost due to the absence of the hydrogen bond, and

the guanine and cytosine fragments move away from each other by about 20 degrees. The bond angle opens up (see Figure 3.7a), while the other two hydrogen bonds shorten in going from the frozen hydrogen abstracted geometry to the optimized minimum. The geometry change and the 8.4 kcal/mol energy relaxation are significant in this case, due to the close stacking of base pairs in a double stranded DNA helix. The loss of one hydrogen bond also helps to reduce the dissociation energy of this radical to 14.8 kcal/mol (Table 4). Puckering of the radical geometry (see Figure 3.7a) facilitates the dissociation of the G-C(N4a) radical into guanine plus the C(N4a) radical.

Table 3.4. Energies of the isolated guanine and cytosine radicals and the G-C radicals; dissociation energies of the optimized guanine-cytosine radicals.

Radicals	Energies in hartrees	Energies in hartrees		Energies in hartrees		Dissociation Energies (D_e) of the Radicals in kcal/mol.
		Isolated Guanine Species	Energies	Isolated Cytosine Species	Energies	
G-C	-937.71968	G	-542.66272	C	-395.01372	27.2 27.2[a], 23.0[b], 23.8[c], 26.3[d] 21.0[e]
G(N9)-C	-937.06740	G(N9)·	-542.00593	C	-395.01372	30.0
G(N2b)-C	-937.05049	G(N2b)·	-542.00306	C	-395.01372	21.1
G(N1)-C	-937.04878	G(N1)·	-542.00325	C	-395.01372	20.0
G-C(N1)	-937.04656	G	-542.66272	C(N1)·	-394.34180	26.4
G(N2a)-C	-937.04331	G(N2a)·	-542.01088	C	-395.01372	11.7
G-C(N4b)	-937.03130	G	-542.66272	C(N4b)·	-394.33784	19.3
G-C(C6)	-937.03041	G	-542.66272	C(C6)·	-394.32708	25.5
G(C8)-C	-937.02625	G(C8)·	-541.96817	C	-395.01372	27.8
G-C(C5)	-937.02464	G	-542.66272	C(C5)·	-394.32042	26.0
G-C(N4a)	-937.01560	G	-542.66272	C(N4a)·	-394.32926	14.8

a. Richardson, Wesolowski, and Schaefer [27].
b. Colson, Besler, and Sevilla [28].
c. Sponer, Leszczynski, and Hobza [29].
d. Sponer, Leszczynski, and Hobza [30].
e. Experiment - Yanson, Teplitski, and Sukhodub [31].

G-C(N4b) – The second hydrogen attached to the cytosine NH_2 group is not hydrogen bonded, so removing this atom does not change the structural features of the base pair qualitatively. This G-C(N4b) radical when optimized releases only 3.1 kcal/mol of energy and goes to a structure (Figure 3.8) which is 22.7 kcal/mol above the lowest energy G(N9)-C radical at the B3LYP/DZP++ level of theory. All three hydrogen bonds elongate compared to the G-C base pair, by 0.150, 0.064, and 0.049 Å, respectively. The dissociation energy of the G-C(N4b) radical is predicted to be 19.3 kcal/mol (Table 3.4).

G-C(C5)—Removal of the other (bonded to C5, C6, or N1) hydrogen atoms on the cytosine does not alter the geometry of the base pair greatly, except for small changes in the bond lengths due to resonance stabilization of the resulting radicals (e.g. G-C(N1)). Structure G-C(C5) is predicted to lie 26.8 kcal/mol above the lowest energy G(N9)-C radical. The energy relaxation with respect to the constrained G-C geometry is small (about 1.3 kcal/mol). The geometry of the G-C(C5) radical is shown in Figure 3.9. The G-C(C5) radical requires 26.0 kcal/mol energy to dissociate into guanine plus the C(C5) radical.

G-C(C6)—Figure 3.10 shows the geometry of the optimized G-C(C6) radical. It is generated by removing a hydrogen atom from atom C6 of cytosine. G-C(C6) lies 23.2 kcal/mol above the lowest energy G(N9)-C radical at the B3LYP/DZP++ level of theory. There is no major change in the geometry relative to G-C, as expected from the position of the radical. Radicals generated far from the hydrogen bonds have little effect on the G-C dissociation energy. The dissociation energy predicted for this radical is 25.5 kcal/mol, rather close to the analogous G-C prediction of 27.2 kcal/mol energy.

G-C(N1)—The last radical structure to be considered is G-C(N1), generated by removing the hydrogen atom from N1 of cytosine. This radical is the lowest in energy among

the radicals generated on cytosine in this series. The radical generated at atom N1 is stable due to resonance delocalization of the radical electron. In addition, the radical electron is qualitatively localized near an electronegative nitrogen atom. This radical is predicted to lie only 13.1 kcal/mol above the lowest energy radical investigated, namely G(N9)-C. Figure 3.11 shows the equilibrium geometry of the G-C(N1) radical. The NH--N and NH--O hydrogen bond lengths shorten somewhat (0.047 and 0.071 Å, respectively) as well as the N1-C6 bond (0.039Å) adjacent to the radical center. Once again the dissociation energy of G-C(N1) radical (-26.4 kcal/mol) is very close that for the guanine-cytosine base pair (27.2 kcal/mol), as reported in Table 3.4.

Hydrogen bond lengths for all the radicals considered in this work using the B3LYP gradient corrected density functional in conjunction with the DZP++ basis set are reported in Table 3.3.

3.5 BIOLOGICAL SIGNIFICANCE

Size complementarity in double stranded DNA ensures that the larger purines (adenine and guanine), pair with thymine and cytosine, the smaller pyrimidines, respectively [51, 52]. Hydrogen bonded base pairs of correct lengths form the rungs of the ladder that is constrained by the uprights, made of the pentose sugar linked by phosphate groups. Size complementarity is probably more important than the hydrogen bonds itself [53-55]. The magnitude of structural perturbations predicted here for some of the radicals described above indicates that they will inject significant amounts of strain into the ladder. Reorientation of the backbone on the G(N1)-C radical is particularly important given that the radical generated releases 21.2 kcal/mol of energy while collapsing (relative to G-C) to a stable

minimum. Other geometrical rearrangements are also significant due to the strain added by loss of planarity and puckering. Estimating the effects of this sort of geometry change in a long DNA ladder will be very interesting.

3.6 CONCLUDING REMARKS

The theoretically obtained bond distances for the closed-shell neutral G-C agree quite well with previous theoretical predictions. As is well known, the gas phase theoretical results at times do not coincide with the experimental crystallographic data. For a number of radicals studied in the present work the structural changes associated with hydrogen atom removal are major. These include base orientation angle changes, reconfiguration of the base pair, and elongation or shortening of the hydrogen bonds responsible for base pairing. The structural perturbations are most profound in the radicals generated at the hydrogen bonding sites, because these break the structural integrity of base pairing. Similarly, in fact, even more profound structural changes can be expected in the adenine-thymine base pair, because it has only two hydrogen bonds. Breaking one of these bonds may cause severe structural disruption.

Lesions generated in the guanine-cytosine base pair will in turn cause strain in the closely stacked base pairing sequence. This strain is most significant (20.7 kcal/mol) in the G(N1)-C radical (Figure 3.2) where the entire base pairing sequence changes due to shift of the guanine-cytosine backbone. In two other radicals (Figure 3.3 and Figure 3.7) the geometry changes in a major way due to openings of the angles between the guanine and cytosine backbones of between 20 and 31 degrees. This deformation pushes one end of the radical (G(N2a)-C) almost 2.2 Å away from the planar geometry. In the other case (G-

C(N4a)) the radical nitrogen atom protrudes out of the plane by approximately 1.7 Å. The rungs of the DNA double helix are separated by 3.4 Å from each other. So the radical formation not only leads to deformation in one rung, it also can create considerable steric and possibly electronic effects on the adjacent rungs of the DNA ladder, by coming too close to them. The relaxation energies due to radical formation and the relative energies of the radicals indicate the relative thermodynamic stabilities of the new optimized G-C radicals. It is to be emphasized that the range of radical relaxation energies is wide, from 1.3 to 20.7 kcal/mol.

Hydrogen bond breakage due to radical formation also has an adverse effect on the radicals due to their reduced dissociation energies. Such a small dissociation energy indicates how easily a base pair radical can be separated into an isolated guanine or cytosine molecule plus the corresponding radical. This dissociation across the hydrogen bonds hints at the breakage of two complementary strands. In two of the radicals (G(N2a)-C and G-C(N4a)) where a radical is formed on a hydrogen bonding site the dissociation energies are as low as 11.7 and 14.8 kcal/mol, less than half of the dissociation energy of neutral G-C base pair. This finding is further justified from the extent of deformation these two base pair radicals undergo. Overall, lesions in the guanine-cytosine system may cause the base pair to undergo fatal structural perturbations leading to possible strand break and loss of genetic information.

3.7 ACKNOWLEDGEMENTS

We appreciate the generous support of the U. S. National Science Foundation, Grant CHE-0136186. P. P. B. thanks Brian Papas for help with Q-Chem.

3.8 REFERENCES

1. Collins, G. P., *Sci. Am.* **2003,** *289*, 26.

2. Berdys, J.; Anusiewicz, I.; Skurski, P.; Simons, J., *J. Am. Chem. Soc.* **2004,** *126*, 6441.

3. Yarnell, A., *Chem. Eng. News* **2003,** *81*, 33.

4. Colson, A. O.; Sevilla, M. D., *Int. J. Radiat. Biol.* **1995,** *67*, 627.

5. Guerra, C. F.; Bickelhaupt, F. M.; Snijders, J. G.; Baerends, E. J., *J. Am. Chem. Soc.* **2000,** *122*, 4117.

6. Rosenberg, J. M.; Seeman, N. C.; Day, R. O.; Rich, A., *Biochem. & Biophys. Res. Comm.* **1976,** *69*, 979.

7. Seeman, N. C.; Rosenberg, J. M.; Suddath, F. L.; Parkkim, J. J.; Rich, A., *J. Mol. Bio.* **1976,** *104*, 109.

8. Rosenberg, J. M.; Seeman, N. C.; Day, R. O.; Rich, A., *J. Mol. Biol.* **1976,** *104*, 145.

9. Hobza, P.; Sponer, J., *Chem. Phys. Lett.* **1998,** *288*, 7.

10. Leszczynski, J., *J. Mol. Struct.* **1999,** *487*, ix.

11. Sponer, J.; Leszczynski, J.; Hobza, P., *J. Phys. Chem. A* **1997,** *101*, 9489.

12. Sponer, J.; Hobza, P., *Chem. Phys. Lett.* **1997,** *267*, 263.

13. Hobza, P.; Sponer, J., *J. Mol. Struct.* **1996,** *388*, 115.

14. Sponer, J.; Hobza, P., *Collect. Czechoslovak Chem. Comm.* **2003,** *68*, 2231.

15. Sponer, J.; Burda, J. V.; Leszczynski, J.; Hobza, P., *J.Biomol. Struct. & Dyn.* **1999,** *17*, 61.

16. Sponer, J.; Burda, J. V.; Mejzlik, P.; Leszczynski, J.; Hobza, P., *J.Biomol. Struct. & Dyn.* **1997,** *14*, 613.

17. Sponer, J.; Hobza, P., *Encyclopedia of Computational Chemistry* **1998**, (John Wiley and Sons.

18. Hobza, P.; Sponer, J.; Leszczynski, J., *J. Phys. Chem. B* **1997,** *101*, 8038.

19. Sponer, J.; Hobza, P.; Leszczynski, J., *Computational Chemistry. Reviews of Current Trends* **1996**, (World Scientific.

20. Steenken, S., *Chem. Rev.* **1989,** *89*, 503.

21. Cadet, J.; Douki, T.; Gasparutto, D.; Ravanat, J. L., *Mutation Research-Fundamental and Molecular Mechanisms of Mutagenesis* **2003,** *531*, 5.

22. Brocklehurst, B., *Radiat. Res.* **2001,** *155*, 637.

23. Tuppurainen, K.; Lotjonen, S.; Laatikainen, R.; Vartiainen, T.; Maran, U.; Strandberg, M.; Tamm, T., *Mutat. Res.* **1991,** *247*, 97.

24. Dee, D.; Baur, M. E., *J. Chem. Phys.* **1974,** *60*, 541.

25. Dee, D.; Baur, M. E., *Bulletin of the Am. Phys. Soc.* **1972,** *17*, 661.

26. Hutter, M.; Clark, T., *J. Am. Chem. Soc.* **1996,** *118*, 7574.

27. Richardson, N. A.; Wesolowski, S. S.; Schaefer, H. F., *J. Am. Chem. Soc.* **2002,** *124*, 10163.

28. Colson, A. O.; Besler, B.; Sevilla, M. D., *J. Phys. Chem.* **1992,** *96*, 9787.

29. Sponer, J.; Leszczynski, J.; Hobza, P., *J. Phys. Chem.* **1996,** *100*, 1965.

30. Sponer, J.; Leszczynski, J.; Hobza, P., *Biopolymers* **2002,** *61*, 3.

31. Yanson, I. K.; Teplitsky, A. B.; Sukhodub, L. F., *Biopolymers* **1979,** *18*, 1149.

32. Wesolowski, S. S.; Leininger, M. L.; Pentchev, P. N.; Schaefer, H. F., *J. Am. Chem. Soc.* **2001,** *123*, 4023.

33. Richardson, N. A.; Wesolowski, S. S.; Schaefer, H. F., *J. Phys. Chem. B* **2003,** *107*, 848.

34. Sponer, J.; Jurecka, P.; Hobza, P., *J. Am. Chem. Soc.* **2004,** *126*, 10142.

35. Steenken, S.; Jovanovic, S. V.; Candeias, L. P.; Reynisson, J., *Chem-Eur. J.* **2001,** *7*, 2829.

36. Cullis, P. M.; Malone, M. E.; Merson-Davies, L. A., *J. Am. Chem. Soc.* **1996,** *118*, 2775.

37. Melvin, T.; Botchway, S. W.; Parker, A. W.; ONeill, P., *J. Am. Chem. Soc.* **1996,** *118*, 10031.

38. Malins, D. C.; Polissar, N. L.; Ostrander, G. K.; Vinson, M. A., *Proc. Natl. Acad. Sci. USA* **2000,** *97*, 12442.

39. Becke, A. D., *J. Chem. Phys.* **1993,** *98*, 5648.

40. Lee, C. T.; Yang, W. T.; Parr, R. G., *Phys. Rev. B* **1988,** *37*, 785.

41. Lee, T. J.; Schaefer, H. F., *J. Chem. Phys.* **1985,** *83*, 1784.

42. Dunning, T. H., *J. Chem. Phys.* **1971,** *55*, 3958.

43. Dunning, T. H., *J. Chem. Phys.* **1970,** *53*, 2823.

44. Huzinaga, S., *J. Chem. Phys.* **1965,** *42*, 1293.

45. Rienstra-Kiracofe, J. C.; Tschumper, G. S.; Schaefer, H. F.; Nandi, S.; Ellison, G. B., *Chem. Rev.* **2002,** *102*, 231.

46. Kong, J.; White, C. A.; Krylov, A. I.; Sherrill, D.; Adamson, R. D.; Furlani, T. R.; Lee, M. S.; Lee, A. M.; Gwaltney, S. R.; Adams, T. R.; Ochsenfeld, C.; Gilbert, A. T. B.; Kedziora, G. S.; Rassolov, V. A.; Maurice, D. R.; Nair, N.; Shao, Y. H.; Besley, N. A.; Maslen, P. E.; Dombroski, J. P.; Daschel, H.; Zhang, W. M.; Korambath, P. P.; Baker, J.; Byrd, E. F. C.; Van Voorhis, T.; Oumi, M.; Hirata, S.; Hsu, C. P.; Ishikawa, N.; Florian, J.; Warshel, A.; Johnson, B. G.; Gill, P. M. W.; Head-Gordon, M.; Pople, J. A., *J. Comput. Chem.* **2000,** *21*, 1532.

47. Bertran, J.; Oliva, A.; Rodriguez-Santiago, L.; Sodupe, M., *J. Am. Chem. Soc.* **1998,** *120*, 8159.

48. Gould, I. R.; Kollman, P. A., *J. Am. Chem. Soc.* **1994,** *116*, 2493.

49. Brameld, K.; Dasgupta, S.; Goddard, W. A., *J. Phys. Chem. B* **1997,** *101*, 4851.

50. Malins, D. C.; Polissar, N. L.; Ostrander, G. K.; Vinson, M. A., *Proc.Natl. Acad. Sci. USA* **2000,** *97*, 12442.

51. Benner, S. A., *Sci.* **2004,** *306*, 625.

52. Benner, S. A., *Acc. Chem. Res.* **2004,** *37*, 784.

53. Lai, J. S.; Kool, E. T., *J. Am. Chem. Soc.* **2004,** *126*, 3040.

54. Moran, S., *Proc. Natl. Acad. Sci. USA* **1997,** *94*, 10506.

55. Goodman, M. F., *Nature Biotechnol.* **1999,** *17*, 640.

3.9 FIGURES

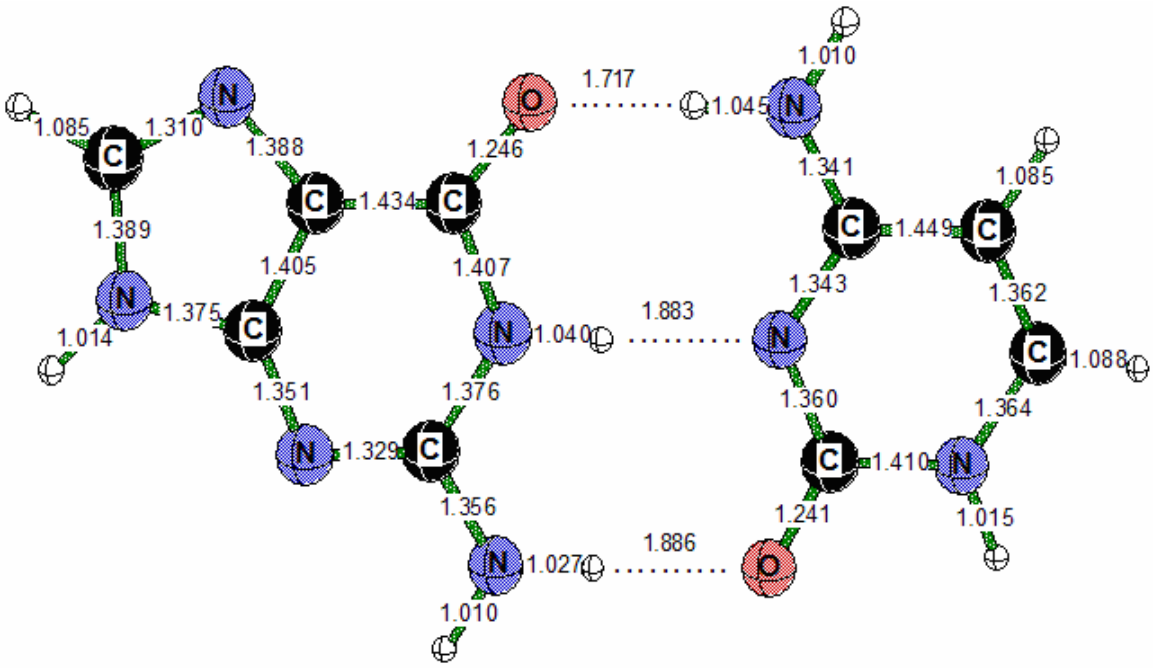

Figure 3.1. Optimized geometry of the neutral guanine-cytosine base pair at the B3LYP/DZP++ level of theory. All bond lengths are reported in angstroms.

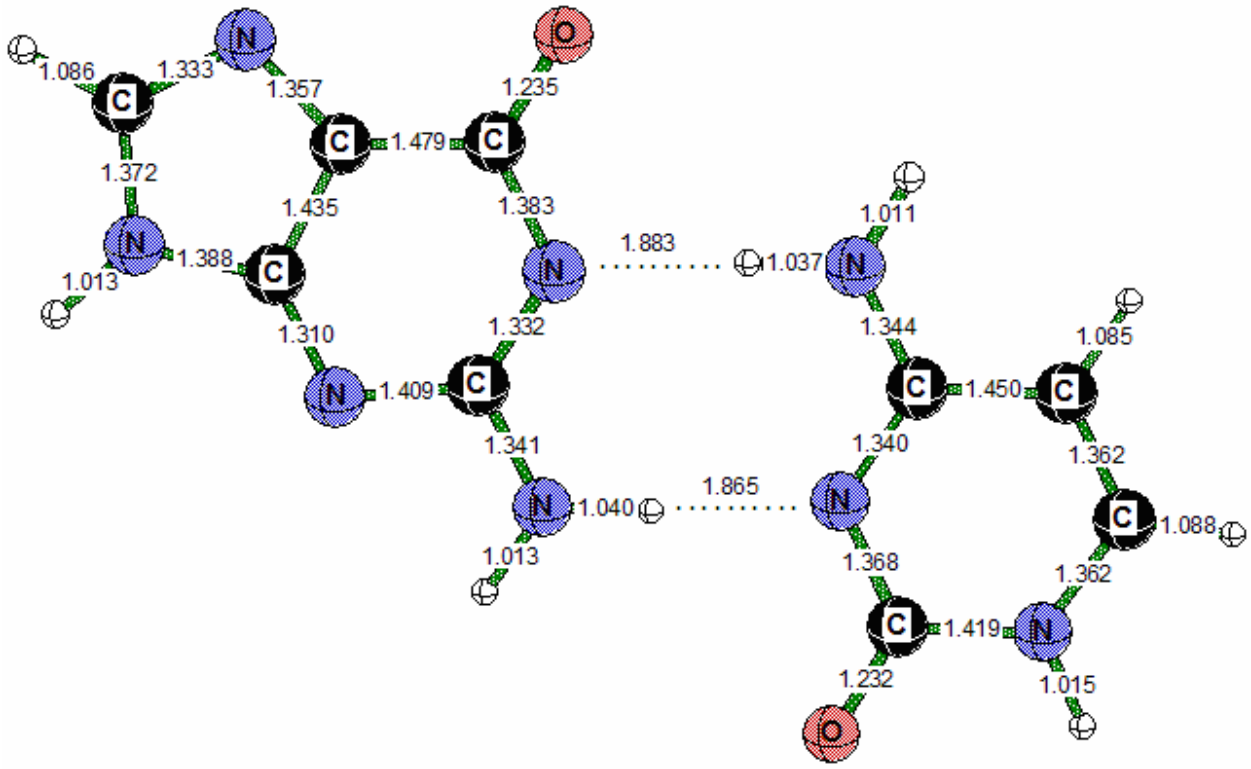

Figure 3.2**.** Optimized geometry of the G(N1)-C radical at the B3LYP/DZP++ level of theory. Note that relative to neutral G-C, the guanine H attached to the N1 has been removed; see Scheme 2 for atom numbering. All bond lengths are reported in angstroms.

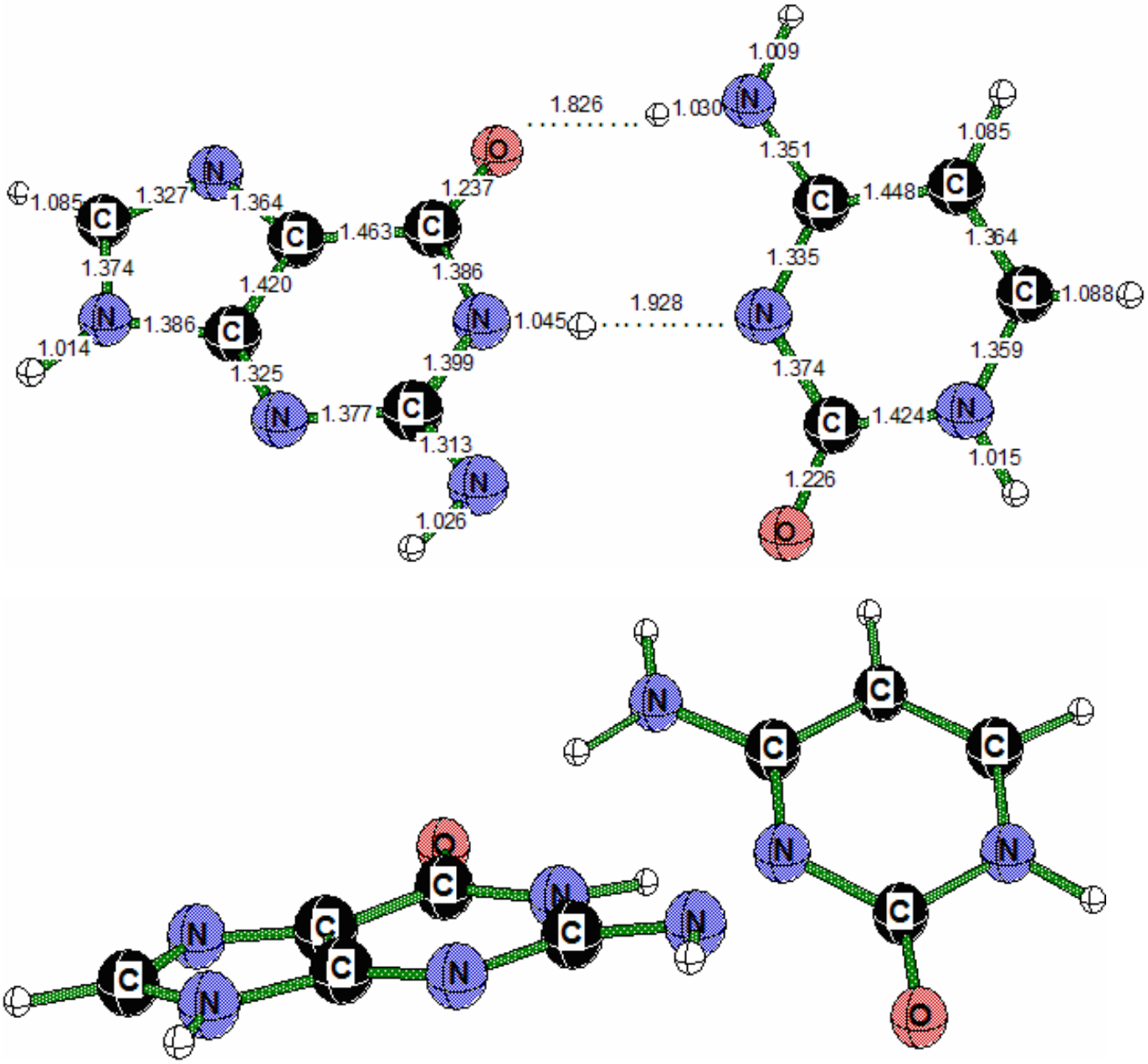

Figure 3.3. Optimized structure of the G(N2a)-C radical at B3LYP/DZP++ level of theory. All bond distances are reported in angstroms. Note that relative to neutral G-C base pair, the guanine atom H_{2a} attached to N2 has been removed.

Figure 3.3a. G(N2a-C) radical from a different perspective, showing the opening angle between the guanine and cytosine rings.

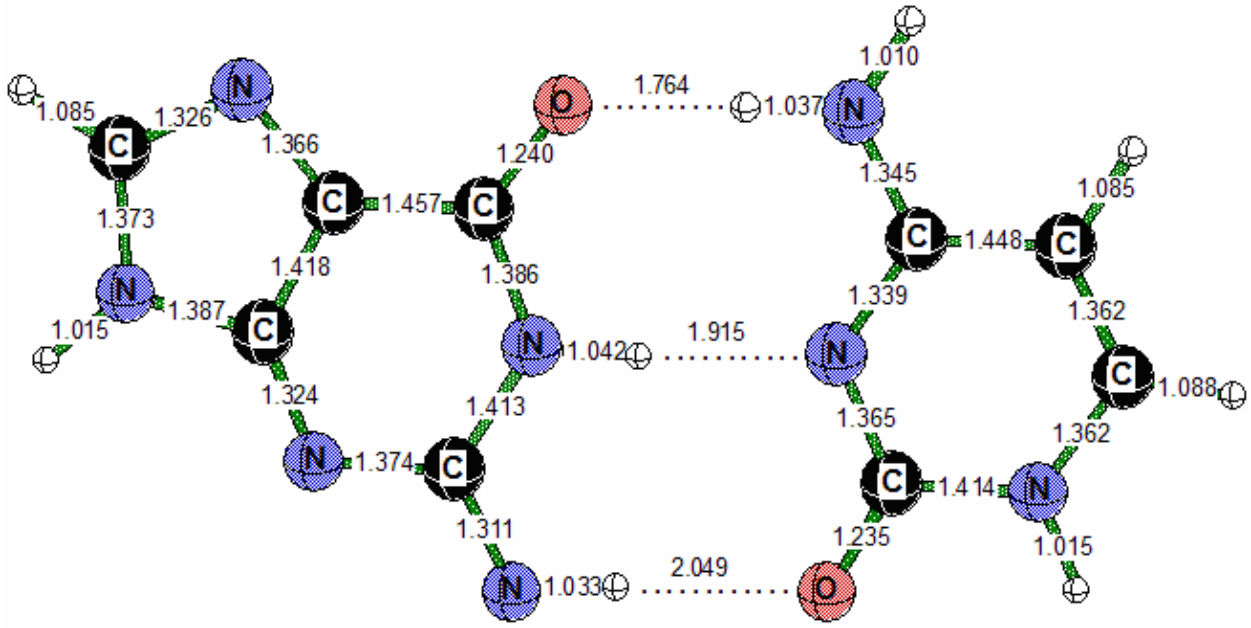

Figure 3.4**.** Optimized structure of the G(N2b)-C radical at the B3LYP/DZP++ level of theory. All bond distances are reported in angstroms. Note that relative to neutral G-C, guanine atom H_{2b} attached to the N2 atom has been removed.

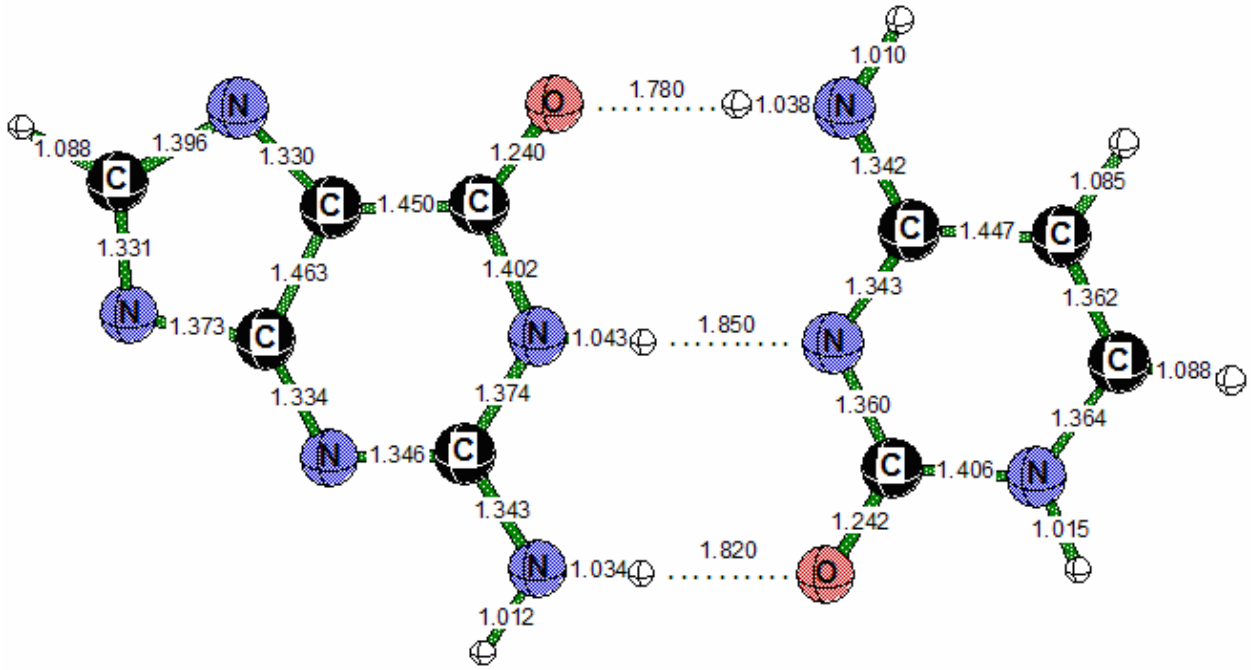

Figure 3.5. Optimized geometry of the G(N9)-C radical at the B3LYP/DZP++ level of theory. All bond lengths are reported in angstroms. Note that relative to G-C, the guanine H atom attached to N9 has been removed.

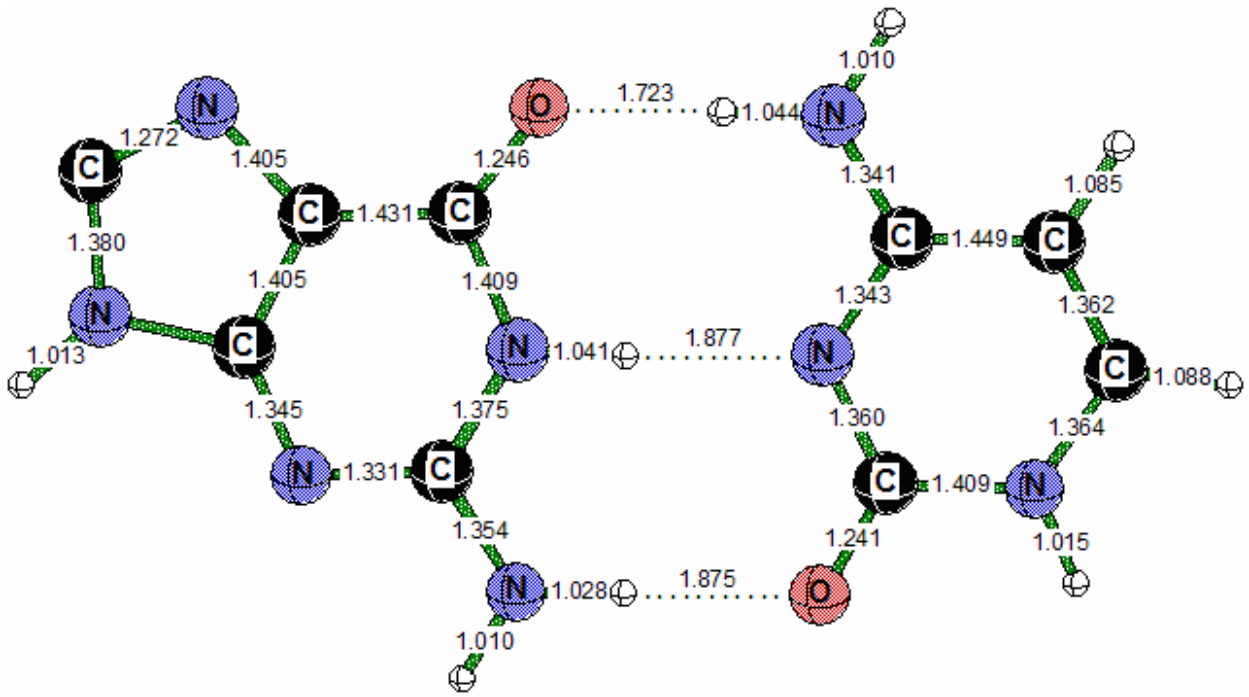

Figure 3.6. Optimized geometry of the G(C8)-C radical at the B3LYP/DZP++ level of theory. All bond lengths are reported in angstroms. Note that relative to neutral G-C, the guanine H atom attached to C8 has been removed.

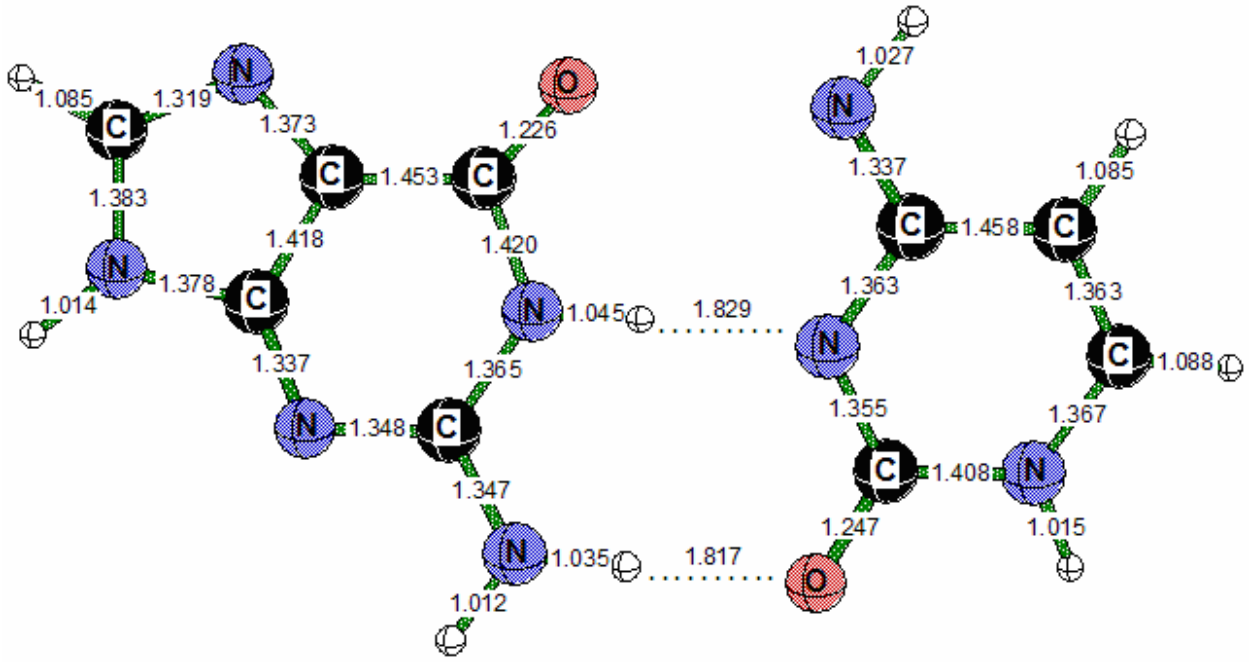

Figure 3.7. Optimized geometry of the G-C(N4a) radical at the B3LYP/DZP++ level of theory. All bond distances are reported in angstroms. Note that relative to G-C, the cytosine H atom attached to N4 has been removed.

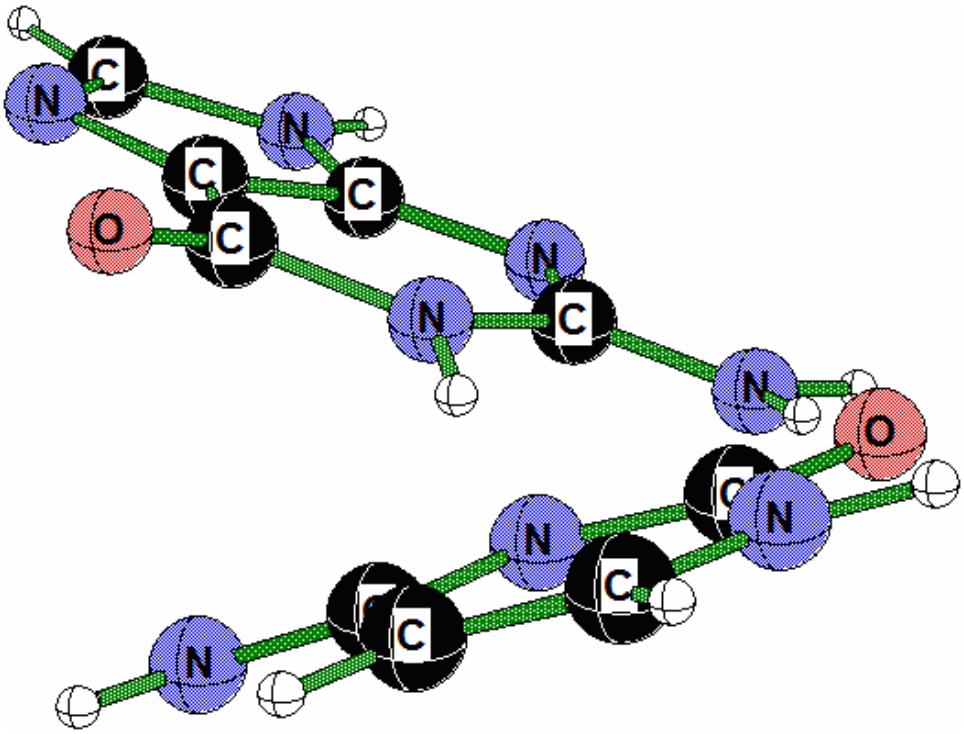

Figure 3.7a**.** A different perspective on the G-C(N4a) radical. Angle opening between the guanine and cytosine rings is about 31 degrees.

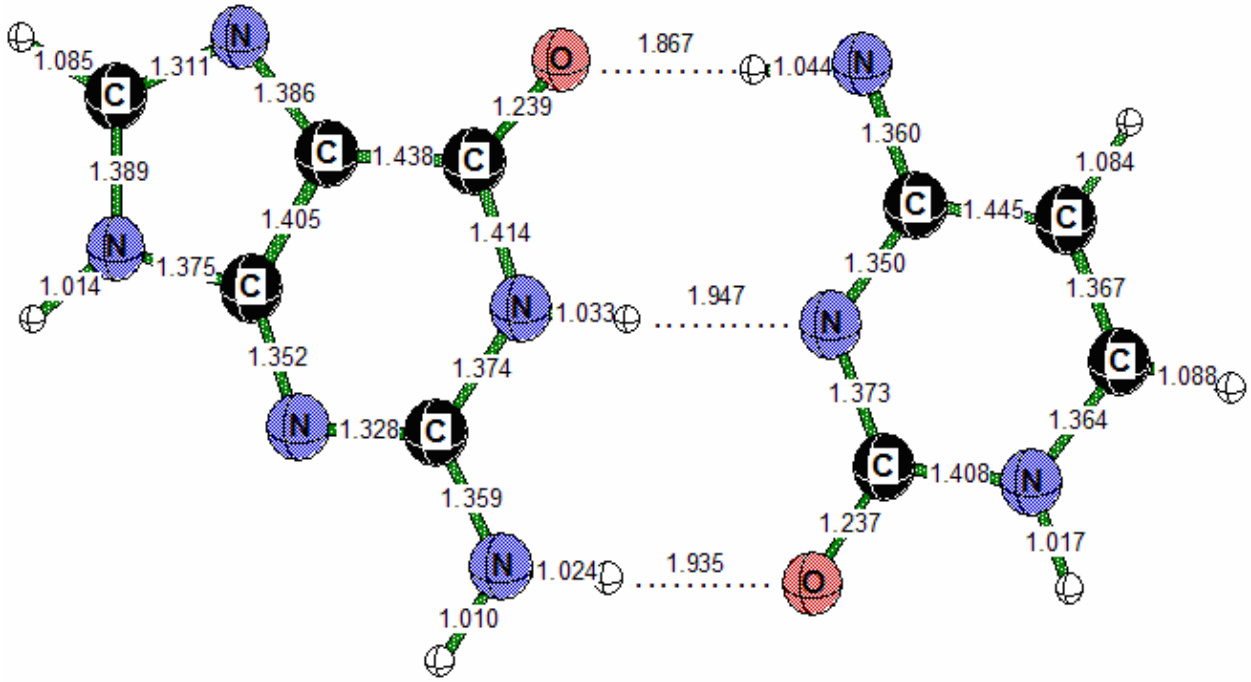

Figure 3.8. Optimized geometry of the G-C(N4b) radical at the B3LYP/DZP++ level of theory. All bond distances are reported in angstroms. Note that relative to G-C, the cytosine H atom attached to N4 has been removed. This is a conformer of G-C(N4a) with three rather than two hydrogen bonds.

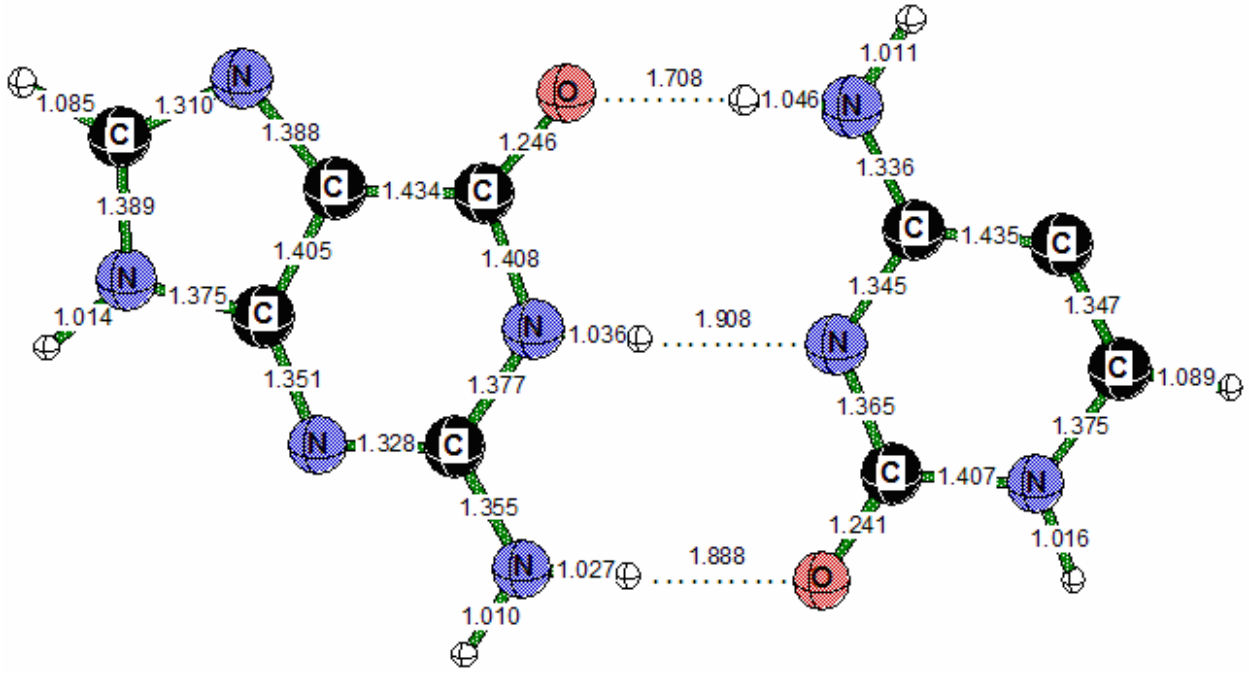

Figure 3.9. Optimized geometry of the G-C(C5) radical at the B3LYP/DZP++ level of theory. All predicted bond distances are shown in angstroms. Note that relative to G-C base pair, cytosine H atom attached to C5 has been removed.

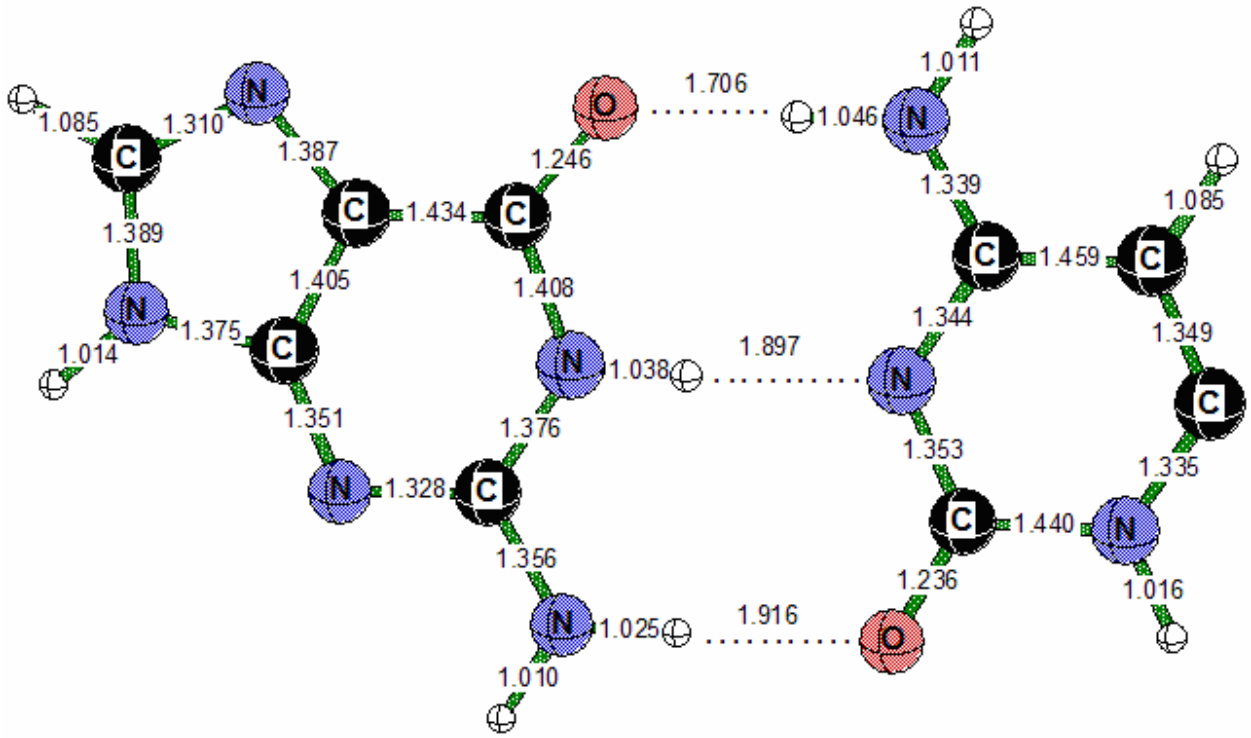

Figure 3.10. Optimized geometry of the G-C(C6) radical at the B3LYP/DZP++ level of theory. All bond distances are reported in angstroms. Note that relative to G-C, the cytosine H atom attached to C6 has been removed.

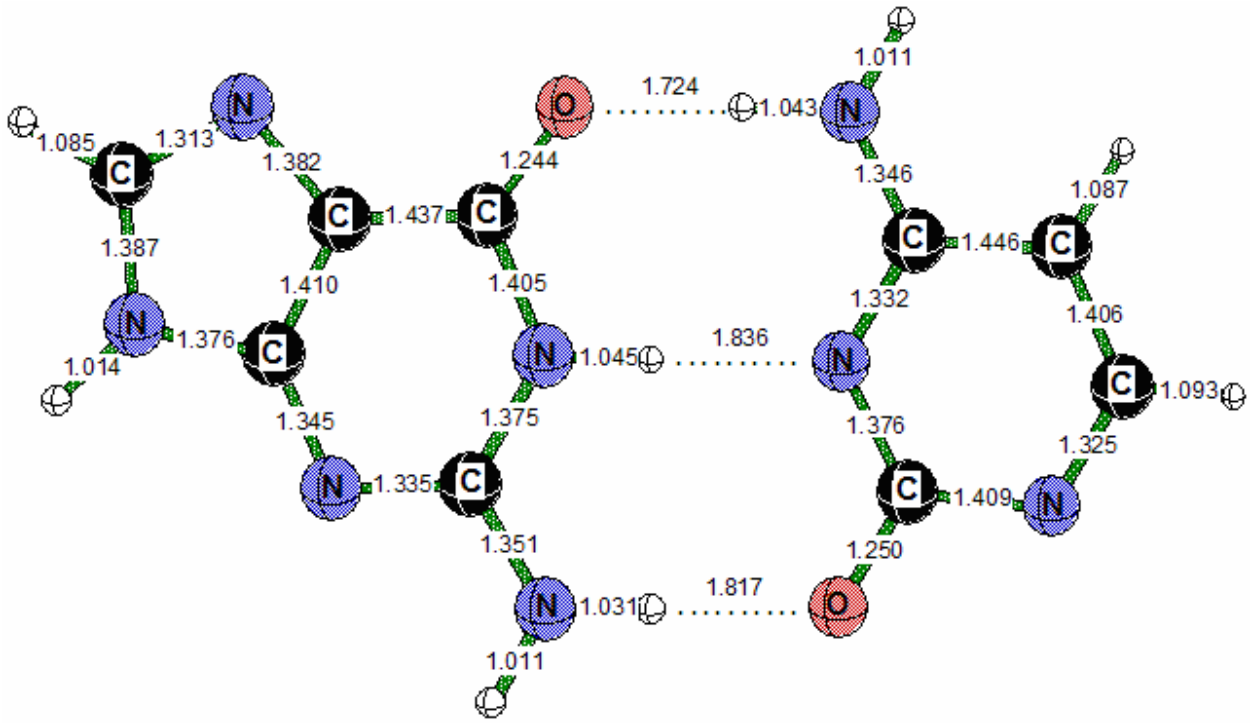

Figure 3.11**.** Optimized structure of the G-C(N1) radical at the B3LYP/DZP++ level of theory. All bond lengths are reported in angstroms. Note that relative to G-C, the cytosine H atom attached to N1 has been removed.

CHAPTER 4

LESIONS IN DNA SUBUNITS: THE NUCLEIC ACID BASES

Bera, Partha P., and Henry F. Schaefer III. 2006. Trends and Perspectives in Modern Computational Science. Volume 6, 245-264. Reprinted by the permission of Brill Academic Publishers.

4.1 ABSTRACT

The nucleic acid bases adenine, thymine, uracil, guanine, and cytosine are among the most important building blocks of life. Molecular modifications, or lesions, in the nucleic acid bases (NABs) can give rise to profound physiological changes. The simplest such set of lesions are considered in this research: radical anions, deprotonated NABs, hydrogen abstracted radicals, hydrogen appended radicals, and hydride appended anions. A whole range of isomeric structures is possible when hydrogen atoms are added to or subtracted from the NABs. This research provides a foundation for the theoretical examination of base pairs, nucleoside pairs, nucleotide pairs, and larger DNA subunits.

Keywords: DNA, lesion, lesions, NAB, nucleic acids, purine, pyrimidine, adenine, guanine, cytosine, thymine, base pair, bases, strand breaks, radiation damage, electron affinities, energies, hydrogen abstraction.

4.2 INTRODUCTION

The flow of genetic information is preserved by the basic building blocks of the nucleic acids DNA and RNA. These macro-molecules contain and transfer the genetic information and misinformation from generation to generation by means of chemical reactions. The stacked and coiled natures of DNA and RNA facilitate charge transfer through their backbones. The core constituents of double helical DNA and RNA are the purine and pyrimidine bases. The information stored in these highly precise structural patterns is enormous, and exceedingly dependent on the structural integrity of the sequence. Behind these complex but discernible structural patterns are the basic forces of nature. These forces

encompass atom-atom attractions, dispersion effects, hydrogen bonding considerations, and the base pair and stacking interactions. The structural integrity is lost by the breaking of bonds and by fragmentation processes. Understanding the underlying chemistry and basic interactions is absolutely vital to science.

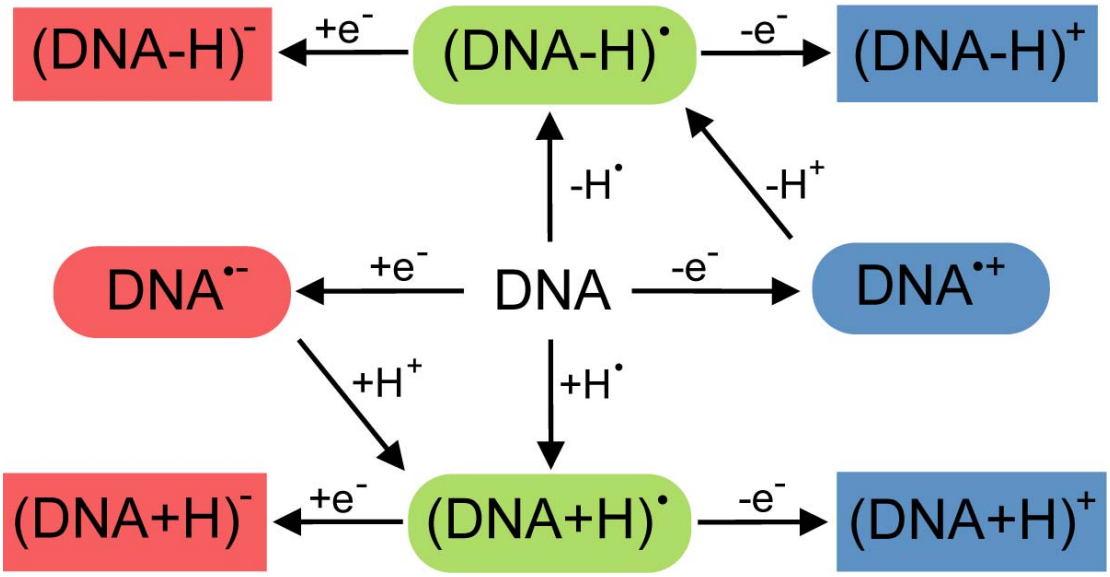

Scheme 4.1. DNA damage reaction scheme.

The present paper is aimed at describing research done using *ab initio* quantum chemistry, specifically density functional methods, on the bases and their fragments in completely isolated environments.[1-10] Investigating the different interactions contributes to the chemical physics of elementary bio-molecules in the gas phase. The philosophy of our research is that the deepest and most comprehensive understanding of biochemistry will result from the study of: i) the isolated bases, base pairs and damaged fragments (cumulatively – molecules); ii) isolated molecules in micro-solvated environments (e.g., discrete numbers of water molecules); and iii) molecules in the fully solvated environment. In this paper we have summarized the understandings obtained from theory for the isolated

bases and the fragments resulting from the abstraction and addition of hydrogen atom and hydride ions to the purine and pyrimidine bases of DNA.

The reaction channels leading to the production of the radicals and anions discussed in this work are represented in the cartoon above (Scheme 4.1).[2] In scheme 4.2 below we show the conceptual reactions of adenine in a pictorial manner to explain the formation of several adenine anions.[2]

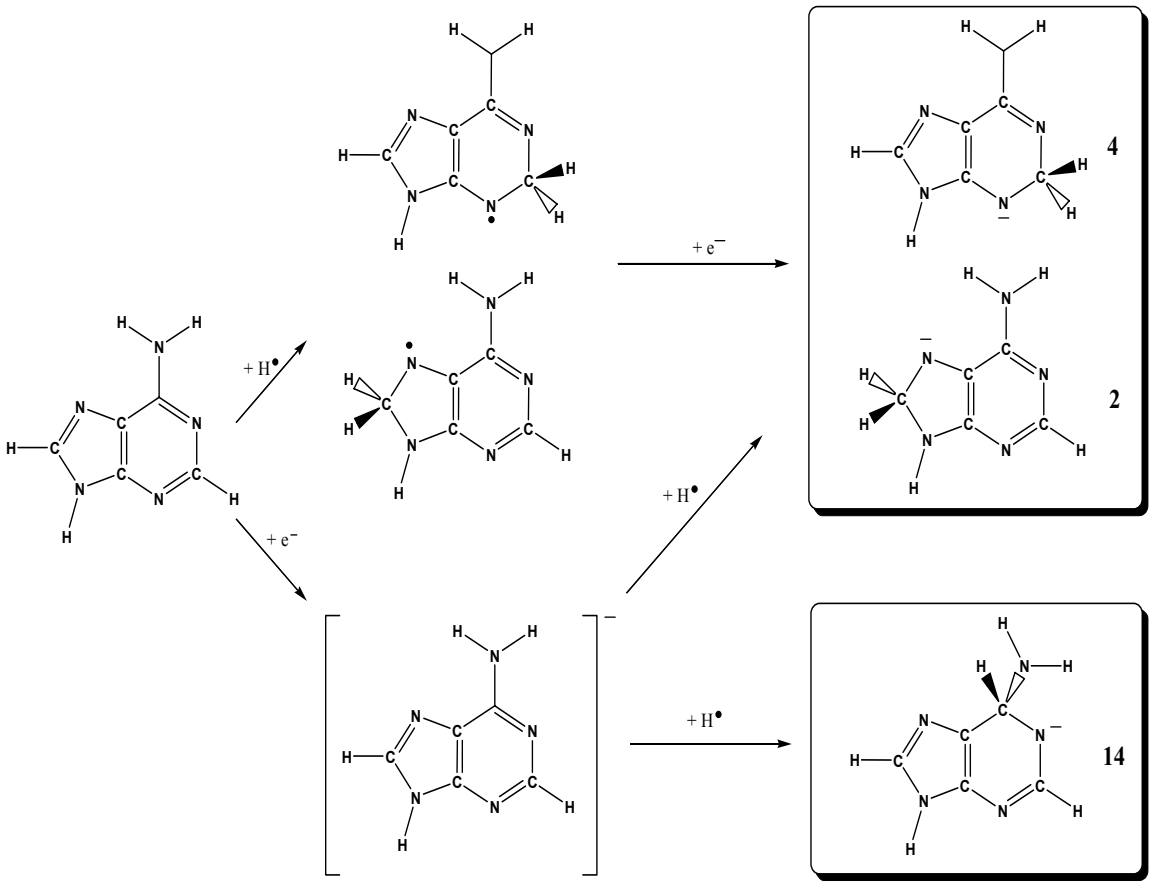

Scheme 4.2. The hydrogen addition and electron captures reactions of Guanine.

The causes of the production of radicals and anions in the DNA subunits, bases and base pairs are manifold; chemical damage, direct radiation damage and indirect damage.[11-15] Direct damage to bio-molecules like purines and pyrimidines are caused by radiation coming from electromagnetic sources including the sun. Direct bond breaking and ionization of the

inner and outer shell electrons are the immediate fallout of this direct radiation damage. The fact that secondary electrons having energies as low as 3 eV, generated by ionizing radiation, plays an important part in the mechanism of indirect radiation damage by electron attachment (see Scheme 4.2) has been discussed at length recently and opened up new dimensions to the exploration of DNA damage.[16] Low energy electron capture and the understanding of subsequent mechanisms for the formation of the fragmented molecules represent a growing field of research[11, 15] due to the alleged role in the formation of cancer cells. Ionizing radiation is one of most important causes of the primary and secondary damage to DNA.[17-19] Hydrogen ions and radicals produced by chemical reactions inside the cell also contribute to the chemical damage done on the molecular level.[16, 20-27] Consequently the fragmentation channels of DNA damage starting from the molecular level have been the focus of intense investigation in recent years, both experimentally and theoretically.[24, 26, 28-33] A variety of damage occurring to nucleic acids including oxidation, reduction, abstraction and addition of electrons, protons or hydrogen atoms are being studied, and pathways of fragment (lesion) formation are being explored by many researchers.[20, 34-50] There is ample experimental evidence pointing toward the formation of the radicals and anions due to irradiation of the bases.[20, 27, 35, 37, 50-53]

From an experimental point of view the group including Abdul-Carime has done extensive explorations of dissociative electron attachment (DEA) to the bases and base pairs.[16, 22, 54, 55] Their research has pointed out various dissociation channels including N-H and C-H bond breaking, following electron capture by the bases. The work of the research groups of Collins,[13] Sanche,[13, 56, 57] Close,[35, 50, 58] and Illenberger[16, 22, 24, 52] have experimentally explored fragmentation channels, by creating and identifying the

intermediates of radiation damage. Other researchers have experimentally established the energetic requirements for lesion formation in DNA subunits and subsequently for single and double strand breaks. [11-13, 51, 58-67]

To contribute to the physical understanding of mechanisms of DNA damage, the theoretical community has also extensively studied the possible intermediates in the fragmentation channels. Theoretical studies of the nucleic acids and the fragments generated from them provide valuable insights into the energetic (e.g., ionization potentials, electron affinities, dissociation energies, gas phase acidities, etc.) and structural (e.g,. dihedral angles and interatomic distances) properties of them. The research efforts of our group,[1, 2, 6-10, 68, 69] Sevilla,[43, 70-73] Wetmore,[41] Turecek,[34, 46] Chen,[51, 74, 75] Hobza,[76-79] and Lesczynski,[58, 79-85] among others, are particularly relevant in this respect.

4.3 AB INITIO AND DENSITY FUNCTIONAL METHODS FOR LARGE MOLECULES

Studies of the physicochemical properties of bio-molecules have been attempted both experimentally and theoretically over the years. The experiments done on these systems can be difficult. Computational approaches towards predicting the fundamental properties are thus becoming ever more popular. Traditionally, wave function based quantum mechanical methods, especially 'post Hartree-Fock' correlated methods, have proved themselves to be possible alternatives to good quality experimental results for small molecules. Although modern computers are getting faster yearly and wave function based *ab initio* quantum chemistry methods are able to solve diverse chemical problems, it is still not possible to compute the physical properties of very large molecules by these methods on a regular basis.

Density Functional Theory (DFT) methods prove to be very important in this context. DFT methods attempt to strike a balance between the theoretical reliability and computational requirements. One important aspect of both the correlated ab initio and DFT based methods is that they involve at most a minimal number of adjustable parameters, unlike typical semi-empirical and empirical procedures. At the same time DFT functionals give reliable structural parameters and other chemical properties of concern.[68, 85] Absolute and mean errors of the theoretical parameters will be discussed in the appropriate sections below.

The DFT functionals used in the research discussed herein are well tested and broadly proven to approach chemically relevant accuracy.[68] The three density functionals discussed here are the pure functional BLYP,[86, 87] the hybrid density functional B3LYP[87, 88] and the pure DFT functional BP86.[86, 89, 90] Interested readers are directed to the detailed report by Papas[91] on the accuracy of the DFT functionals using different grids and various computational packages. The double zeta plus polarization and diffuse function basis set, DZP++[92-94] suggested by Lee and Schaefer has proven to provide excellent geometries and some energetic properties within a few kcal/mol of the experimental values, as discussed in the review article of by Rienstra-Kiracofe et. al.[68]

All the results shown here were carried out using the Gaussian 94 suite of density functional programs.[95] Default integration grids were used for all energy and analytic gradient evaluations.

4.4 NUMBERING SCHEME

Throughout this review we have followed the IUPAC recommended numbering scheme for the all the bases as shown below.

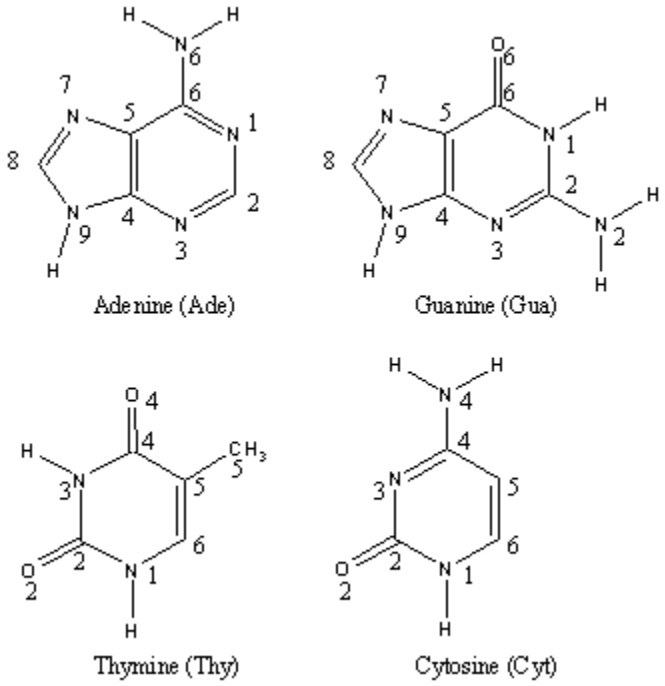

Figure 4.1 The numbering convention for nucleic acid bases.

The radicals, cations and anions arising from the above are represented using the number of the particular atom (in parentheses) from which an electron of H atom is abstracted or added. For example, the radical generated by the homolytic cleavage of the N9-H bond of Guanine (Gua) is represented as G(N9-H)$^{\cdot}$. The closed shell anion created by adding (pedagogically) an electron to N9 of the open shell radical G(N9-H)$^{\cdot}$ is labeled G(N9-H)$^{-}$, and the cation qualitatively generated by removing an electron from the same radical is represented as G(N9-H)$^{+}$.

All the important tautomers of the gas phase purine and pyrimidine bases are considered with respect to the addition of a hydrogen atom or a proton. The amino-oxo Watson-Crick and the amino-hydroxy tautomers of cytosine, and the subsequent hydrogen added species are shown in Figure 2. The three tautomers of cytosine considered in this work are named as follows;

Watson-Crick amino-oxo	C
Amino-hydroxy-trans	*t-amino-hyd*C
Amino-hydroxy-cis	*c-amino-hyd*C

The other purine and pyrimidine bases are named in similar fashion to maintain uniformity and simplicity.

4.5 RESULTS AND DISCUSSION

A. STRUCTURAL

Important gas phase isolated structural parameters were predicted using the density functionals mentioned above.

BOND DISTANCES

The accuracy of predicted structural parameters from the density functional methods used to study the bio-molecules is high. The average error in the predicted bond lengths is on the order of hundredth of an angstrom. The theoretical bond distances are often comparable to those from higher accuracy MP2 or coupled cluster (CC) methods. All the structures discussed in this review are fully optimized and represent true minima on the potential energy hypersurfaces for the species of concern. The structures discussed here fall on the ground electronic state potential energy surfaces of the particular molecules, radicals or anions considered.

Figures 4.5 and 4.6 in the paper by Profeta[6] describe the bond angle and bond distance differences between neutral thymine and the analogous radical and/or anionic species. In the gas phase the bond lengths vary by as

much as 0.04 angstroms for the radical T(N3-H)˙. Bond angle changes relative to neutral thymine molecule are also profound for this radical. This radical is the only one of all the thymine radicals that departs from the puckered neutral (C_1 symmetry) radical to a planar anion geometry.

Hydrogen abstraction from the isolated guanine molecule creates more structural deformations in the five-membered ring of the molecule than in its six-member ring. This indicates the substantial amount of electron delocalization in the five-member part of this purine. Nitrogen centered radicals show greater stability compared to the carbon centered structures, as explained by Luo.[5] The structural deformations in the lowest energy radical G(N2-H2)˙ (**6**) and the lowest energy anion, G(N9-H)¯ (**9**) are profound in the vicinity of the lesion. The largest changes in bond distances occur for the N-C bond and are more than 0.1 Å. A detailed study of all the radicals and anions is provided by Luo.[5]

The purine base adenine shows similar trends to the guanine molecule. Hydrogen abstraction from the exocyclic nitrogen leads to two rotational isomers A(N6-H1)˙ and A(N6-H2)˙. These two isomers are structurally very similar, and are within one kcal/mol of each other, unlike guanine, where the analogous energy separation is slightly higher. Electron addition to these radicals requires considerable electron redistribution, and hence produces significant change in the bond lengths. Comparison of the bond distances in some of the radicals shows the C_4-N_9 and N_9-C_8 bond distances to change by almost 0.1 Å. Some of the planar radicals depart from planarity when an

electron is added to generate the anion. A detailed structural analysis is also given in Table 1 in the paper of Evangelista.[1]

For cytosine also both radical formation and subsequent electron addition lead to structural deformations. While the radicals and anions retain their planar structures, hydrogen abstraction leads to a redistribution of electrons and resultant bond length changes, in some cases, by more than a tenth of an angstrom. Luo[4] discussed the detailed structural changes (see Figure 4.3) due to radical formation from cytosine. The rigid cyclic structures of the bases make the potential energy surface rather steep. The existence of a small number of conformational isomers for these molecules enables the separation of the radicals and anions by their geometrical positions.

Structural aspects of H^+, $H^\cdot$, and H^- addition to the DNA bases are addressed in the research by Zhang,[9, 10] Evangelista,[2] and Ipek.[96] For the sake of simplicity we will restrict ourselves to the discussion of the species originating from the hydrogen addition to the Watson-Crick tautomers. For a more thorough discussion, interested readers are directed to the original papers.

Hydrogen addition to the N_7, C_8 and C_2 positions leads to the most stable guanine radical species, as explained by Zhang.[9] Hydrogen addition inevitably comes at the expense of a double bond. The single and double bonds in the vicinity shorten or elongate quite significantly.

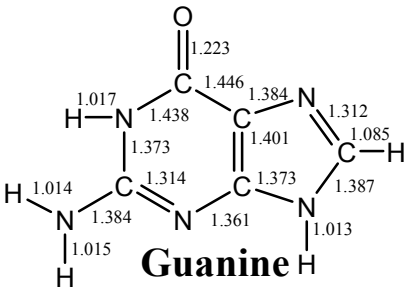

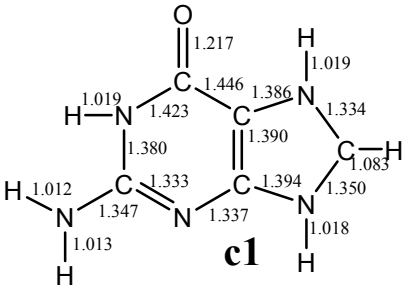

G(N7+H+)

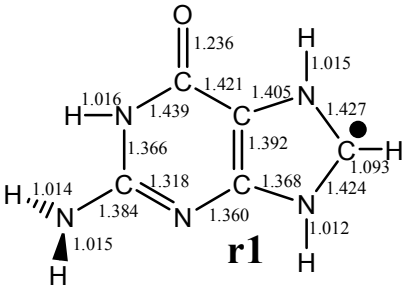

G(N7+H˙)

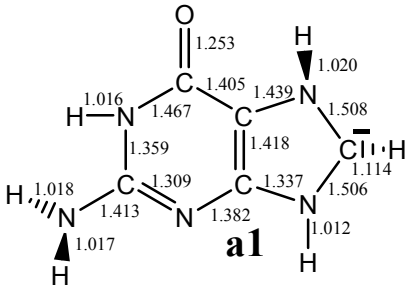

G(N7+H¯)

Figure 4.2.

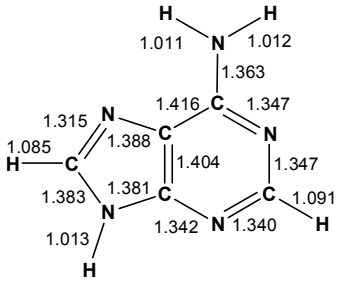

Adenine

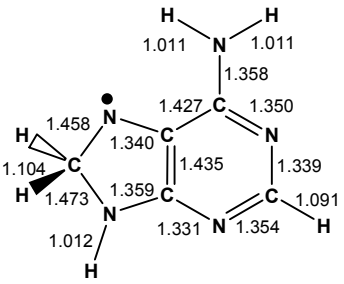

A(C8+H)˙

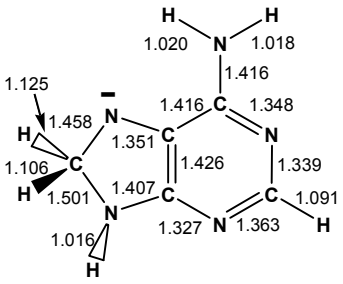

A(C8+H)¯

Figure 4.3.

On going from the radical to the anion, again the extra electron causes the bonds to lengthen so as to nullify the effect of radical formation. Figure 4.2 shows the effects of H^+, $H^\cdot$ and H^- addition to the N7 nitrogen of the isolated guanine molecule.

Figure 4.3. shows the neutral adenine molecule and the hydrogen added adenine molecules. The lowest energy radical and anions are $A(C8+H)^\cdot$ and $A(C8+H)^-$. The breaking of the double bond due to the addition of a hydrogen atom is clear from the elongation of the C-N bond. The other radicals and anions show analogous bond lengthening whenever a double bond is broken. The carbon atom to which the hydrogen atom is added displays a tetrahedral geometry, and the amino group of the adenine goes out of plane for some radicals and anions.

Hydrogen atom and hydride anion addition to the double bonds of the cytosine molecule bring in geometrical changes by transforming the appropriate double bond to a single bond distance and shrinking the adjacent bonds. The lowest energy radical (shown in Figure 4) accepts an electron to become an anion (equivalent to addition of a hydride anion to cytosine) with subsequent changes in the bond lengths. Some of these radicals and anions will still be able to associate with the guanine moiety in a G-C pair. A hydrogen atom added to the C5 or C6 positions of cytosine will still be able to pair up with guanine. Of course, the energetic ordering of these radicals ($C(C+H)^\cdot$-G) will be different from the energetic orders of the isolated $C(C+H)^\cdot$ radicals.[1, 4, 5]

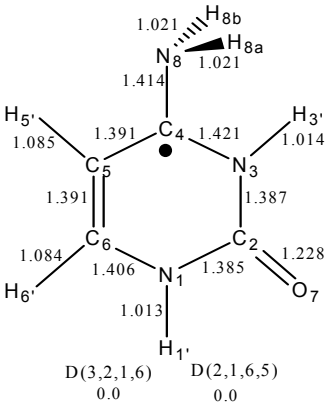

rO1

C(N3+H)$^{\cdot}$

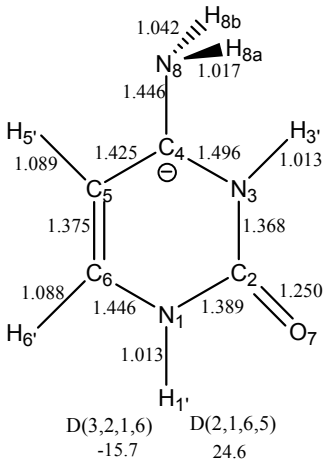

aO1

C(N3+H)$^{-}$

Figure 4.4.

BOND ANGLES

The bond angles and the dihedral angles are important geometrical parameters because they play a vital role in keeping the overall structural features of DNA intact. Large and/or abrupt changes (Figures 3-6, reference 10) in the angles and dihedrals can cause a fatal disruption of the chain. For example, the out of plane dihedral angles D(3,4,8, 8a) and D(3,4,8,8b) of the cytosine radical **10** and anion **11** (see Figure 2 of reference 4) change by 12 and 18 degrees, respectively, due to acceptance of an extra electron. Changes in bond angles and dihedral angles are common in other bases and radicals as well.

B. ENRGETICS

The expected accuracies of the absolute and relative energies associated with the different DFT functionals are discussed at length in the *Chemical Reviews* paper of Rienstra-Kiracofe. In this section we will discuss fundamental physical properties like the adiabatic electron affinities (AEA), vertical detachment energies (VDE), gas phase acidities (GPA) and association/dissociation energies of the bases and the radicals and anions treated by the various methods discussed in the introduction.

RELATIVE STABILTIES/ ENERGY ORDERING

The total energies of the isolated gas phase bases, radicals and anions were computed using the above discussed levels of theory. In Table 4.6, reported are the optimized total energies of the radicals and anions generated by the abstraction of an exo-cyclic hydrogen from the isolated bases at the B3LYP/DZP++ level of theory. The corresponding papers[1, 4, 5] report the total and zero point vibrationally corrected energies of the radicals and anions at other (BLYP and BP86) levels of theory.

All three functionals show the same energetic ordering of the radicals and the anions. For adenine, the energetic trend reported in Table 6 shows that the nitrogen centered radicals A(N9-H)$^{\cdot}$, A(N6-H1)$^{\cdot}$ and A(N6-H)$^{\cdot}$ are close in energy and more stable than the carbon centered radicals A(C1-H)$^{\cdot}$ and A(C2-H)$^{\cdot}$. The energetically most favorable radical is A(N9-H)$^{\cdot}$, created by removing a H atom from the N9 position of the isolated adenine molecule. The anions, like the radicals, prefer the nitrogen centers to the carbon centers for the qualitative location of the extra electron. The three nitrogen centered

anions are lower in energy than the carbon centered structures with the A(N9-H)$^-$ being the lowest of the group. In adenosine, the N9 position is attached to the ribose by a carbon-nitrogen glycosidic bond; thus the formation of radical A(N9-H)$^\cdot$ or anion A(N9-H)$^-$ would break the glycosidic bond. The carbon centered radicals switch their energetic position in passing from the radical to the anion. The corresponding anion A(C1-H)$^-$ is much lower in energy than the other carbon centered anion, namely A(C2-H)$^-$.

For the guanine molecule, five distinct radicals can be generated by removing a hydrogen atom. It is to be remembered that three of these hydrogen atoms are H-bonded to the cytosine molecule in the GC base pair. Removing a hydrogen from the N2 position of guanine results in two rotational isomers G(N2-H2)$^\cdot$ and G(N2-H1)$^\cdot$. These radicals can be formed from the one-electron-oxidized guanine by reversible proton loss from the external nitrogen (N2). The radical G(N1-H1)$^\cdot$ is predicted to lie lowest in energy of the guanine radicals generated by H abstraction, while the radical at the N9 position is the second lowest in energy. Deprotonation at the N9 position produces the lowest energy anion. Due to the greater electronegativity of nitrogen, the nitrogen centered radicals and anions are lower in energy than the carbon centered structures. The carbon center radical G(C8-H)$^\cdot$ and the corresponding anion are separated from the nearest nitrogen centered radicals and anions by 21 and 35 kcal/mol. The energy ordering, in going from the radicals to anions, remains the same except for the two lowest energy anions, which are switched (see Table 4.6). The other functionals

predict same energy ordering for the radicals and anions as that predicted by B3LYP/DZP++, as shown in Table 4.6. Three nitrogen-centered and two carbon centered anions are generated by removing the five exo-cyclic hydrogens of the cytosine molecule. In Table 4.6 are given the energies of the radicals and the anions produced by the abstraction of each such hydrogen at the B3LYP/DZP++ level of theory. The other density functionals (BLYP and BP86) predict the same energetic ordering of the radicals and the anions. The ZPVE corrected energies are discussed in the paper of Luo.[4] The radicals produced by hydrogen abstraction are close to each other in energy, within 15 kcal/mol. As seen for the isolated purines, the nitrogen centered radicals C(N1-H)$^{\cdot}$, C(N2-H1)$^{\cdot}$, and C(N8-H2)$^{\cdot}$ are lower in energy than the carbon centered structures C(C5-H)$^{\cdot}$ and C(C6-H)$^{\cdot}$ for the pyrimidine also. Addition of an electron to the radicals does not alter the relative stabilities of the anions. The lowest energy cytosine radicals and anions are created by abstracting a H atom or a proton from N1 which is the sugar binding site in a cytidine residue. The rotational isomers, created by removing the hydrogen or proton from the amino group, are very close in energy to the lowest lying radical or anion. This fact indicates that the radical generated at the C8 position is very likely to be formed under suitable experimental conditions. The energetic ordering is confirmed by other levels of theory, with minor differences in the energy spacings.

ELECTRON AFFINITIES

An electron affinity is best measured in a photodetachment experiment by knocking out the most weakly bound electron of the anion and generating the appropriate neutral species. The energy difference between the anion and the neutral gives the electron affinity (EA).

$$B + e = B^-$$

Adiabatic Electron Affinities: Each adiabatic electron affinities (AEA) is predicted from the energy difference between the neutral base or the hydrogen abstracted/added base and the corresponding anion, both at their theoretical equilibrium geometries. The anions are conceptually produced by adding an electron to the bases and re-optimizing the geometries of the species. The extra electron can go into a valence orbital or an anti-bonding orbital of the neutral species. However, the anion orbitals obtained this way are fully relaxed and hence are not identical to the corresponding orbitals of the neutral species. The predicted adiabatic electron affinities (AEA) from the DFT methods used here are typically within 0.15 eV of the experimental electron affinities. The accuracy of the different DFT functionals for the prediction of the electron affinities is described in detail in the review by Reinstra-Kiracofe.[68]

The adiabatic electron affinities of the neutral nucleobases show some functional dependence, as discussed in the work of Wesolowski.[32] (see Table 5 reference 33). The predicted AEA of three of the pyrimidine bases by the B3LYP, BLYP and BP86 are in good agreement with the available

experimental values. The absolute values of the adiabatic electron affinities of the pyrimidine bases cytosine, thymine and uracil are greater than those for the purine bases. The final relative electron binding ability of the neutral nucleobases are summarized as follows.

$$U > T > C \sim G > A$$

The purines have five hydrogen atoms that can be abstracted due to reaction or interaction with radiation. In both purines, adenine and guanine, the radical created at the N9 position has the largest adiabatic electron affinity. The N9 position happens to be the site of the sugar-base connection. The absolute values of these dehydrogenated radical electron affinities are much higher than those of the neutral purines. The doublet radicals generated due to the loss of hydrogen are ravenous for another electron. The qualitative nitrogen sites are more favorable for the "last" electron than the carbon sites due to the greater electronegativity of nitrogen. This nitrogen bias of the "last" electron has been explained by Evangelista.[1] All the hydrogen abstracted radicals of adenine and guanine have high adiabatic electron affinities (AEA), as shown in Table 4.2.

Thymine has six and cytosine has five dissociable hydrogen atoms. The radicals generated by hydrogen abstraction from cytosine and thymine are discussed in the two work of Luo[4, 5] and Profeta.[6] The radicals generated from either of the pyrimidines have high electron affinities (AEA), ranging from 1 eV to 3 eV. Like the purine radicals the cytosine radicals preferentially bind an extra electron on the N1 position, which is the sugar binding site in a

normal strand. However, radical T(N3-H)$^{\cdot}$ possesses the largest electron affinity of all the thymine radicals generated by hydrogen abstraction. The two carbonyl groups next to the N3 position bring in considerable electron delocalization to the anion, and lower its energy, yielding the largest AEA.

In this section we discuss the electron affinities of the species resulting from the addition to the single bases of a hydrogen atom (see cartoon, Scheme 1). In gas phase experimental studies of bio-molecules, both the Watson-Crick and non-Watson-Crick structures (tautomers) of the bases are important species, as pointed out by Bowen and coworkers.[97] All the species resulting from the addition of a hydrogen atom to the unsaturated part of the Watson-Crick amino-oxo and other tautomers of the purine and pyrimidine bases are considered. The following equations set out the electron capture processes.

$$B + H \rightarrow (B+H)^{\cdot} \; ; \quad (B+H)^{\cdot} + e \rightarrow (B+H)^{-}$$

$$B + H^{-} \rightarrow (B+H)^{-}$$

The AEA values of the hydrogen-appended purine and pyrimidine bases are summarized in Table 4.3. The results show the familiar trend; BP86 with the highest AEA among all three functionals followed by B3LYP and BLYP. The electron affinities are much higher than those of the neutral bases but smaller compared to the hydrogen abstracted bases. Hydrogen atom addition to the double bonds was considered, leading to the formation of radicals. Most of the radicals readily accept an electron, except the radicals generated on the N1 nitrogen of adenine and cytosine. As a group, the AEAs span a wide range, from 0.01 eV to 3.0 eV. Some of the predicted AEAs are

too small to be able to absolutely establish their signs, because the predicted values are smaller than the average errors of the methods employed. The AEAs for the radicals produced by adding H atom to one of the carbon atoms are higher than the AEA of the radicals produced by the addition of H to one of the N atoms.

The pure functional BLYP shows the smallest energy differences between the radical and the corresponding anion with a given basis set (DZP++), and hence predicts the smallest electron affinities. Among the three functionals used in these studies, BP86 predicts the highest electron affinities. The values for the most commonly used hybrid Hartree-Fock/density functional B3LYP method fall in between the pure (BLYP) and the hybrid (BP86) functionals.

Vertical Detachment Energies (VDE): Each vertical detachment energy is evaluated as the difference of energies between the anion and the neutral species, both at the optimized anion geometry. In a typical photodetachment experiment the vertical detachment energy of the anion is measured by knocking out one electron from the valence shell of the anion to produce the neutral species. The geometry may be assumed to be fixed in the short time period following electron removal. The anion geometry being different from that of the radical, the vertical dissociation energies are always upper bounds to the adiabatic electron affinities. This may be visualized from the cartoon (Figure 1; reference 68) presented in the review on the electron affinities of small molecules by Rienstra-Kiracofe.

From Tables 4.4 and 4.5 it may be seen that the VDEs of the anions are larger by a tenth of an eV to one eV than the AEAs of the corresponding radicals. In Table 4.5 are reported the VDEs of the radicals produced by the addition of H to the bases. With all the bases being closed shell species, hydrogen abstraction or addition and subsequent electron capture binds the electrons strongly. This is manifested in the relatively high VDE predictions at all levels of theory. The nitrogen centered anions are energetically more stable than the carbon centered anions. Hence, all the N-deprotonated anions have higher VDEs than the C-deprotonated structures (see Table 4.4). However, hydrogen (H) addition to a carbon center leaves an unpaired electron on the nitrogen (in the Lewis dot sense). So the anions for which the hydrogen is added to the carbon are more stable and have higher VDE values than the anions where the hydrogen atom is added to nitrogen.

Most of the anions, being valence bound, should be stable in the gas phase. The stabilizing effects of electron addition to either hydrogen abstracted or hydrogen added bases are manifested in their typically high electron affinities.

4.6 CONCLUDING REMARKS

Results from several theoretical studies done on isolated gas phase purine and pyrimidine bases using carefully calibrated electronic structure methods are presented here. Three density functionals B3LYP, BLYP and BP86 were used in conjunction with the

DZP++ basis set in all the computations. The results described above may be summarized as follows.

1. All the nitrogen centered radicals possess greater adiabatic electron affinities than the carbon centered radicals.
2. Both the dehydrogenated and hydrogenated radicals of the nucleic acid bases show typically high electron affinities. This indicates that the formation of these radicals will lead to electron transfer in or out of the bases, and eventually formation of the either the proton transferred or hydride transferred species in the gas phase.
3. Distortions of the geometries of the bases may jeopardize the integrity of the base pairing.

4.7 ACKNOWLWDGEMENTS

This research was funded by the U. S. National Science Foundation, Grant CHE-0451445. P. P. B. will like to thank Francesco Evangelista for his helpful advices and for providing some special graphics. P. P. B. will also like to thank Semran Ipek for providing access to her results prior to publication and David Zhang for some graphics. Dr. Luboš Horný and Dr. Chaitanya S. Wannere have helped a great deal by their constant encouragement throughout this work.

4.8 TABLES

Table 4.1. Adiabatic Electron Affinities (AEA in eV) of the Four Neutral DNA Bases.

Level of theory	Adenine	Guanine	Thymine	Cytosine
B3LYP	-0.28	-0.10	0.20	0.03
BLYP	-0.19	-0.01	0.12	-0.01
BP86	-0.05	0.11	0.28	0.13
Experiment [a]	-0.045			-0.055
Experiment [b]	0.95±0.05	1.51±0.05	0.79±0.05	0.56±0.05
Experiment [c]			0.120±0.120	0.130±0.120

[a] Gas phase data[30]

[b] Scaled reduction potential data.[75]

[c] Extrapolated AEAs from the photoelectron spectra of neucleobase·$(H_2O)_n$ clusters.[31]

Table 4.2. Adiabatic Electron Affinities (in eV) of the H-Abstracted Radicals of the DNA Bases.

Structure	B3LYP	BLYP	BP86
Adenine	-0.28	-0.19	-0.05
A(N9-H)$^{\cdot}$	3.26	3.05	3.28
A(N6-H1)$^{\cdot}$	2.55	2.43	2.65
A(N6-H2)$^{\cdot}$	2.58	2.46	2.68
A(C2-H)$^{\cdot}$	0.90	0.87	0.98
A(N1-H)$^{\cdot}$	2.38	2.27	2.42
Thymine	0.20	0.12	0.28
T(N1-H)$^{\cdot}$	3.22	3.18	3.26
T(N3-H)$^{\cdot}$	3.74	3.34	3.53
T(C6-H)$^{\cdot}$	2.60	2.41	2.56
T(C7-H2)$^{\cdot}$	1.04	1.04	1.22
T(C7-H2)$^{\cdot}$	1.04	1.04	1.22
T(C7-H3)$^{\cdot}$	1.04	1.04	1.22
Guanine	-0.10	-0.01	0.11
G(N1-H)$^{\cdot}$	2.95	2.75	2.95
G(N2-H1)$^{\cdot}$	2.75	2.57	2.77
G(N2-H2)$^{\cdot}$	2.77	2.58	2.79
G(N9-H)$^{\cdot}$	2.99	2.80	3.01
G(C8-H)$^{\cdot}$	2.18	2.10	2.24
Cytosine	-0.01	0.03	0.13
C(N1-H)$^{\cdot}$	3.00	2.84	3.05
C(N8-H1)$^{\cdot}$	2.97	2.83	3.03
C(N8-H2)$^{\cdot}$	2.94	2.81	3.02
C(C5-H)$^{\cdot}$	2.22	2.05	2.22
C(C6-H)$^{\cdot}$	2.41	2.17	2.32

Table 4.3. Adiabatic Electron Affinities (AEA in eV) of the Base plus H Radicals.

Structure	B3LYP	Structure	B3LYP
Adenine	-0.28	**Guanine**	-0.10
A(C8+H)	1.22	G(N7+H)	0.01
A(C2+H)	1.38	G(C8+H)	0.12
A(N7+H)	0.27	G(C6+H)	0.58
A(N1+H)	-0.05	G(N3+H)	0.65
A(N3+H)	0.02	G(C5+H)	0.84
A(C5+H)	0.68	G(C4+H)	1.48
A(C6+H)	1.99	G(C6+H)	2.10
A(C4+H)	1.57	G(C2+H)	2.24
		G(N2+H)	3.00
Thymine	0.20	**Cytosine**	-0.01
diketo-T(C6+H)$^{\cdot}$	0.43	amino-oxoC(N3+H)	0.13
2-keto-T(N3+H)$^{\cdot}$	0.30	amino-oxoC(C6+H)	1.97
2-keto-T(C6+H)$^{\cdot}$	2.25	amino-oxoC(C5+H)	0.62
2-keto-T(C2+H)$^{\cdot}$	-0.28	amino-oxoC(C4+H)	2.59
4-keto-T(C6+H)$^{\cdot}$	1.65	amino-oxoC(C2+H)	2.34
Dienol-T(C6+H)$^{\cdot}$	0.95	amino-oxoC(C2+H)	2.38
diketo-T(C2+H)$^{\cdot}$	1.01	t-amino-	-0.20

		hydC(N3+H)	
4keto-T(C4+H)˙	0.53	t-amino-hydC(C6+H)	1.63
diketo-T(C4+H)˙	2.5	t-amino-hydC(C5+H)	0.44
Dienol-T(N3+H)˙	0.13	t-amino-hydC(C4+H)	2.24
4keto-T(N1+H)˙	0.74	t-amino-hydC(C2+H)	2.10
Dienol-T(C4+H)˙	2.06	t-amino-hydC(C2+H)	2.04
		c-amino-hydC(N1+H)	-0.16
		c-amino-hydC(C6+H)	1.67
		c-amino-hydC(C5+H)	0.45
		c-amino-hydC(C4+H)	2.22
		c-amino-hydC(C2+H)	2.09
		c-amino-hydC(C2+H)	2.05

Table 4.4. Vertical Detachment Energies (VDE in eV) of Deprotonated DNA Bases.

Structure	B3LYP	BLYP	BP86	Structure	B3LYP	BLYP	BP86
Adenine				**Guanine**			
A(N9-H)$^{\cdot}$	3.61	3.35	3.58	G(N1-H)$^{\cdot}$	3.17	2.94	3.15
A(N6-H1)$^{\cdot}$	2.64	2.50	2.72	G(N2-H1)$^{\cdot}$	2.86	2.66	2.87
A(N6-H2)$^{\cdot}$	2.67	2.53	2.75	G(N2-H2)$^{\cdot}$	2.87	2.66	2.87
A(C2-H)$^{\cdot}$	1.73	1.66	1.78	G(N9-H)$^{\cdot}$	3.34	3.13	3.33
A(C1-H)$^{\cdot}$	2.89	2.73	2.90	G(C8-H)$^{\cdot}$	2.68	2.55	2.71
Thymine				**Cytosine**			
T(N1-H)$^{\cdot}$	3.17	3.17	3.38	C(N1-H)$^{\cdot}$	3.12	2.96	3.17
T(N3-H)$^{\cdot}$	4.59	4.59	4.23	C(N8-H1)$^{\cdot}$	3.17	2.97	3.18
T(C6-H)$^{\cdot}$	2.87	2.87	3.03	C(N8-H2)$^{\cdot}$	3.14	2.96	3.17
T(C7-H2)$^{\cdot}$	1.16	1.18	1.34	C(C5-H)$^{\cdot}$	2.67	2.45	2.64
T(C7-H2)$^{\cdot}$	1.16	1.18	1.34	C(C6-H)$^{\cdot}$	2.94	2.60	2.77
T(C7-H3)$^{\cdot}$	1.16	1.18	1.34				

Table 4.5. Vertical Detachment Energies (VDE in eV) of Hydride (H^-) Appended DNA Bases.

Structure	B3LYP	Structure	B3LYP
Adenine		**Guanine**	
$A(C8+H)^-$	1.44	$G(N7+H)^-$	1.06
$A(C2+H)^-$	1.76	$G(C8+H)^-$	1.21
$A(N7+H)^-$	1.21	$G(C6+H)^-$	1.20
$A(N1+H)^-$	0.53	$G(N3+H)^-$	1.25
$A(N3+H)^-$	0.75	$G(C5+H)^-$	1.23
$A(C5+H)^-$	0.90	$G(C4+H)^-$	1.83
$A(C6+H)^-$	2.14	$G(C6+H)^-$	2.72
$A(C4+H)^-$	1.88	$G(C2+H)^-$	2.30
		$G(N2+H)^-$	3.18
Thymine		**Cytosine**	
diketo-$T(C6+H)^-$	4.48	amino-oxoC$(N3+H)^-$	0.75
2-keto-$T(N3+H)^-$	5.03	amino-oxoC$(C6+H)^-$	2.30
2-keto-$T(C6+H)^-$	5.13	amino-oxoC$(C5+H)^-$	1.37
2-keto-$T(C2+H)^-$	0.21	amino-oxoC$(C4+H)^-$	2.94
4-keto-$T(C6+H)^-$	3.65	amino-oxoC$(C2+H)^-$	2.82
Dienol-$T(C6+H)^-$	1.31	amino-oxoC$(C2+H)^-$	2.86
diketo-$T(C2+H)^-$	0.52	t-amino-hydC$(N3+H)^-$	0.81
4keto-$T(C4+H)^-$	4.47	t-amino-hydC$(C6+H)^-$	1.90
diketo-$T(C4+H)^-$	4.56	t-amino-hydC$(C5+H)^-$	0.88
Dienol-$T(N3+H)^-$	-0.29	t-amino-hydC$(C4+H)^-$	2.43
4keto-$T(N1+H)^-$	2.67	t-amino-hydC$(C2+H)^-$	2.39
Dienol-$T(C4+H)^-$	3.16	t-amino-hydC$(C2+H)^-$	2.38
		c-amino-hydC$(N1+H)^-$	1.06
		c-amino-hydC$(C6+H)^-$	1.93
		c-amino-hydC$(C5+H)^-$	0.90
		c-amino-hydC$(C4+H)^-$	2.43
		c-amino-hydC$(C2+H)^-$	2.38
		c-amino-hydC$(C2+H)^-$	2.36

Table 4.6. Total Energies of the Hydrogen Abstracted Radicals and the Corresponding Anions Derived from the Bases at B3LYP/DZP++.

Radicals	B3LYP	Anion	B3LYP	Radical	B3LYP	Anion	B3LYP
Adenine				**Guanine**			
A(N9-H)$^{\cdot}$	-466.73827	A(N9-H)$^{\cdot}$	-466.85796	G(N2-H2)$^{\cdot}$	-542.01025	G(N9-H)$^{\cdot}$	-542.11524
A(N6-H1)$^{\cdot}$	-466.73409	A(N6-H1)$^{\cdot}$	-466.82778	G(N9-H)$^{\cdot}$	-542.00549	G(N2-H2)$^{\cdot}$	-542.11205
A(N6-H2)$^{\cdot}$	-466.73238	A(N6-H2)$^{\cdot}$	-466.82706	G(N1-H)$^{\cdot}$	-542.00277	G(N1-H)$^{\cdot}$	-542.11110
A(C2-H)$^{\cdot}$	-466.72310	A(N1-H)$^{\cdot}$	-466.79846	G(N2-H1)$^{\cdot}$	-542.00240	G(N2-H1)$^{\cdot}$	-542.10335
A(C1-H)$^{\cdot}$	-466.71107	A(C2-H)$^{\cdot}$	-466.75625	G(C8-H)$^{\cdot}$	-541.96769	G(C8-H)$^{\cdot}$	-542.04776
Thymine				**Cytosine**			
T(N1-H)$^{\cdot}$	-453.56938	T(N1-H)$^{-}$	-453.58310	C(N1-H)$^{\cdot}$	-394.34116	C(N1-H)$^{\cdot}$	-394.45144
T(N3-H)$^{\cdot}$	-453.53045	T(N3-H)$^{-}$	-453.56432	C(N8-H1)$^{\cdot}$	-394.33742	C(N8-H1)$^{\cdot}$	-394.44652
T(C6-H)$^{\cdot}$	-453.54340	T(C6-H)$^{-}$	-453.54539	C(N8-H2)$^{\cdot}$	-394.32879	C(N8-H2)$^{\cdot}$	-394.43700
T(C7-H1)$^{\cdot}$	-453.58282	T(C7-H1)$^{-}$	-453.58704	C(C5-H)$^{\cdot}$	-394.32658	C(C5-H)$^{\cdot}$	-394.41507
T(C7-H2)$^{\cdot}$	-453.58281	T(C7-H2)$^{-}$	-453.58704	C(C6-H)$^{\cdot}$	-394.31997	C(C6-H)$^{\cdot}$	-394.40154
T(C7-H3)$^{\cdot}$	-453.58282	T(C7-H3)$^{-}$	-453.58704				

Table 4.7. Total Energies (in Hartrees) of the Radicals and Anions Generated from the Addition of H to Nucleic Acid Bases. The Abbreviation C(N3+H) Represents Amino-oxoC(N3+H) in the Watson-Crick Form.

Radicals	B3LYP	Anion	B3LYP	Radical	B3LYP	Anion	B3LYP
Adenine				**Guanine**			
A(C8+H)$^{\cdot}$	-467.96688	A(C8+H)$^{-}$	-468.01164	G(N7+H)$^{\cdot}$	-543.20691	G(N7+H)$^{-}$	-543.20667
A(C2+H)$^{\cdot}$	-467.95358	A(C6+H)$^{-}$	-468.00651	G(C8+H)$^{\cdot}$	-543.22268	G(C8+H)$^{-}$	-543.25349
A(N7+H)$^{\cdot}$	-467.94586	A(N7+H)$^{-}$	-468.00443	G(C6+H)$^{\cdot}$	-543.19648	G(C6+H)$^{-}$	-543.20080
A(N1+H)$^{\cdot}$	-467.94337	A(N1+H)$^{-}$	-467.99039	G(N3+H)$^{\cdot}$	-543.19012	G(N3+H)$^{-}$	-543.21153
A(N3+H)$^{\cdot}$	-467.94217	A(N3+H)$^{-}$	-467.96428	G(C5+H)$^{\cdot}$	-543.19773	G(C5+H)$^{-}$	-543.22176
A(C5+H)$^{\cdot}$	-467.93942	A(C5+H)$^{-}$	-467.95589	G(C4+H)$^{\cdot}$	-543.20105	G(C4+H)$^{-}$	-543.25546
A(C6+H)$^{\cdot}$	-467.93346	A(C6+H)$^{-}$	-467.94281	G(C6+H)$^{\cdot}$	-543.17382	G(C6+H)$^{-}$	-543.25617
A(C4+H)$^{\cdot}$	-467.93269	A(C4+H)$^{-}$	-467.94162	G(C2+H)$^{\cdot}$	-543.20930	G(C2+H)$^{-}$	-543.28633
				G(N2+H)$^{\cdot}$	-543.15876	G(N2+H)$^{-}$	-543.26919
Thymine				**Cytosine**			
diketo-T(C6+H)$^{\cdot}$	-454.66484	Diketo-T(C6+H)$^{-}$	-454.68073	C(N3+H)$^{\cdot}$	-395.57852	C(N3+H)$^{-}$	-395.58319
2-keto-T(N3+H)$^{\cdot}$	-454.51485	2-keto-T(N3+H)$^{-}$	-454.52591	C(C6+H)$^{\cdot}$	-359.56521	C(C6+H)$^{-}$	-395.63759
2-keto-T(C6+H)$^{\cdot}$	-454.64683	2-keto-T(C6+H)$^{-}$	-454.72159	C(C5+H)$^{\cdot}$	-395. 56846	C(C5+H)$^{-}$	-395.59120
2-keto-T(C2+H)$^{\cdot}$	-454.63703	2-keto-T(C2+H)$^{-}$	-454.62667	C(C4+H)$^{\cdot}$	-395.53060	C(C4+H)$^{-}$	-395.62566

4-keto-T(C6+H)$^{\cdot}$	-454.63667	4-keto-T(C6+H)$^{-}$	-454.69760	C(C2+H)$^{\cdot}$	-395.51002	C(C2+H)$^{-}$	-395.59608
Dienol-T(C6+H)$^{\cdot}$	-454.63612	Dienol-T(C6+H)$^{-}$	-454.67101	C(C2+H$^{\cdot}$)	-395.50838	C(C2+H)$^{-}$	-395.59588
diketo-T(C2+H)$^{\cdot}$	-454.63035	Diketo-T(C2+H)$^{\cdot}$	-454.67057	t-amino-hydC(N3+H)$^{\cdot}$	-395.55850	t-amino-hydC(N3+H)$^{-}$	-395.55116
4keto-T(C4+H)$^{\cdot}$	-454.62991	4keto-T(C4+H)$^{-}$	-454.64930	t-amino-hydC(C6+H)$^{\cdot}$	-395.55521	t-amino-hydC(C6+H)$^{-}$	-395.61517
diketo-T(C4+H)$^{\cdot}$	-454.49337	Diketo-T(C4+H)$^{-}$	-454.58714	t-amino-hydC(C5+H)$^{\cdot}$	-395.56303	t-amino-hydC(C5+H)$^{-}$	-395.57938
Dienol-T(N3+H)$^{\cdot}$	-454.62837	Dienol-T(N3+H)$^{-}$	-454.63305	t-amino-hydC(C4+H)$^{\cdot}$	-395.53634	t-amino-hydC(C4+H)$^{-}$	-395.61862
4keto-T(N1+H)$^{\cdot}$	-454.62791	4keto-T(N1+H)$^{-}$	-454.65512	t-amino-hydC(C2+H)$^{\cdot}$	-395.53707	t-amino-hydC(C2+H)$^{-}$	-395.61355
Dienol-T(C4+H)$^{\cdot}$	-454.60033	Dienol-T(C4+H)$^{-}$	-454.67641	t-amino-hydC(C2+H)$^{\cdot}$	-395.53642	t-amino-hydC(C2+H)$^{-}$	-395.61316
				c-amino-hydC(N1+H)$^{\cdot}$	-395.56029	c-amino-hydC(N1+H)$^{-}$	-395.55441

	c-amino-hydC(C6+H).	-395.55350	c-amino-hydC(C6+H)-	-395.61475
	c-amino-hydC(C5+H).	-395.56162	c-amino-hydC(C5+H)-	-395.57821
	c-amino-hydC(C4+H).	-395.53709	c-amino-hydC(C4+H)-	-395.61865
	c-amino-hydC(C2+H).	-395.53694	c-amino-hydC(C2+H)-	-395.61323
	c-amino-hydC(C2+H).	-395.53646	c-amino-hydC(C2+H)-	-395.61231

Figure 4.5. Radicals Generated by the Addition of a Hydrogen Atom to Cytosine.

Cytosine	Hydrogenated Cytosine Radicals $(C+H)^{\bullet}$ ($\bullet$ shows the formal radical center)						
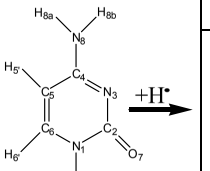 amino-oxo (A-O)	amino-oxoC(N3+H)	amino-oxoC(C6+H)	amino-oxoC(C5+H)	amino-oxoC(C4+H)	Amino-oxoC(C2+H)	amino-oxoC(C2+H)	
	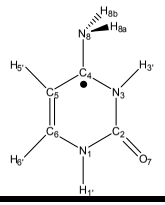	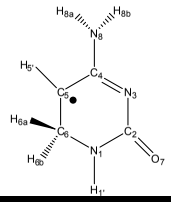	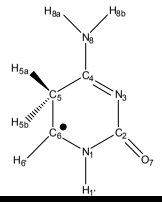	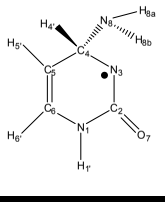	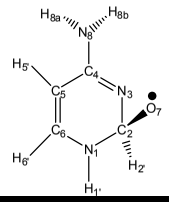	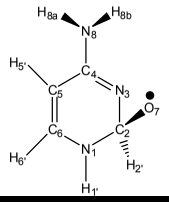	
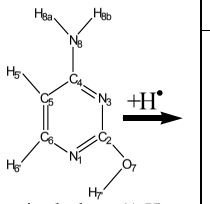 amino-hydroxy (A-H) Trans	t-amino-hydC(N3+H)	t-amino-hydC(C6+H)	t-amino-hydC(C5+H)	t-amino-hydC(C4+H)	t-amino-hydC(C2+H)	t-amino-hydC(C2+H)	c-amino-hydC(N1+H)
	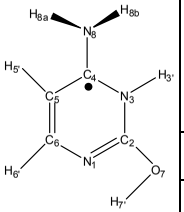	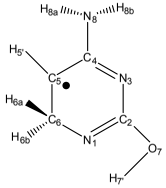	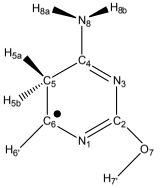	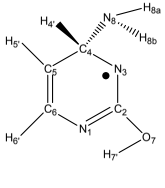	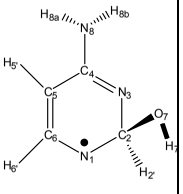	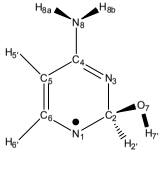	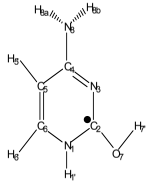
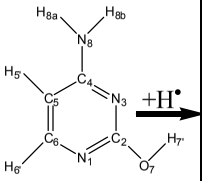 amino-hydroxy (A-H) Cis		c-amino-hydC(C6+H)	c-amino-hydC(C5+H)	c-amino-hydC(C4+H)	t-amino-hydC(C2+H)	t-amino-hydC(C2+H)	
		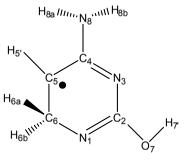	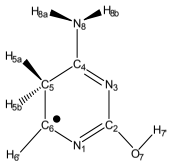	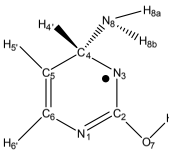	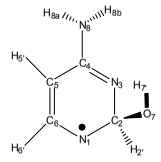	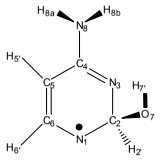	

4.9 REFERENCES

1. Evangelista, F. A.; Paul, A.; Schaefer, H. F., *J. Phys. Chem. A* **2004,** *108*, 3565.

2. Evangelista, F. A.; Schaefer, H. F., *Chem. Phys. Chem.* **2006,** *7*, 1471.

3. Ipek, S.; Bera, P. P.; Schaefer, H. F., **2006**, In preparation.

4. Luo, Q.; Li, J.; Li, Q. S.; Kim, S.; Wheeler, S. E.; Xie, Y. M.; Schaefer, H. F., *Phys. Chem. Chem. Phys.* **2005,** *7*, 861.

5. Luo, Q.; Li, Q. S.; Xie, Y. M.; Schaefer, H. F., *Collect. Czech. Chem. Comm.* **2005,** *70*, 826.

6. Profeta, L. T. M.; Larkin, J. D.; Schaefer, H. F., *Mol. Phys.* **2003,** *101*, 3277.

7. Richardson, N. A.; Wesolowski, S. S.; Schaefer, H. F., *J. Am. Chem. Soc.* **2002,** *124*, 10163.

8. Richardson, N. A.; Wesolowski, S. S.; Schaefer, H. F., *J. Phys. Chem. B* **2003,** *107*, 848.

9. Zhang, J. D.; Xie, Y. M.; Schaefer, H. F., *J. Phys. Chem. A* **2006**, submitted.

10. Zhang, J. D.; Xie, Y. M.; Schaefer, H. F.; Luo, Q.; Li, Q., *Mol. Phys.* **2006,** *104*, 2347.

11. Berdys, J.; Anusiewicz, I.; Skurski, P.; Simons, J., *J. Am. Chem. Soc.* **2004,** *126*, 6441.

12. Brocklehurst, B., *Radiat. Res.* **2001,** *155*, 637.

13. Collins, G. P., *Sci. Am.* **2003,** *289*, 26.

14. Swarts, S. G.; Sevilla, M. D.; Becker, D.; Tokar, C. J.; Wheeler, K. T., *Radiat. Res.* **1992,** *129*, 333.

15. Yarnell, A., *Chem. Eng. News* **2003,** *81*, 33.

16. Abdoul-Carime, H.; Gohlke, S.; Illenberger, E., *Phys. Rev. Lett.* **2004,** *92*, 168103.

17. Douki, T.; Angelov, D.; Cadet, J., *J. Am. Chem. Soc.* **2001,** *123*, 11360.

18. Douki, T.; Ravanat, J. L.; Angelov, D.; Wagner, J. R.; Cadet, J., *Top. Curr. Chem.* **2004,** *236*, 1.

19. Steenken, S.; Goldbergerova, L., *J. Am. Chem. Soc.* **1998,** *120*, 3928.

20. Steenken, S., *Chem. Rev.* **1989,** *89*, 503.

21. Steenken, S.; Jovanovic, S. V.; Candeias, L. P.; Reynisson, J., *Chem. Eur. J.* **2001,** *7*, 2829.

22. Abdoul-Carime, H.; Gohlke, S.; Fischbach, E.; Scheike, J.; Illenberger, E., *Chem. Phys. Lett.* **2004,** *387*, 267.

23. Chatgilialoglu, C.; Guerra, M.; Mulazzani, Q. G., *J. Am. Chem. Soc.* **2003,** *125*, 3839.

24. Huels, M. A.; Hahndorf, I.; Illenberger, E.; Sanche, L., *J. Chem. Phys.* **1998,** *108*, 1309.

25. Pogozelski, W. K.; Tullius, T. D., *Chem. Rev.* **1998,** *98*, 1089.

26. Ramirez-Arizmendi, L. E.; Heidbrink, J. L.; Guler, L. P.; Kenttamaa, H. I., *J. Am. Chem. Soc.* **2003,** *125*, 2272.

27. Vieira, A. J. S. C.; Steenken, S., *J. Am. Chem. Soc.* **1990,** *112*, 6986.

28. Desfrancois, C.; Abdoul-Carime, H.; Schermann, J. P., *J. Chem. Phys.* **1996,** *104*, 7792.

29. Huels, M. A.; Boudaiffa, B.; Cloutier, P.; Hunting, D.; Sanche, L., *J. Am. Chem. Soc.* **2003,** *125*, 4467.

30. Periquet, V.; Moreau, A.; Carles, S.; Schermann, J. P.; Desfrancois, C., *J. Elec. Spec. Rel. Phenom.* **2000,** *106*, 141.

31. Schiedt, J.; Weinkauf, R.; Neumark, D. M.; Schlag, E. W., *Chem. Phys.* **1998,** *239*, 511.

32. Wesolowski, S. S.; Leininger, M. L.; Pentchev, P. N.; Schaefer, H. F., *J. Am. Chem. Soc.* **2001,** *123*, 4023.

33. Wiley, J. R.; Robinson, J. M.; Ehdaie, S.; Chen, E. C. M.; Chen, E. S. D.; Wentworth, W. E., *Biochem. Biophys. Res. Comm.* **1991,** *180*, 841.

34. Chen, X. H.; Syrstad, E. A.; Nguyen, M. T.; Gerbaux, P.; Turecek, F., *J. Phys. Chem. A* **2005,** *109*, 8121.

35. Close, D. M.; Nelson, W. H.; Sagstuen, E.; Hole, E. O., *Radiat. Res.* **1994,** *137*, 300.

36. Lichter, J. J.; Gordy, W., *Proc. Natl. Acad. Sci. USA* **1968,** *60*, 450.

37. Nelson, W. H.; Sagstuen, E.; Hole, E. O.; Close, D. M., *Radiat. Res.* **1992,** *131*, 272.

38. Reynisson, J.; Steenken, S., *Phys. Chem. Chem. Phys.* **2005,** *7*, 659.

39. Schmidt, J.; Borg, D. C., *Radiat. Res.* **1971,** *46*, 36.

40. Sieber, K.; Huttermann, J., *Int. J. Radiat. Biol.* **1989,** *55*, 331.

41. Wetmore, S. D.; Boyd, R. J.; Eriksson, L. A., *J. Phys. Chem. B* **1998,** *102*, 10602.

42. Zehner, H.; Westhof, E.; Flossmann, W.; Muller, A., *Z. Naturforschung. C: Biosciences* **1977,** *32*, 1.

43. Colson, A. O.; Becker, D.; Eliezer, I.; Sevilla, M. D., *J. Phys. Chem. A* **1997,** *101*, 8935.

44. Debije, M. G.; Bernhard, W. A., *J. Phys. Chem. A* **2002,** *106*, 4608.

45. Debije, M. G.; Close, D. M.; Bernhard, W. A., *Radiat. Res.* **2002,** *157*, 235.

46. Turecek, F.; Yao, C. X., *J. Phys. Chem. A* **2003,** *107*, 9221.

47. Greco, F.; Liguori, A.; Sindona, G.; Uccella, N., *J. Am. Chem. Soc.* **1990,** *112*, 9092.

48. Jang, Y. H.; Goddard, W. A.; Noyes, K. T.; Sowers, L. C.; Hwang, S.; Chung, D. S., *J. Phys. Chem. B* **2003,** *107*, 344.

49. Podolyan, Y.; Gorb, L.; Leszczynski, J., *J. Phys. Chem. A* **2000,** *104*, 7346.

50. Close, D. M., *Radiat. Res.* **1993,** *135*, 1.

51. Chen, E. S. D.; Chen, E. C. M.; Sane, N., *Biochem. Biophys. Res. Comm.* **1998,** *246*, 228.

52. Gohlke, S.; Abdoul-Carime, H.; Illenberger, E., *Chem. Phys. Lett.* **2003,** *380*, 595.

53. Kar, L.; Bernhard, W. A., *Radiat. Res.* **1983,** *93*, 232.

54. Abdoul-Carime, H.; Cloutier, P.; Sanche, L., *Radiat. Res.* **2001,** *155*, 625.

55. Abdoul-Carime, H.; Sanche, L., *Int. J. Radiat. Biol.* **2002,** *78*, 89.

56. Sanche, L., *Radiat. Protect. Dos.* **2002,** *99*, 57.

57. Sanche, L., *Physica Scripta* **2003,** *68*, C108.

58. Close, D.; Forde, G.; Gorb, L.; Leszczynski, J., *Struct. Chem.* **2003,** *14*, 451.

59. Bertran, J.; Oliva, A.; Rodriguez-Santiago, L.; Sodupe, M., *J. Am. Chem. Soc.* **1998,** *120*, 8159.

60. Bixon, M.; Jortner, J., *J. Phys. Chem. A* **2001,** *105*, 10322.

61. Boudaiffa, B.; Cloutier, P.; Hunting, D.; Huels, M. A.; Sanche, L., *M S-Medicine Sciences* **2000,** *16*, 1281.

62. Cadet, J.; Douki, T.; Gasparutto, D.; Ravanat, J. L., *Mutat. Res. Funda. Mol. Mech. of Mutat.* **2003,** *531*, 5.

63. Cullis, P. M.; Malone, M. E.; Merson-Davies, L. A., *J. Am. Chem. Soc.* **1996,** *118*, 2775.

64. Dee, D.; Baur, M. E., *J. Chem. Phys.* **1974,** *60*, 541.

65. Malins, D. C.; Polissar, N. L.; Ostrander, G. K.; Vinson, M. A., *Proceedings of the National Academy of Sciences of the USA* **2000,** *97*, 12442.

66. Malins, D. C.; Polissar, N. L.; Ostrander, G. K.; Vinson, M. A., *Proceedings of the National Academy Sciences of the USA* **2000,** *97*, 12442.

67. Melvin, T.; Botchway, S. W.; Parker, A. W.; ONeill, P., *J. Am. Chem. Soc.* **1996,** *118*, 10031.

68. Rienstra-Kiracofe, J. C.; Tschumper, G. S.; Schaefer, H. F.; Nandi, S.; Ellison, G. B., *Chem. Rev.* **2002,** *102*, 231.

69. Bera, P. P.; Schaefer, H. F., *Proc. Natl. Acad. Sci. USA* **2005,** *102*, 6698.

70. Colson, A. O.; Besler, B.; Close, D. M.; Sevilla, M. D., *J. Phys. Chem.* **1992,** *96*, 661.

71. Colson, A. O.; Sevilla, M. D., *J. Phys. Chem. A* **1995,** *99*, 13033.

72. Colson, A. O.; Sevilla, M. D., *Int. J. Radiat. Biol.* **1995,** *67*, 627.

73. Colson, A. O.; Sevilla, M. D., *J. Phys. Chem.* **1996,** *100*, 4420.

74. Chen, E. C. M.; Chen, E. S., *Abs. of Papers Am. Chem. Soc.* **2000,** *220*, U497.

75. Chen, E. C. M.; Chen, E. S., *J. Phys. Chem. B* **2000,** *104*, 7835.

76. Hobza, P.; Sponer, J., *THEOCHEM* **1996,** *388*, 115.

77. Hobza, P.; Sponer, J., *Chem. Phys. Lett.* **1998,** *288*, 7.

78. Hobza, P.; Sponer, J., *Chem. Rev.* **1999,** *99*, 3247.

79. Hobza, P.; Sponer, J.; Leszczynski, J., *J. Phys. Chem. B* **1997,** *101*, 8038.

80. Hagelberg, F.; Yanov, I.; Leszczynski, J., *THEOCHEM* **1999,** *487*, 183.

81. Leszczynski, J., *THEOCHEM* **1999,** *487*, ix.

82. Sponer, J.; Hobza, P., *Encyc. Comput. Chem.* **1998,** *1*, 777.

83. Sponer, J.; Hobza, P.; Leszczynski, J., *Comput. Chem. Rev. Curr. Trends* **1996,** *1*, (World Scientific.

84. Sponer, J.; Leszczynski, J.; Hobza, P., *J. Phys. Chem.* **1996,** *100*, 1965.

85. Sponer, J.; Leszczynski, J.; Hobza, P., *Biopolymers* **2001,** *61*, 3.

86. Becke, A. D., *Phys. Rev. A* **1988,** *38*, 3098.

87. Lee, C. T.; Yang, W. T.; Parr, R. G., *Phys. Rev. B* **1988,** *37*, 785.

88. Becke, A. D., *J. Chem. Phys.* **1993,** *98*, 5648.

89. Perdew, J. P., *Phys. Rev. B* **1986,** *33*, 8822.

90. Perdew, J. P., *Phys. Rev. B* **1986,** *34*, 7406.

91. Papas, B. N.; Schaefer, H. F., *THEOCHEM* **2006**, In press.

92. Dunning, T. H., *J. Chem. Phys.* **1970,** *53*, 2823.

93. Huzinaga, S., *J. Chem. Phys.* **1965,** *42*, 1293.

94. Lee, T. J.; Schaefer, H. F., *J. Chem. Phys.* **1985,** *83*, 1784.

95. Frisch, M. J.; Trucks, G. W.; Schlegel, H. B.; Scuseria, G. E.; Gill, P. M. W.; Johnson, B. G.; Robb, M. A.; Cheeseman, J. R.; Keith, T.; Montgomery, J. A.; Stratmann, R. E.; Burant, J. C.; Daprich, S.; Millam, J. M.; Daniels, A. D.; Kudin, K. N.; Strain, M. C.; Farcas, O.; Tomasi,

J.; Barone, V.; Cossi, M.; Cammi, R.; Mennuchi, B.; Pomelli, C.; Adamo, C.; Clifford, S.; Ochterski, J.; Petersson, G. A.; Cui, Q.; Morukuma, K.; Salvador, P.; Dannenberg, J. J.; Malick, D. K.; Rabick, A. D.; Baboul, A. G.; Raghavachari, K.; Stefanov, B. B.; Liu, G.; Liashenko, A.; Piskorz, P.; Komaromi, I.; Gomperts, R.; Al-Laham, M. A.; Zakrzewski, V. G.; Ortiz, J. V.; Foresman, J. B.; Cioslowski, J.; Stefanov, B. B.; Nanayakkara, A.; Challacombe, M.; Peng, C. Y.; Ayala, P. Y.; Chen, W.; Wong, M. W.; Andres, J. L.; Replogle, E. S.; Gomperts, R.; Martin, R. L.; Fox, D. J.; Binkley, J. S.; Defrees, D. J.; Baker, J.; Stewart, J. P.; Head-Gordon, M.; Gonzalez, C.; Pople, J. A. *Gaussian 94, Revision E.2*, Gaussian, Inc., Pittsburgh PA.: 1995.

96. Ipek, S.; Bera, P. P.; Schaefer, H. F., Hydrogen atom and hydride ion addition to tautomers of thymine: structures and energetics. In In Preparation.

97. Radisic, D.; Bowen, K. H.; Dabkowska, I.; Storoniak, P.; Rak, J.; Gutowski, M., *J. Am. Chem. Soc.* **2005,** *127*, 6443.

CHAPTER 5

MINDLESS CHEMISTRY

Bera, Partha P., Kurt W. Sattelmeyer, Martin Saunders, Henry F. Schaefer III and Paul v R. Schleyer. Journal of Physical Chemistry 2006 110, 4287-4290. Repreinted by the permission of American Chemical Society.

5.1 ABSTRACT

Applications of an automated stochastic search procedure for locating all possible minima with a given composition are illustrated by the pentatomic molecules BCNOS, CAlSiPS, $C_4B(-)$, $C_4Al(-)$, and $CBe_4(2-)$, as well as by C_6Be, the $C_6Be(2-)$ dianion, and C_6H_2. All previously identified minima were reproduced, and many new structures, often with non-intuitive geometries, were found.

5.2 INTRODUCTION

After more than two centuries, chemists are still not able to predict the structures of all isomers with a given composition logically, thoroughly, and reliably. This is not surprising. As the number of atoms comprising a molecule increases, the possible connectivities scale factorially! Hundreds, thousands, and then many more minima become conceivable. Experience, knowledge, and chemical intuition may offer suggestions, but the task of enumerating and establishing the relative stability of all possible structures rapidly becomes ill-suited and unfeasible for humans. Most chemists hesitate even to venture a guess as to what the most stable isomer of a compound with an unfamiliar composition might be.

Such problems can be daunting even for small molecules, especially when all atoms are different. Such species are seldom considered. Even small clusters with more than two elements are rare. Sun et al.[1-4] employed manual exploration techniques to find stable isomers of intriguing interstellar molecule candidates, such as SiC_2N, SiC_2P, SiC_3N, SiC_3P, and NC_3S. Each search began by choosing five or six possible connectivities for each molecule. Chemical intuition was used to guess all possible isomers with each of these connectivities. The task of evaluating all of them must have been very tedious and time consuming.

Predicting the lowest energy structure of a hypothetical pentatomic molecule, composed of five different, but familiar atoms, e.g., B, C, N, O, S, would be an order of magnitude more complex! A thorough listing of all the possible connectivities must include those illustrated in Figure 5.1, along with all the associated permutations of the various atoms. Their geometric and conformational isomers may also be minima. The challenge of finding all the isomers of this and other examples is addressed in the present paper.

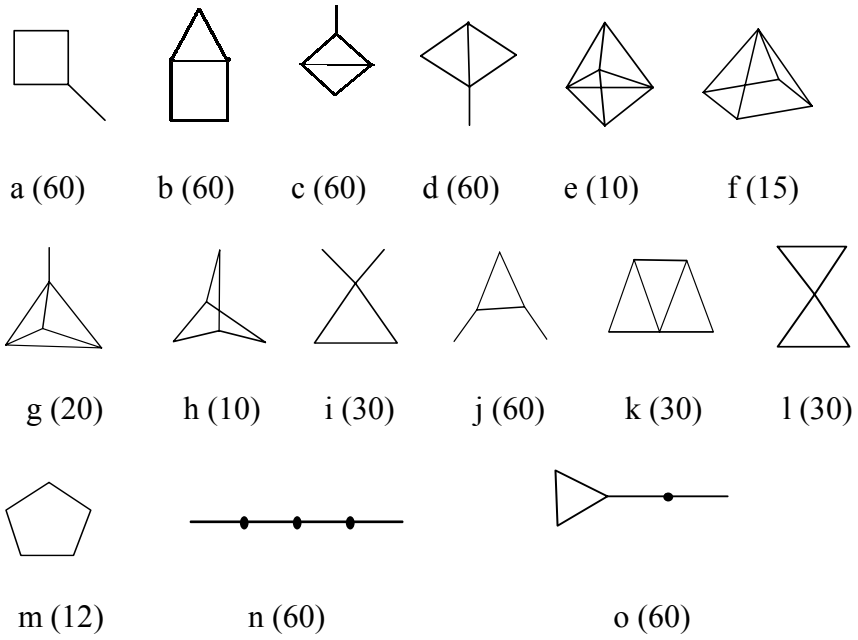

Figure 5.1. Connectivities of pentatomic molecules; the conformations also may vary. The number of possible permutations when all five atoms are different, as in BCONS and CAlSiPS, are given in parentheses.

While conceivable, the manual exploration of each of the many hundred structural possibilities for BCNOS suggested by Figure 5.1 using quantum chemistry methods is an uninviting task, uncertain in its outcome. The rigorous manual solution of the next largest six unique atom puzzle, e.g., BCNOPS, surely would be precluded by the enormous labor required.

There have been many efforts to deal with problems of similar complexity using automated procedures, but generally with the objective of finding the global minimum. In 2004, Zhao and Xie reviewed comprehensively the genetic algorithm–based methods employed to determine the most stable geometry of clusters.[5] R. Car and M. Parrinello's well-known "dynamic simulated annealing" combines molecular dynamics and density functional theory.[6] Searches employing "simulated annealing" "Monte Carlo metropolis search" and various "genetic algorithm techniques" are also well documented.[6-9] Tomasulo and Ramakrishna gradually replaced the atoms of a starting structure one by one,[10] and used the Car-Parrinello technique to relax the atomic positions and optimize electronic wave functions. But most of the structures obtained this way could be anticipated easily since only the relative positions of the atoms change. Babadova-Parvanova, et al. used the density functional tight binding level to search for low energy isomers using the "single parent genetic algorithm" (DFTB/SPGA) method.[11] Bertolus et al. combined Car-Parrinello molecular dynamics with local energy minimization using DFT;[12] several molecular dynamics trajectories generated a large number of structures, e.g., several interesting Si_mC_n clusters. R. O. Jones has employed density functional methods for many years to study the structure and bonding of elemental as well as mixed element clusters.[13-15] Starting geometries were generated either by MD simulated annealing, density functional tight binding, or selected from DFT–based computations or experimental results. Choosing starting geometries becomes more and more complex when the number of atoms increases. Even though their energies were lowest or competitive, hollow cage isomers of gold clusters were not located in a recent genetic algorithm search.[16] Alexandrova et al. used genetic algorithm–based techniques on randomly generated structures to search for global minima.[17] Godecker in 2004 proposed a 'minima hopping' method to scan the entire potential energy surface.[18] Then there are other methods like

'conformational flooding' which address the similar issue.[19] A major problem existing *for any search method* is that the potential energy surface (PES) at lower theoretical levels, employed initially for practical considerations, may differ from the PES at higher, more accurate levels. We have encountered cases where structures, important on higher-level PES's, do not exist as minima at lower levels!

5.3 PROCEDURE

The purpose of this paper is to present illustrative examples demonstrating how structures generated through stochastic methodology[20] can be used to explore PES's having many minima automatically with the least possible human involvement. *Truly rigorous searches require knowledge of all possible isomers to be certain that the global minimum has been located.*

Fortunately, Saunders' fast, comprehensive, and automated "kick" method produces isomers and conformers simply and effectively with little thought or effort.[20] A similar random search and minimization technique was proposed by Lloyd and Johnston while exploring aluminum clusters.[21] The automated random structure generation procedure implemented here enables searches for unknown isomers much more easily than manual explorations. Neither preconceived structures nor bonding principles are involved! All the atoms are placed at the same point initially, and then are "kicked" randomly within a box of chosen dimensions, e.g. a 2 Å cube. The method developed further in this work generates up to 1000 unbiased starting geometries and submits them automatically for optimization with e.g., Gaussian 94,[22] as employed here, or other electronic structure programs, to a bank of rapid, coarse-grain parallelized PC's. While many jobs die quickly (the atoms are too close or the SCF convergence is not achieved) and other jobs do not achieve geometrical convergence, the "yield" of completed optimizations

typically ranges between 10 and 50%. Most of these completed jobs from initial batches of e.g., 100 "kick runs" are unique minima in the examples we have explored! (If desired, promising partially optimized jobs may be completed in the usual manner and other search procedures, e.g., utilizing the gradient and Hessian information, may be employed. However, this requires human effort. It is easier just to run more "batches.")

Subsequently, an auxiliary program searches each batch of outputs for successful completion (convergence to a minimum), eliminates redundancies, orders the energies, and lists the archive summaries of the unique isomers. Selected structures (e.g., the most stable or otherwise attractive isomers) obtained in this manner at lower levels of theory may then be refined manually employing more sophisticated methods. In essence, lower level searches generate "candidates" for refinement at higher levels rapidly. All "kick" optimizations proceed in point group C_1, but often lead very nearly to higher symmetries, which may then be imposed and the harmonic frequencies computed.

To insure that all the minima have been located, additional batches of kick jobs are run until no new structures are obtained. While it is impossible to be absolutely certain that all minima have been found, this problem exists to a greater extent with other methods. Minima may lie beyond the resolution capabilities of the method employed, or the "box" dimensions may be too restrictive. However, the latter may be varied to increase the percentage of successful optimizations or the probability of finding structures with planar or elongated shapes. The purpose of this paper is to illustrate the method we have developed by applying it to several diverse problems. Singlet PES′ of the following molecules were explored using the method explained above.

5.4 ILLUSTRATIVE EXAMPLES

BCONS. In 1976 Baudisch synthesized a chemical novelty, a substituted five membered BCNOS ring comprised of five different atoms.[23] This feat inspired us to search for all the possible singlet pentatomic minima involving only these five familiar main group elements (without any substituents). Independent batches of 100 or 200 jobs employed the kick method at the respectable B3LYP/6-31G* level of theory. The kick size in the cubic box was varied from 2.0 to 2.5 Å. Since some atoms must move far to reach an equilibrium position, the number of optimization cycles permitted was increased (from the default). Ten PC's running simultaneously processed about 20 jobs per hour; roughly 30% of the jobs completed satisfactorily. Redundancies in each batch (energies within 0.00001 a.u.) were eliminated; duplicates appearing in more than one batch were noted; and the kick runs were continued until no new structures were generated. A total of 1000 kicks gave 103 unique geometries. The energies of these minima ranged over 314 kcal/mol!

The best isomers had type **n** (Figure 5.1) topologies. Surprisingly, linear SCNBO was the global minimum, despite its seemingly unfavorable S=C double bond. Linear OCNBS followed next, then NCSBO (bent at sulphur), NCOBS (bent at oxygen), linear SNCBO, and other permutations of these elements. Many isomers of type **o** (Figure 5.1) with a three membered ring and a two-atom side chain constituted the second most stable structural group. Of these, planar NCB(OS) followed by CNB(OS) had the lowest energies.

As a check, we explored all 60 possible type **n** permutations manually; 28 of these survived as minima, but some were bent rather than linear. Others rearranged and a few formed three membered rings. *All of these minima had been found previously by the kick procedure.* Remarkable variety illustrating the connectivities of Figure 5.1 characterized the other, higher

energy structures and included a five membered ring, cages, and bridged isomers, as well as examples of partially dissociated CO, NO, and CS complexes (with the corresponding three-atom fragments). The refinement and characterization of these minima using a higher level of theory (cc-pVTZ/CCSD) resulted in the same ordering of energies for the ten lowest energy isomers (see SI-Table 1). Figure 2 shows the geometry of the global minimum reoptimized at the cc-pVTZ/CCSD level of theory.

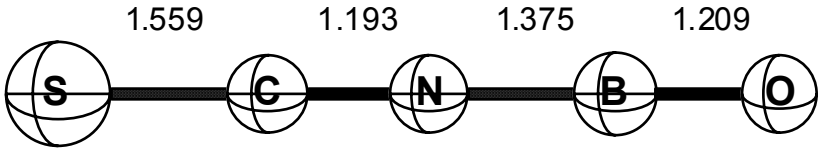

Figure 5.2. The linear BCONS global minimum geometry (in Å) at the cc-pVTZ/CCSD *ab initio* level.

CAlSiPS. Our second example retained carbon, but included four second row elements known to eschew multiple bonding. Indeed, the results were quite different from BCNOS: there were *no linear minima*. The fourth 100 run batch did not result in any significant new isomers. Fifty minima in an 86 kcal/mol energy range were found. Oddly, **1** (type c) was the lowest energy form (global minimum) at B3LYP/6-31G* (the CCSD/cc-pVTZ geometry is shown below). Type **o** structures were favored by the next several lower energy isomers at B3LYP/6-31G*.

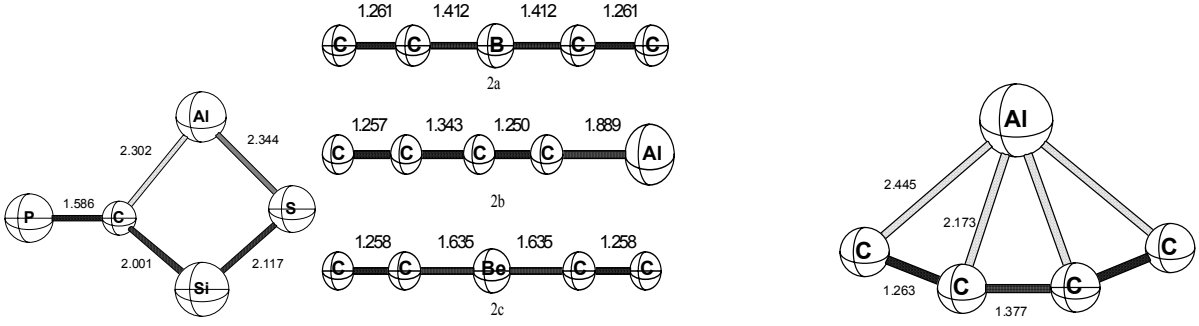

Figure5.3. **1** **2** anion[C4B-, C4Al-, C4Be(2-)] **3** anion (C_4Al^-)

$C_4B(-)$, $C_4Al(-)$, and $C_4Be(2-)$. The search for all the isomers of these isoelectronic species is inherently much less complex since four atoms are the same. While the global minima of the $C_4Be(2-)$ and the "magic number" $C_4B(-)$ species have been predicted by analogy with the isoelectronic linear neutral C_5,[24-27] many of their isomers have been overlooked.

The $C_4B(-)$ anion signal was, by far, the most intense in a 1988 experiment on the cluster ions formed in the laser-ablation plasma of boron carbide.[28] The kick method located 12 singlet minima, ranging in energy by more than 127 kcal/mol at B3LYP/6-31G*. The best of these, CCBCC(1-) (**2a**), is 30 kcal/mol more stable than its linear BCCCC(1-) counterpart. The third and fifth best species (relative energies 60 and 78 kcal/mol, respectively) are of type **k** (Figure 5.1), with a planar tetracoordinate boron and carbon. There are no analogous isoelectronic neutral C_5 or even $C_4Be(2-)$ minima, but a similar C_{2v} planar tetracoordinate aluminum structure (**3 anion**) is the second most stable $C_4Al(-)$ isomer. The $C_4Al(-)$global minimum, linear CCCCAl(1-), is 17 kcal/mol more stable; a D_{2d} **l**–type structure is the only other low energy isomer (**2b**).

Although small dianions in isolation are generally metastable toward Coulomb explosion, $C_4Be(2-)$ has been observed experimentally in the gas phase.[29] Dreuw and Cederbaum computed 10 structures, but claimed that only the three linear forms, the lowest energy CCBeCC(2–) (**2c**) as well as BeCCCC(2–) and CBeCCC(2-), were minima.[30] Shi and Kais reported that two other isomers (planar types **o** and **l**, with Be in the center of each) also were minima.[31]

The kick method, run at the B3LYP/6-31G* level some 500 times until no new minima appeared, revealed 12 isomers with energies ranging over 163 kcal/mol. (In contrast, *only five minima were obtained at HF/6-31G**.) Besides the three linear forms, three were of type **o** and two of type **j**. Type **a** (external Be), **c**, **e** (trigonal Be), and **l** (D_{2d} rather than the reported planar

form,[28] which has three imaginary vibrational frequencies), also were represented. Other singlet minima at B3LYP/6-31G* are unlikely.

C_6Be and $C_6Be(2-)$. About 500 kick computations resulted in 33 C_6Be minima at the B3LYP/STO-3G level; only 15 of these survived when refined at B3LYP/6-31G*. A cyclic C_{2V} structure (**4**) was the most stable isomer. Both structures 4 and 6 dianions are optimized and reported at the cc-pVTZ/CCSD level of theory.

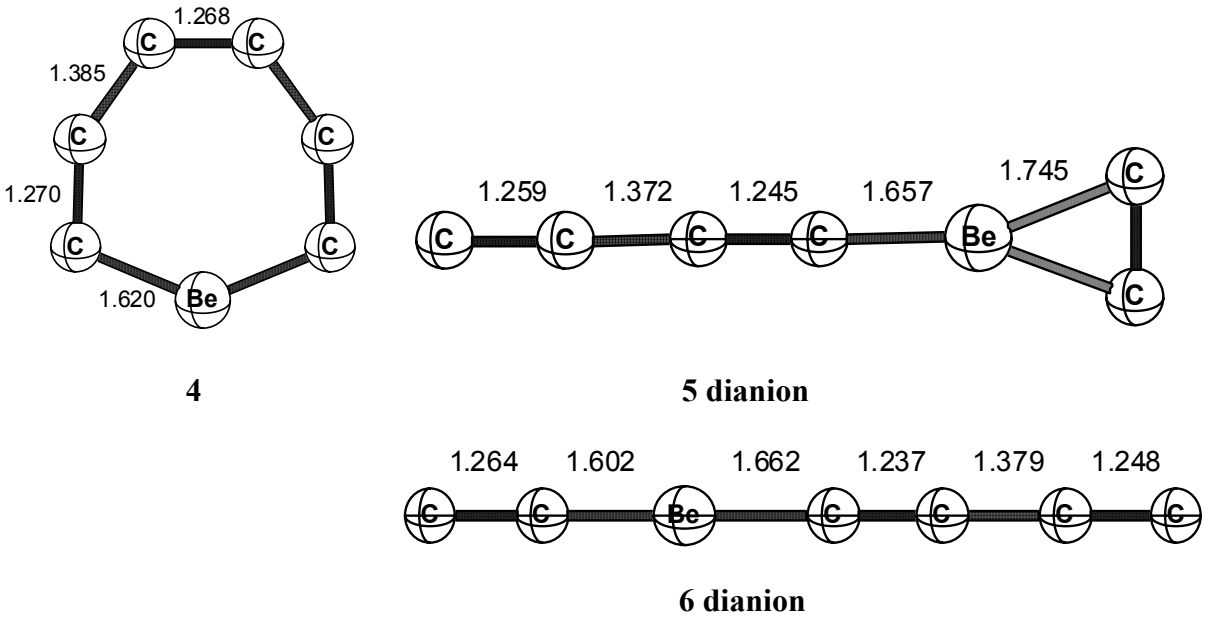

4 **5 dianion**

6 dianion

Figure 5.4. BeC_6 and BeC_6^{2-}

Dreuw and Cederbaum[30] examined the experimentally known $C_6Be(2-)$[29] and claimed that only "linear isomer[s]….correspond to minima on the potential energy surface." The kick method disagrees. Both the HF/STO-3G and B3LYP/6-31G* PES's have more than ten minima ranging over 120 kcal/mol. At the B3LYP level, the C_{2v} C2BeCCCC(2–) structure (**5 dianion**) is only 4 kcal/mole less stable the linear CCBeCCCC(2–) global minimum (**6 dianion**).

C_6H_2. The C_6H_2 system[32-34] extends the original C_6 search by Saunders.[20] Triacetylene (HCCCCCCH) is, by far, the global minimum, being more than 50 kcal/mol lower in energy

(CCSD(T)/cc-pVTZ)[34] than the two other experimentally–observed isomers, $CCCCCCH_2$ hexapentaenylidene)[32] and CCCCHCCCH (ethynylbutatrienylidene).[33]

The two additional hydrogen atoms in C_6H_2 increase the number of minima from those reported for C_6[20] dramatically. Indeed, an earlier attempt "to investigate 'all' reasonable structures" was defeated by the "depressingly large"[34] number of structures which would have to be processed manually. Several thousand "kicks" located 80 C_6H_2 isomers, spanning a range of 175 kcal/mol at B3LYP/DZP. *These included all nine reported earlier.*[32, 33] Moreover, of the 32 isomers within 100 kcal/mol of triacetylene at the B3LYP/DZP level, 30 survived further refinement; all are minima at CCSD(T)/cc-PVTZ. As expected, structure **7** has the lowest energy also at this level.

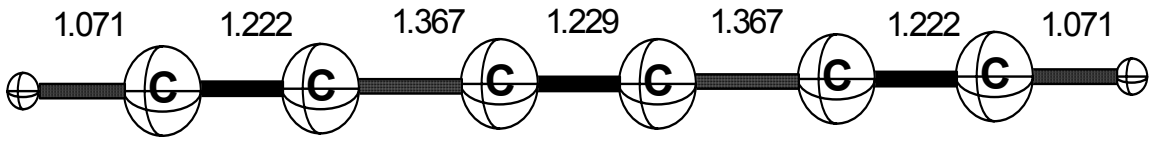

7

Figure 5.5. Triacetylene.

In conclusion, the kick procedure facilitates unbiased and nearly automatic searches of potential energy surfaces. It is an important addition to the existing methods. Little thought and human effort are required, and numerous isomers not anticipated by chemical intuition are located. While no method can guarantee 100 per cent recovery of all possible minima, this goal can be approached by repeating the "kick" procedure again and again. While low starting theoretical levels employ fewer computational resources and result in a large number of isomers, it may be better strategy to begin with higher levels as these are less likely to be misleading.

The often-employed genetic algorithm (GA) method[5, 7, 8] only attempts to locate the global energy minimum structure. In practice, this not always is achieved.[5, 7, 8, 16] The concept of GA is

inferior compared to methods that search for all the minima. However, the latter methods are not applicable currently to larger systems, which often are investigated by GA procedures. When two or more isomers have nearly the same energy, there is the further general problem that entropy differences may determine the lowest free energy. Many approaches, for example systematic search, thermal annealing, distance geometry and genetic algorithm,[5-15, 17, 21] have been promoted, but, for systems of the moderate size we have discussed, none of these alternatives appear to be superior to the stochastic search procedure employed here.

5.5 ACKNOWLEDGEMENT

The research in Georgia was supported by National Science Foundation Grant CHE01-36186. Initial results were reported in a conference poster.[35] PPB thanks Dr. Yukio Yamaguchi and Justin Turney for helpful discussions.

5.6 REFERENCES

1. Ding, Y.; Li, Z.; Huang, X.; Sun, C., *J. Phys. Chem. A* **2001,** *105*, 5896.

2. Chen, G.; Ding, Y.; Huang, X.; Zhanng, H.; Li, Z.; Sun, C., *J. Phys. Chem. A* **2002,** *106*, 10408.

3. Liu, H.; Huang, X.; Chen, G.; Ding, Y.; Sun, C., *J. Phys. Chem. A* **2004,** *108*, 6919.

4. Liu, H.; Huang, X.; Chen, G.; Ding, Y.; Sun, C., *J. Phys. Chem. A* **2004,** *108*, 11828.

5. Zhao, J.; Xie, R., *J. Comp. & Theo. Nanosci.* **2004,** *1*, 117.

6. Car, R.; Parrinello, M., *Phys. Rev. Lett.* **1985,** *55*, 2471.

7. Back, T., *Evolutionary Algorithm in Theory and Practice: Evolutionary Programming, Genetic Algorithms*. Oxford University Press, Oxford: 1990.

8. Chaudhuri, P.; Bhattacharyya, S. P., *Chem. Phys.* **1999,** *241*, 313.

9. Metropolis, N.; Rosenbluth, A. W.; Rosenbluth, M. N.; Teller, A. H.; Teller, E., *J. Chem. Phys.* **1953,** *21*, 1087.

10. Tomasulo, A.; Ramakrishna, M. V., *J. Chem. Phys.* **1996,** *105*, 10449.

11. Babadova-Parvanova, P.; Jackson, K. A.; Srinivas, S.; Horoi, M.; Kohler, C.; Seifert, G., *J. Chem. Phys.* **2002,** *116*, 3576.

12. Bartolus, M.; Finocchi, F.; Millie, P., *J. Chem. Phys.* **2004,** *120*, 4333.

13. Jones, R. O.; Gantefor, G.; Hunsicker, S.; Pieperhoff, P., *J. Chem. Phys.* **1995,** *103*, 9549.

14. Jones, R. O.; Lichtenstein, A. I.; Hutler, J., *J. Chem. Phys.* **1997,** *106*, 4556.

15. Jones, R. O., *J. Chem. Phys.* **1999,** *110*, 5189.

16. Wang, J.; Jellinek, J.; Zhao, J.; Chen, Z.; King, R. B.; Schleyer, P. v. R., *J. Phys. Chem. A* **2005,** *Web Release,17-Sep-2005*.

17. Alexandrova, A.; Boldyrev, A.; Fu, Y.; Yang, X.; Wang, X.; Wang, L., *J. Chem. Phys.* **2004,** *120*, 5709.

18. Goedecker, S., *J. Chem. Phys.* **2004,** *120*, 9911.

19. Grubmuller, H., *Phys. Rev. Lett.* **1995,** *E52*, 1893.

20. Saunders, M., *J. Comp. Chem.* **2004,** *25*, 621.

21. Lloyd, L. D.; johnston, L., *Chem. Phys.* **1998,** *236*, 107.

22. Frisch, M. J.; Trucks, G. W.; Schlegel, H. B.; Gill, P. M. W.; Johnson, B. G.; Robb, M. A.; Cheeseman, J. R.; Keith, T.; Peterson, G. A.; Montgomery, J. A.; Raghavachari, K.; Al-Laham, M. A.; Zakrzewski, V. G.; Oritz, J. V.; Foresman, J. B.; Cioslowski, J.; Stefanov, B. B.; Nanayakkara, A.; Challacombe, M.; Peng, C. Y.; Ayala, P. Y.; Chen, W.; Wong, M. W.; Andres, J. S.; Defrees, D. J.; Baker, J.; Stewart, J. P.; Head-Gordon, M.; Gonzalez, C.; Pople, J. A., ***Gaussian 94,*** *Gaussian, Inc: Pittsburgh, PA,* ***1995****.*

23. Baudisch, H. University of Erlangan-Nuremberg, Erlangan, 1976.

24. Galazutdinov, G.; Musaev, F.; Nirski, J.; Krelowski, J., *Monthly Notices to the Royal Astron. Soc.* **2001,** *325*, 1332.

25. Bernath, P. F.; Hinkle, K. H.; Keady, J. J., *Science* **1989,** *244*, 562.

26. Motylewski, T.; Vaizert, O.; Giesen, T. F.; Linnartz, H.; Maier, J. P., *J. Chem. Phys.* **1999,** *111*, 6161.

27. Galazutdinov, G.; Petlewski, A.; Musaev, F.; Moutou, C.; Lo Curto, G.; Krelowski, J., *Astron. & Astrophys.* **2002,** *395*, 969.

28. Becker, S.; Dietze, H. J., *Int. J. Mass Spect. & Ion Proc.* **1988,** *82*, 287.

29. Klein, J.; Middleton, R., *Nucl. Instrum. Methods. Phys. Res. Sect B* **1999,** *159*, 8.

30. Dreuw, A.; Cederbaum, L. S., *J. Chem. Phys.* **2000,** *112*, 7400.

31. Shi, Q.; Kais, S., *J. Am. Chem. Soc.* **2002,** *124*, 11723.

32. Langer, W. D.; Velusamy, T.; Kuiper, T. B. H.; Peng, R.; McCarthy, M. C.; Travers, M. J.; Kovacs, A.; Gottlieb, C. A.; Thaddeus, P., *Astrophys. J.* **1997,** *480*, L63.

33. McCarthy, M. C.; Thaddeus, P., *Astrophys. J.* **2002,** *569*, L55.

34. Sattelmeyer, K. W.; Stanton, J. F., *J. Am. Chem. Soc.* **2000,** *122*, 8220.

35. Bera, P. P.; Sattelmeyer, K. W.; Saunders, M.; Schaefer, H. F.; Schleyer, P. v. R. S. In *Automated Stochastic Method to search for Isomers and Conformers*, Molecular Quantum Mechanics Conference: The No Nonsense Path to Progress, Cambridge University, England, 2004; Cambridge University, England, 2004.

CHAPTER 6

THE LOW-LYING QUARTET ELECTRONIC STATES OF NITROGEN DIOXIDE

Bera, Partha P., Yukio Yamaguchi, and H. F. Schaefer III. To be submitted to Journal of Chemical Physics.

6.1 ABSTRACT

Environmentally active molecule nitrogen dioxide (NO_2) has been revisited. Electronic ground state and the low-lying quartet states of NO_2 have been investigated using high-level *ab* initio electronic structure methods. Single-reference restricted open-shell Hartree-Fock (ROHF) self-consistent-field (SCF), configuration interaction with single and double excitations (CISD), coupled cluster with single and double excitations (CCSD), and CCSD with perturbative triple excitations [CCSD(T)] methods along with Dunning's correlation consistent polarized valence cc-pVXZ and augmented cc-pVXZ (where X = T, Q, and 5) basis sets were used in this research. The adiabatic excitation energies of the low lying quartet excited states are 84.17 kcal/mol (3.63 eV) for the $^4A_2$ state, 93.86 kcal/mol (4.07 eV) for the $^4B_2$ state, and 101.69 kcal/mol (4.41 eV) for the $^4A_1$ state. The lowest quartet linear Renner-Teller $^4\Pi$ state in a bent configuration gives rise to a $^4A_2$ state at 112.8° and a $^4B_2$ state at 124.4° <(ONO) angles. In the C_{2v} geometry the second lowest quartet state ($^4B_2$) shows an imaginary asymmetric stretching frequency which indicates a lowering of symmetry and the presence of a C_s equilibrium geometry. The $^4A_1$ state has a very small bond angle of about 85.6°. The potential energy diagrams with respect to bond angles of the ground state and the quartet states are also reported.

6.2 INTRODUCTION

In environmental chemistry nitrogen dioxide (NO_2) holds key interest being one of the most environmentally active nitrogen oxides.(ref) Concentration of nitrogen oxides in the atmosphere is more than the concentration of carbon dioxide. NO_2 has been known to be a greenhouse gas as well as having high global worming potential (GWP). It contributes to the depletion of ozone layer by taking part in the generation of NO radicals and NO^+ cations.

Electronic states of NO_2 have encouraged both experimental[1-9] and theoretical scientists over several decades.

Gillespie and Khan used multi configuration self-consistent-field (MCSCF) approach to study the C_{2v} potential energy surfaces of NO_2 and concluded the excitation energies of the $^4A_2$ and $^4B_2$ states to be very close to each other.[10] Use of *d* orbitals significantly improved the computed vertical excitation energies. Jackels and Davidson in a pioneering work in 1976 used $^4B_2$ molecular orbital as a starting reference in a 'Internally Consistent Self-Consistent-Field' (ICSCF) scheme and a double zeta basis set (DZ) to investigate several doublet electronic states as well as the quartet states.[11, 12] Their results show a $^4B_2$ state ($2b_1 \leftarrow 1a_2$) to be of lower energy than the $^4A_2$ state by 0.22 ev (vertical energy difference).

In 1979, Handy, Goddard, and Schaefer investigated the six lowest lying electronic states of NO_2 using configuration interaction (CI) technique.[13] Beside the $^2A_1$ ground state they predicted the five lowest lying excited electronic states to be $^2B_1$, $^2B_2$, $^2A_2$, $^4A_2$, and $^4B_2$. All CI calculations performed in the ground electronic state experimental geometry of R_{NO}1.1934 Å and <ONO 134.1° provided reasonable excitation energies. A *d* polarization function added to the Dunning's DZ (4s2p) quality basis set predicted 4.15 and 4.30 eV for the excitation energies of $^4A_2$ and $^4B_2$ electronic states, respectively.[14-17]

Neutral open-shell species like NO_2 particularly posed some challenges computationally. But the advances made in the last two decades in the field of computational quantum chemistry made it worthwhile to elucidate excited state properties with greater accuracy and reliability. Purpose of this work is to investigate the relatively less studied low-lying quartet electronic states of NO_2 with highly correlated *ab initio* methods in conjunction with considerably large atomic basis sets.

6.3 ELECTRONIC STRUCTURE CONSIDERATIONS

In the previous theoretical studies,[10, 11, 18, 19] the ground state of the NO_2 molecule,

$$[\text{core}](3a_1)^2(2b_2)^2(4a_1)^2(3b_2)^2(1b_1)^2(5a_1)^2(1a_2)^2(4b_2)^2(6a_1) \qquad \tilde{X}\ ^2A_1 \qquad (1)$$

was found to have a bent structure which is consistent with Walsh' rules. In Eq. (1), [core] denotes the three lowest-lying core orbitals (N and O: 1s like). In a linear geometry the ground electronic $^2A_1$ state connects to the linear $^2\Pi_u$ state

$$[\text{core}](3\sigma_g)^2(2\sigma_u)^2(4\sigma_g)^2(3\sigma_u)^2(1\pi_u)^4(1\pi_g)^4(2\pi_u) \qquad \tilde{X}\ ^2\Pi_u\,. \qquad (2)$$

The lowest quartet state is formed from $\tilde{X}\ ^2A_1$ by a $2b_1 \leftarrow 4b_2$ single excitation

$$\ldots\ (1b_1)^2(5a_1)^2(1a_2)^2(4b_2)(6a_1)(2b_1) \qquad \tilde{a}\ ^4A_2 \qquad (3)$$

where, ... designates the seven doubly occupied low lying orbitals.

The second lowest quartet state $^4B_2$ is derived from the $\tilde{X}\ ^2A_1$ state by a single $2b_1 \leftarrow 1a_2$ transition,

$$\ldots (1b_1)^2(5a_1)^2(1a_2)(4b_2)^2(6a_1)(2b_1) \qquad \tilde{b}\ ^4B_2. \quad (4)$$

In a linear geometry the lowest two quartet states, $^4A_2$ and $^4B_2$ states, connect to the $^4\Pi_g$ state,

$$\ldots\ (1\pi_u)^4(1\pi_g)^3(2\pi_u)^2 \qquad \tilde{a}\ ^4\Pi_g, \qquad (5)$$

or in a real orbital notation

$$\ldots\ (1\pi_{ux})^2(1\pi_{uy})^2(1\pi_{gx})^2(1\pi_{gy})(2\pi_{ux})(2\pi_{uy}) \qquad \tilde{a}\ ^4\Pi_g\,. \qquad (6)$$

The third lowest quartet state is formed from the $\tilde{X}\ ^2A_1$ state by a $2b_16a_1 \leftarrow 4b_21a_2$ double excitation

$$\ldots(1b_1)^2(5a_1)^2(1a_2)(4b_2)(6a_1)^2(2b_1) \qquad \tilde{c}\ ^4A_1. \qquad (7)$$

The fourth lowest quartet state is derived from the $\tilde{X}\ ^2A_1$, by a $2b_1 \leftarrow 4b_21a_2$ double excitation,

$$\ldots(1b_1)^2(5a_1)^2(1a_2)(4b_2)(6a_1)(2b_1)^2 \qquad \tilde{d}\ ^4B_1\ . \qquad (8)$$

In the C_{2v} molecular point group symmetry, the eight electronic states presented in Eqs. (1)–(8) are mutually orthogonal to each other with respect to spin/spatial symmetry. Therefore, geometries, dipole moments, and totally symmetric vibrational frequencies may be determined correctly without the fear of variational collapse.

6.4 STABILITY ANALYSIS

For open-shell systems, it is helpful to analyze the molecular orbital (MO) Hessian of the reference SCF wave functions. The MO Hessian is defined as the second derivatives of the SCF energy with respect to independent MO rotations. The signs and magnitudes of the eigenvalues for the MO Hessian provide useful information concerning the instability (or stability) of the SCF wave functions.

At the linear configuration, the MO Hessian matrix for the $^4\Pi_g$ state of NO_2 has one zero eigenvalue. The eigenvector of the zero eigenvalue is associated with a $^2\pi_{ux}$ - $^2\pi_{uy}$ MO rotation. Therefore, an exchange of two MOs does not alter the SCF energy.

For the bent $\tilde{a}\ ^4A_2$ state of NO_2, the eigenvalues of the MO Hessian are all positive, as expected. Thus, the SCF wave functions for the lowest quartet state are *stable* at its equilibrium geometry. There is one negative eigenvalue (for example, λ_1 = -0.00861 hartree at the cc-pVTZ/SCF level of theory) of the MO Hessian for the bent $\tilde{b}\ ^4B_2$ state. The eigenvector of the negative eigenvalue is related to a $1a_2 – 4b_2$ MO rotation. Therefore, the bent $\tilde{b}\ ^4B_2$ state SCF wave functions are *unstable* with respect to orbital rotation, and a de-excitation of an electron from the $4b_2$ to $1a_2$ orbital leads to the lower-lying $\tilde{a}\ ^4A_2$ state. The bent $\tilde{c}\ ^4A_1$ state has two negative eigenvalues of the MO Hessian (for example, λ_1 = -0.00394 and λ_2 = -0.00361 hartree at the cc-pVTZ/SCF level of theory). The bent $\tilde{c}\ ^4A_1$ SCF wave functions are again *unstable*. The

larger negative eigenvalue corresponding to a $4b_2 - 6a_1$ rotation connects to $\tilde{a}\ ^4A_2$ state, whereas the smaller negative eigenvalue corresponding to a smaller negative eigenvalue connects to the $\tilde{b}\ ^4B_2$ state.

The $^4\Pi_g$ state presents two distinct imaginary frequencies along its bending co-ordinate. Therefore, the $\tilde{a}\ ^4\Pi_g$ state of NO_2 is subject to a Renner-Teller interaction, and it is classified as a type D Renner molecule, as discussed by Lee, Fox, Schaefer, and Pitzer[20] for linear triatomic molecules. The imaginary bending frequency with the larger magnitude [ω_2 (Π^-)] leads to the $\tilde{b}\ ^4B_2$ state in a bent molecular geometry, whereas the [ω_2 (Π^+)] mode leads to the $\tilde{a}\ ^4A_2$ state when the molecule is bent. As a result, the $\tilde{b}\ ^4B_2$ state is lower-lying in the vicinity of linearity. However, the two states cross at about 140° band angle as seen in figure 6.1. The analysis based on the bending frequencies is consistent with the discussion based on the MO Hessians mentioned above.

6.5 THEORETICAL METHODS

Geometries, energies, dipole moments, and harmonic vibrational frequencies of NO_2 in all the states considered were determined using four distinct levels of theory and six basis sets. *Ab initio* theoretical techniques included restricted open shell Hartree-Fock (ROHF) self-consistent-field (SCF), complete active space self-consistent field (CASSCF), configuration interaction including singles and doubles excitation (CISD), coupled cluster including all single and double excitations (CCSD),[21, 22] and CCSD including perturbative triples [CCSD(T)][23, 24] excitations. Six correlation consistent basis sets cc-pVXZ (X=T, Q, and 5) and aug-cc-pVXZ (X=T, Q, and 5) developed by Dunning and co-workers[25-27] were used throughout the investigation. All the calculations were performed using MOLPRO[28] computational quantum

chemistry package. The SCF calculations under MOLPRO used ROHF reference and the open shell restricted coupled cluster theory (RCCSD) for all the calculations. The calculation were also carried using ACES II[29] suit of programs and compared with the results obtained using MOLPRO. Other than some numerical issues (originating from the different implementation of CC theory in these two programs) the results are in qualitative agreement with each other. Three core orbitals (1s-like orbitals of O and N) have been frozen in all correlated calculations. Analytic gradient method was used to optimize geometries and to determine the harmonic vibrational frequencies when available. In other cases harmonic vibrational frequencies were obtained by numerical differentiation of the total energies. All the quartet states investigated here are of different spatial symmetry in C_{2v} point group molecular structures, which makes it possible to determine the equilibrium geometries without collapsing to other states.

6.6 RESULTS AND DISCUSSIONS

The electronic ground state of NO_2 is $\tilde{X}\ ^2A_1$. The main focus of our investigation is the lowest lying quartet electronic states. These quartet electronic states are difficult to measure experimentally because the transitions from the ground state to these states are spin forbidden. The geometrical parameters, dipole moments and harmonic vibrational frequencies of the $\tilde{a}\ ^4A_2$, $\tilde{b}\ ^4B_2$, and $\tilde{c}\ ^4A_1$ states are tabulated and discussed below. Figure 6.1 shows the energies of the doublet ground state and excited $^4A_2$, $^4B_2$ and $^4A_1$ electronic states as a function of changes in the ONO bond angle.

A. Ground Electronic State; $\tilde{X}\ ^2A_1$

For the ground electronic state of NO_2 the experimental ONO angle is 134.1 degrees and the NO bond length is 1.195 Å. The structure and harmonic vibrational frequencies predicted in

this work are in excellent agreement with the experimental findings. The predicted bond lengths at CCSD(T)/aug-cc-pVQZ level of theory differ from the experimentally obtained bond lengths by Hardwick et.al[7] and Lafferty et.al by less then 0.001 Å. The equilibrium bond angle differs from the experimental bond angles by less than 0.5 degrees at the same level of theory. Both the bond length and bond angle of this triatomic C_{2v} molecule converge close to the experimental value with larger basis and more sophisticated method. With increase of electron correlation effects bond lengths elongate slowly as seen in Figure 6.2. Increasing basis set size causes the bond lengths to shrink, while augmenting the basis set seems to have little effect on this geometrical parameter. The bond angle gradually decreases with electron correlation and converge close to the equilibrium experimental value. Especially inclusion of the triples correction to CCSD and augmented correlation consistent basis sets considerably improves the quality of theoretical prediction. Harmonic vibrational frequencies are associated with the bond length. With longer bond lengths (better levels of correlation), the harmonic vibrational frequencies becomes lower as seen in table 6.1. The symmetric, anti-symmetric stretching and bending frequencies fall within 33 cm^{-1}, 12 cm^{-1}, and 54 cm^{-1} of the experimental vibrational frequencies. The little difference between the predicted harmonic frequencies at the CCSD(T)/aug-cc-pVQZ and the experimental frequencies may be attributed to the anharmonicity of the vibrational modes.

B. Lowest quartet excited state: $\tilde{a}\ ^4A_2$

At the CCSD(T)/aug-cc-pVQZ level of theory, 3.65 eV (see Table 6.6) above the ground electronic state, the $^4A_2$ state is the lowest-lying quartet state of NO_2. Although the experimental data is scarce for any of the quartet electronic states, the estimated value of the excitation energy matches with the previous calculations of this quartet state.[10, 15] From the qualitative picture

presented in the Walsh diagram a smaller bond angle (relative to the ground state) is expected due to the excitation of an electron from the $4b_2$ orbital to $2b_1$ orbital. The ONO bond angle is indeed predicted to reduce to 112.8 degrees from 134.2 degrees in the ground state (see figure 6.3). The decrease in the bond angle is partially compensated by the NO bond length elongation. The NO bond length at this level of theory is 1.293 Å, which is 0.1 Å longer than NO, ground state bond length. The excitation energy (3.65 eV) is close to the value (3.77 eV) obtained using a CI scheme with double zeta quality basis set with 3 frozen core orbitals by Handy et. al.[13] The qualitative picture presented by Jackels and Davidson[11, 12] in their pioneering paper on electronic states of NO_2 shows that at the equilibrium geometry the $^4B_2$ state is actually lower than the $^4A_2$ state. The present day coupled cluster methods with high degree electron correlation along with correlation consistent basis sets better estimates the excited states than the SCF-CI treatment with a double zeta quality basis set done by Jackels and Davidson. Excitation energy of the $^4A_2$ state obtained in this work is significantly lower than that obtained in our calculations. The most comprehensive work done on the quartet potential energy surface was by Gillespie et al.[10] Based on MCSCF calculation with a DZ+P basis set they predicted the excitation energy to be 4.4 eV. The total energies and harmonic vibrational frequencies are predicted at CCSD(T)/aug-cc-pVQZ level of theory in table 6.2.

C. Second lowest quartet excited state: $\tilde{b}\ ^4B_2$

Excitation corresponding to this $^4B_2$ state is $2b_1 \leftarrow 1a_2$. At the best level of theory (CCSD(T)/aug-cc-pVQZ) it appears at 4.07 eV above the ground state (see table 6.6). According to Walsh diagram excitation of an electron from $1a_2$ to $2b_1$ causes the system to bend from the ground state geometry to lower the energy of the system. However, the effect is not profound enough to bend the bond angle as much as it does for the $^4A_2$ state. The equilibrium bond angle

at the CCSD(T)/aug-cc-pVQZ level of theory is re(NO)= 1.293 Å and θ_e(ONO)=124.7 degrees. Figure 6.4 shows the bond length and bond angles of the C_{2v} geometry of this state with correlated levels of theory. Adiabatic excitation energies from previous works are 3.84 eV (Handy et al.[13]), 4.4 eV (Gillespie et al.[10]) and 2.38 eV (Jackels and Davidson[11]). The $^4A_2$ and $^4B_2$ states go to linearity and connect a $^4\Pi_g$ state. The orbital energies (of the highest occupied molecular orbital - HOMO) drawn as a function of bond angle (Figure 6.1) shows that the first two states of quartet spin, namely the $^4A_2$ and the $^4B_2$ states cross each other at around 140 degrees ONO bond angle.

At the C_{2v} geometry however, the $^4B_2$ state has an imaginary frequency of the anti-symmetric mode at all correlated levels of theories as seen in table 6.3. This indicates the existence of C_s equilibrium geometry. At the Cs geometry the 4B2 state becomes the $^4A'$ state. There is another $^4A'$ state (the 4A1 state in C2v symmetry) which is close in energy. Therefore an attempt to find the Cs equilibrium geometry was doused by the state mixing and a resultant bad HF reference for the lowest $^4A'$ state. A state averaged complete active space SCF (SA-CASSCF) calculation with two roots of the 4A′ and following the lowest root (corresponds to the $^4B_2$ state at C_{2v} geometry) results in the correct Cs equilibrium geometry. Figure 6.5 reveal the double minimum nature of the $^4A'$ potential surface at the SA-CASSCF/cc-pVTZ level of theory where the two minima correspond to the Cs equilibrium and the center bump corresponds to the C_{2v} transition state between them. CCSD and CCSD(T) optimization and frequency calculations at this geometry, shown in table 6.4, confirms it to be the real minimum of the 4A′ state.

D. The third lowest quartet excited state; $\tilde{c}\ ^4A_1$

The third lowest quartet electronic state is $^4A_1$ state. This arises from the two electron excitation $1a_2 4b_2 \rightarrow 6a_1 2b_1$. At the best level of theory CCSD(T).cc-pV5Z the $^4A_1$ state is 4.41 eV above the ground state. Electrons in the $1a_2$ and $4b_2$ orbitals of XY_2 type triatomic molecule prefer a linear geometry over bent, as seen from the Walsh diagram. Excitation of an electron from any of these orbitals to $6a_1$ orbital makes the geometry to bend because the $6a_1$ orbital comes crashing down in energy with a smaller bond angle. Similarly excitation of an electron from either $1a_2$ or $4b_2$ orbitals makes the geometry to bend by the electron going from extremely unfavorable situation to a slightly favorable situation. As expected the bond angle is only 85.4° at the above mentioned level of theory. Such a short bond angle is only affordable by the molecule if the bond length elongates a little to make room for the oxygen. Figure 6.6 shows the geometric parameters of the $^4A_1$ state of NO_2. As seen in table 6.5, with increase of electron correlation effects the bond distances increase and larger basis set has a little but visible effect on the geometry. At the best level of theory considered (CCSD(T)/cc-pV5Z) the harmonic vibrational frequencies of the three modes are: symmetric stretching (a_1 sym) 1216 cm^{-1}, anti-symmetric stretching (a_1 sym) 665 cm^{-1} and bending (b_2 sym) 309 cm^{-1}.

6.7 ACKNOWLEDGEMENTS

P. P. B. thanks Dr. Luboš Horný for critical remarks about the project and encouragement, and Dr. Justin Turney for helpful discussions. The authors will also like to thank Dr. T. Daniel Crawford for sharing some experience about this critical molecule. This research was funded by The National Science Foundation of USA under the grant CHE0451445.

6.8 REFERENCES

1. Aoki, K.; Hoshina, K.; Shibuya, K., *Journal of Chemical Physics* **1996,** *105*, 2228.

2. Arakawa, E. T.; Nielsen, A. H., *Journal of Molecular Spectroscopy* **1958,** *2*, 413.

3. Bieler, C. R.; Sanov, A.; Hunter, M.; Reisler, H., *Journal of Physical Chemistry* **1994,** *98*, 1058.

4. Bigio, L.; Grant, E. R., *Journal of Chemical Physics* **1987,** *87*, 360.

5. Bird, G. R.; Rastrupandersen, J.; Bransford, J. W.; Curl, R. F.; Kunkle, A. C.; Hodgeson, J. A.; Jache, A. W.; Baird, J. C.; Rosenthal, J., *Journal of Chemical Physics* **1964,** *40*, 3378.

6. Brand, J. C. D.; Chan, W. H.; Hardwick, J. L., *Journal of Molecular Spectroscopy* **1975,** *56*, 309.

7. Hardwick, J. L.; Brand, J. C. D., *Chemical Physics Letters* **1973,** *21*, 458.

8. Jost, R.; Michalski, G.; Thiemens, M., *Journal of Chemical Physics* **2005,** *123*.

9. Weaver, A.; Metz, R. B.; Bradforth, S. E.; Neumark, D. M., *Journal of Chemical Physics* **1989,** *90*, 2070.

10. Gillispie, G. D.; Khan, A. U.; Wahl, A. C.; Hosteny, R. P.; Krauss, M., *Journal of Chemical Physics* **1975,** *63*, 3425.

11. Jackels, C. F.; Davidson, E. R., *Journal of Chemical Physics* **1976,** *65*, 2941.

12. Jackels, C. F.; Davidson, E. R., *Journal of Chemical Physics* **1976,** *64*, 2909.

13. Handy, N. C.; Goddard, J. D.; Schaefer, H. F., *Journal of Chemical Physics* **1979,** *71*, 426.

14. Benioff, P. A., *Journal of Chemical Physics* **1978,** *68*, 3405.

15. Gangi, R. A.; Burnelle, L., *Journal of Chemical Physics* **1971,** *55*, 843.

16. Gangi, R. A.; Burnelle, L., *Journal of Chemical Physics* **1971,** *55*, 851.

17. Shih, S. K.; Peyerimhoff, S. D.; Buenker, R. J., *Chemical Physics Letters* **1977,** *46*, 201.

18. Blahous, C. P.; Yates, B. F.; Xie, Y. M.; Schaefer, H. F., *Journal of Chemical Physics* **1990,** *93*, 8105.

19. Crawford, T. D.; Schaefer, H. F., *Journal of Chemical Physics* **1993,** *99*, 7926.

20. Lee, T. J.; Fox, D. J.; Schaefer, H. F.; Pitzer, R. M., *Journal of Chemical Physics* **1984,** *81*, 356.

21. Purvis, G. D.; Bartlett, R. J., *Journal of Chemical Physics* **1982,** *76*, 1910.

22. Rittby, M.; Bartlett, R. J., *Journal of Physical Chemistry* **1988,** *92*, 3033.

23. Raghavachari, K.; Trucks, G. W.; Pople, J. A.; Headgordon, M., *Chemical Physics Letters* **1989,** *157*, 479.

24. Scuseria, G. E., *Chemical Physics Letters* **1991,** *176*, 27.

25. Dunning, T. H., *Journal of Chemical Physics* **1989,** *90*, 1007.

26. Kendall, R. A.; Dunning, T. H.; Harrison, R. J., *Journal of Chemical Physics* **1992,** *96*, 6796.

27. Woon, D. E.; Dunning, T. H., *Journal of Chemical Physics* **1993,** *98*, 1358.

28. Werner, H.-J.; Knowles, P. J., **2002,** *MOLPRO, Version 2002.1*.

29. Stanton, J. F.; Gauss, J.; Lauderdale, W. J.; D., W. J.; Bartlett, R. J., *ACES II.*

6.8 TABLES

Table 6.1. Theoretical predictions of the total energies (in hartree), dipole moment (in debye), harmonic vibrational frequencies (in cm^{-1}) and zero-point vibrational energies (ZPVE in kcal/mol) for the ground electronic state $\tilde{X}\ ^2A_1$ of NO_2.

Level of theory	Total Energy	$\omega_1(a_1)$	$\omega_2(a_1)$	$\omega_3(b_2)$
cc-pVTZ/SCF	-204.107661	1621	855	1924
aug-cc-pVTZ/SCF	-204.110881	1615	854	1908
cc-pVQZ/SCF	-204.123843	1622	858	1913
aug-cc-pVQZ/SCF	-204.124956	1620	857	1910
cc-pVTZ/CISD	-204.692751	1516	811	1867
aug-cc-pVTZ/CISD	-204.705372	1510	810	1854
cc-pVQZ/CISD	-204.747125	1526	817	1872
aug-cc-pVQZ/CISD	-204.752307	1524	816	1867
cc-pVTZ/CCSD	-204.763000	1431	782	1756
aug-cc-pVTZ/CCSD	-204.778060	1423	780	1742
cc-pVQZ/CCSD	-204.822174	1441	787	1761
aug-cc-pVQZ/CCSD	-204.828229	1438	786	1756
cc-pVTZ/CCSD(T)	-204.799793	1352	758	1687
aug-cc-pVTZ/CCSD(T)	-204.816669	1343	756	1671
cc-pVQZ/CCSD(T)	-204.862081	1362	763	1692
aug-cc-pVQZ/CCSD(T)	-204.868852	1358	762	1686
Expt. 1983				

Table 6.2 Theoretical predictions of the total energies (in hartree), dipole moment (in debye), harmonic vibrational frequencies (in cm^{-1}) and zero point vibrational energies (ZPVE in kcal/mol) for the $\tilde{a}\ ^4A_2$ state of NO_2.

Level of theory	Total Energy	$\omega_1(a_1)$	$\omega_2(a_1)$	$\omega_3(b_2)$
cc-pVTZ/SCF	-204.039483	1170	617	1151
aug-cc-pVTZ/SCF	-204.042635	1165	618	1151
cc-pVQZ/SCF	-204.054776	1172	620	1154
aug-cc-pVQZ/SCF	-204.055908	1171	621	1157
cc-pVTZ/CISD	-204.576144	1177	577	967
aug-cc-pVTZ/CISD	-204.588241	1170	578	968
cc-pVQZ/CISD	-204.628281	1191	583	981
aug-cc-pVQZ/CISD	-204.633351	1189	584	983
cc-pVTZ/CCSD	-204.642210	1177	552	908
aug-cc-pVTZ/CCSD	-204.656922	1170	553	908
cc-pVQZ/CCSD	-204.698977	1192	559	927
aug-cc-pVQZ/CCSD	-204.704983	1191	560	928
cc-pVTZ/CCSD(T)	-204.668178	1158	536	862
aug-cc-pVTZ/CCSD(T)	-204.684733	1150	536	860
cc-pVQZ/CCSD(T)	-204.728055	1173	542	881
aug-cc-pVQZ/CCSD(T)	-204.734792	1171	543	882

Table 6.3 Theoretical predictions of total energies (Hartree), dipole moment (debye), harmonic vibrational frequencies and zero point vibrational energies (kcal/mol) for the $\tilde{b}\ ^4B_2$ state of NO_2

Level of theory	Total Energy	$\omega_1(a_1)$	$\omega_2(a_1)$	$\omega_3(b_2)$
cc-pVTZ/SCF	-204.007745	1334	659	289
aug-cc-pVTZ/SCF	-204.010285	1330	659	203
cc-pVQZ/SCF	-204.022782	1337	662	247
aug-cc-pVQZ/SCF	-204.023706	1336	662	226
cc-pVTZ/CASSCF	-204.14137	1066	570	574i
aug-cc-pVTZ/CASSCF	-204.14366	1062	569	588i
cc-pVQZ/CASSCF	-204.15592	1070	572	574i
aug-cc-pVQZ/CASSCF	-204.15672	1071	573	574i
cc-pVTZ/CISD	-204.555541	1308	634	784i
aug-cc-pVTZ/CISD	-204.567318	1304	632	819i
cc-pVQZ/CISD	-204.607417	1320	639	798i
aug-cc-pVQZ/CISD	-204.612357	1319	639	811i
cc-pVTZ/CCSD	-204.623908	1207	603	325i
aug-cc-pVTZ/CCSD	-204.638375	1201	601	346i
cc-pVQZ/CCSD	-204.680332	1220	608	314i
aug-cc-pVQZ/CCSD	-204.686234	1218	608	321i
cc-pVTZ/CCSD(T)	-204.652795	1156	585	228i
aug-cc-pVTZ/CCSD(T)	-204.669218	1147	581	248i
cc-pVQZ/CCSD(T)	-204.712403	1168	589	188i
aug-cc-pVQZ/CCSD(T)	-204.719070	1165	588	191i

Table 6.4. Theoretical predictions of total energies (Hartree), bond lengths (Å), bond angles (degrees) and harmonic vibrational frequencies (cm^{-1}) for the $\tilde{b}\ ^4A'$ state of NO_2

Level of theory	Total Energy	r_e(NO)	r_e(ON)	θ_e(ONO)	$\omega_1(a)$	$\omega_2(a_1)$	$\omega_3(b_2)$
cc-pVTZ/CCSD	-204.62412	1.379	1.226	124.13	1420	559	333
aug-cc-pVTZ/CCSD	-204.63865	1.387	1.224	123.82	1441	549	361
cc-pVTZ/CCSD(T)	-204.65307	1.427	1.227	122.92	1493	508	439
aug-cc-pVTZ/CCSD(T)	-204.66958	1.427	1.228	122.72	1480	552	476

Table 6.5 Theoretical prediction of total energies (in hartree), harmonic vibrational frequencies (in cm^{-1})for the $\tilde{c}\ ^4A_1$ state of NO_2

Level of theory	Energy	$\omega_1(a_1)$	$\omega_2(a_1)$	$\omega_3(b_2)$
cc-pVTZ/SCF	203.96298	1440	788	270i
aug-cc-pVTZ/SCF	203.96599	1436	784	354i
cc-pVQZ/SCF	203.97788	1442	788	312i
aug-cc-pVQZ/SCF				
cc-pVTZ/CISD	204.53327	1396	746	1067
aug-cc-pVTZ/CISD	204.54584	1391	742	1034
cc-pVQZ/CISD	204.58437	1405	751	1082
aug-cc-pVQZ/CISD				
cc-pVTZ/CCSD	204.60592	1267	699	346
aug-cc-pVTZ/CCSD	204.62146	1257	695	322
cc-pVQZ/CCSD	204.66185	1277	704	382
aug-cc-pVQZ/CCSD				
cc-pVTZ/CCSD(T)	204.64141	1207	649	254
aug-cc-pVTZ/CCSD(T)	204.65902	1197	655	224
cc-pVQZ/CCSD(T)	204.72070	1218	664	308
aug-cc-pVQZ/CCSD(T)				

Table 6.6 Table of excitation energies (in kcal/mol and electron volts) of low-lying quartet electronic states of NO_2

Electronic States	$\tilde{X}\ ^2A_1$		$\tilde{a}\ ^4A_2$		$\tilde{b}\ ^4B_2$		$\tilde{c}\ ^4A_1$	
Level of Theory	Kcal/mol	eV	Kcal/mol	eV	Kcal/mol	eV	Kcal/mol	eV
cc-pVTZ/SCF	0	0	42.78	1.86	62.70	2.72	90.79	3.94
aug-cc-pVTZ/SCF	0	0	42.82	1.86	63.12	2.74	90.92	3.94
cc-pVQZ/SCF	0	0	43.34	1.88	63.42	2.75	91.59	3.97
aug-cc-pVQZ/SCF	0	0	43.32	1.88	63.54	2.76		
cc-pVTZ/CISD	0	0	73.17	3.17	86.10	3.73	100.07	4.34
aug-cc-pVTZ/CISD	0	0	73.50	3.18	86.63	3.75	100.11	4.34
cc-pVQZ/CISD	0	0	74.57	3.23	87.67	3.80	102.13	4.43
aug-cc-pVQZ/CISD	0	0	74.64	3.24	87.82	3.81		
cc-pVTZ/CCSD	0	0	75.79	3.29	87.28	3.78	98.57	4.27
aug-cc-pVTZ/CCSD	0	0	76.01	3.30	87.65	3.80	98.57	4.26
cc-pVQZ/CCSD	0	0	77.30	3.35	89.01	3.86	100.61	4.36
aug-cc-pVQZ/CCSD	0	0	77.33	3.35	89.10	3.86		
cc-pVTZ/CCSD(T)	0	0	82.58	3.58	92.24	4.00	99.39	4.31
aug-cc-pVTZ/CCSD(T)	0	0	82.79	3.59	92.53	4.01	98.93	4.29
cc-pVQZ/CCSD(T)	0	0	84.10	3.65	93.92	4.07	101.71	4.41
aug-cc-pVQZ/CCSD(T)	0	0	84.12	3.65	93.99	4.08		

6.10 FIGURES

Figure 6.1 Orbital energies plotted against bond angles at SCF/cc-pVTZ level of theory.

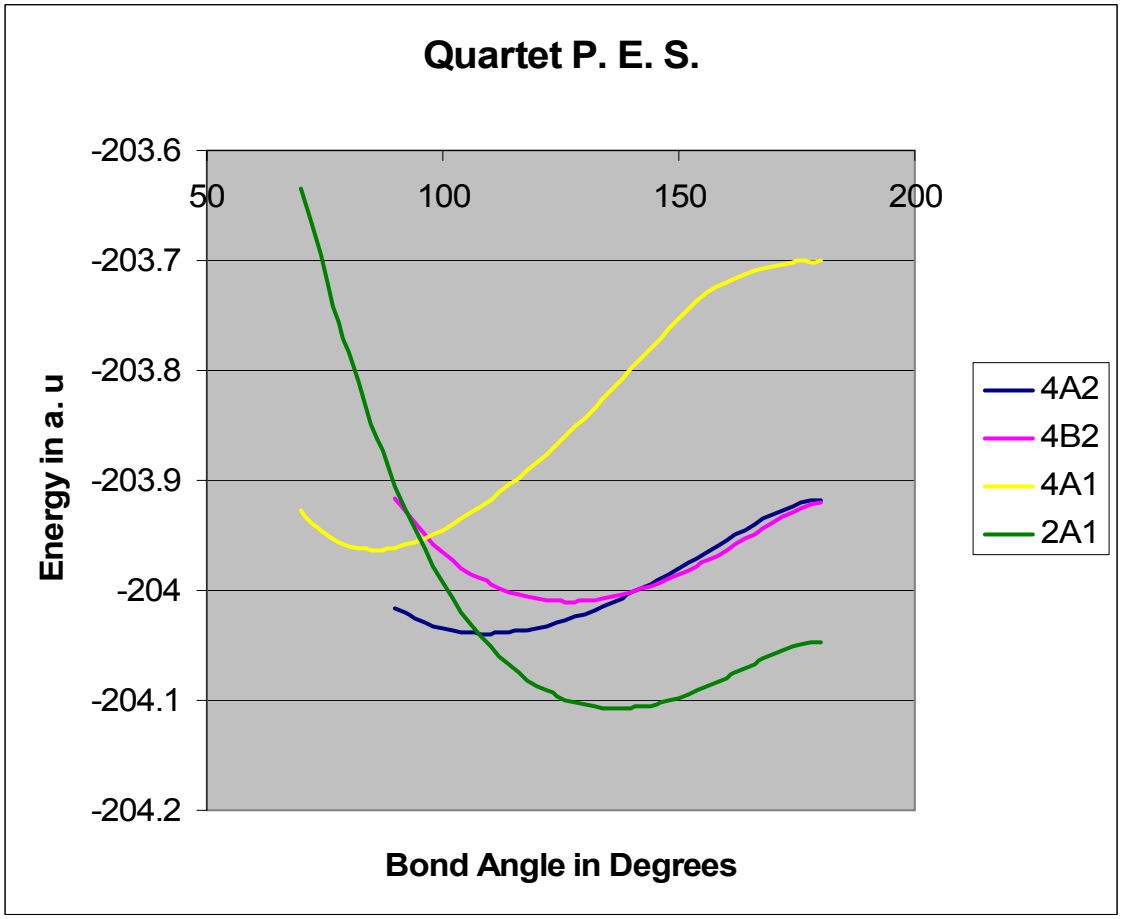

Figure 6.2 $^2A_1$

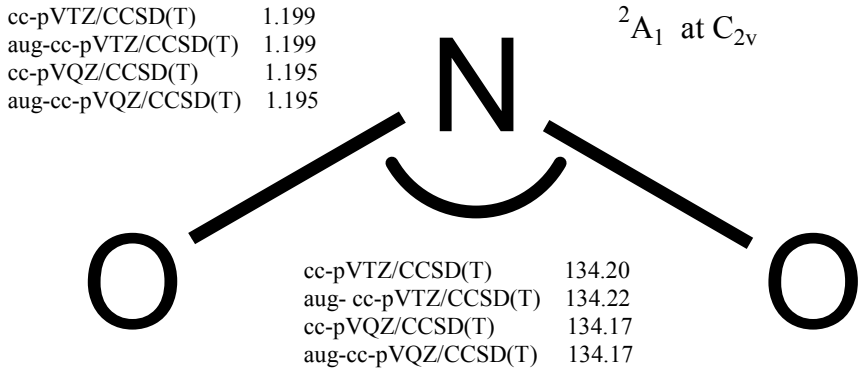

Figure 6.3 $^4A_2$

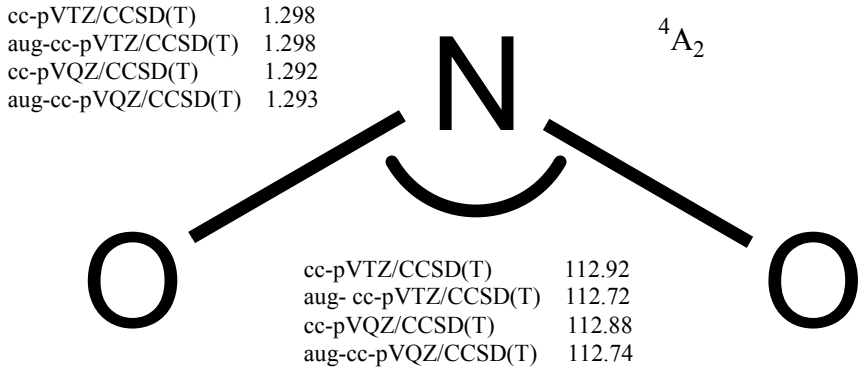

Figure 6.4 $^4B_2$

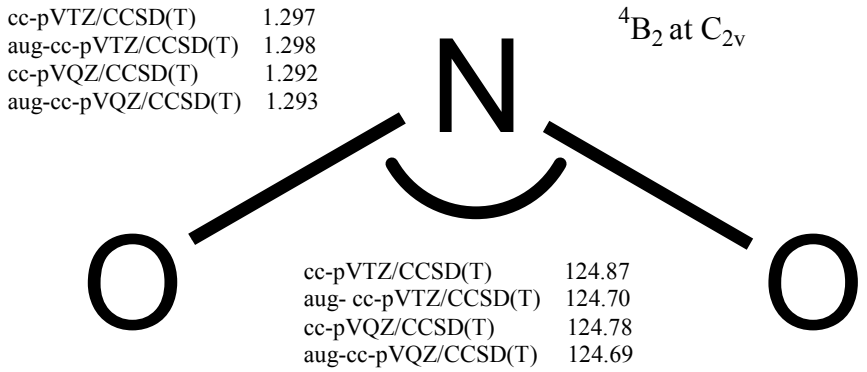

CHAPTER 7

CONCLUSION

In this second generation of quantum chemistry, the applications of DFT and *ab initio* (AIQC) techniques are proving more fruitful in predicting the chemistry of gas phase radicals and anions than ever before. A range of methods are used to predict problems of various levels of complication. Inevitably system size plays an important role in the reliability of quantum chemical predictions.

Highly correlated methods are used to predict the structures and spectroscopic properties sometimes with better than experimental accuracy. However, issues still exist and a plethora of research approaches are tried to improve upon the reliability and accuracy. Ions, radicals and open shell species still pose some challenge to the theoretical community. However, the good news is that the recipe for systematic improvement of the AIQC techniques exists.

DFT mainly focuses on its ability to predict structures and energies of larger systems which are still unmanageable by AIQC. Hundreds of new molecules exist with peculiar empirical formulae and bonding pattern. Most chemists do not even venture a guess at the structures of the possible isomers on the PES such molecules. Brute force efforts using chemical intuition limits ones ability to look at large systems because of the depressingly large number of possibilities. The unbiased stochastic search procedure developed here can be really suitable in predicting all the possible structures that represent minima on the PES of novel molecules of modest size (<15 atoms current capability). It has been applied to systems with handful of atoms with some success.

DFT methods are, also, very helpful in predicting the physical properties like electron affinities of large molecules, like DNA bases and base pairs. A number of density functionals have been successfully used for this purpose. However, at least a few

pure and hybrid density functionals should be used, and compared against each other, to predict chemistry of biomolecules in order to bracket the desired physical property with confidence. Predicting chemical physics of biomolecules are routine these days with acceptable accuracy. The modeling of solvation of biomolecules is widening the already open door of doing chemistry with computers. Therefore field of quantum chemistry is poised to experience huge success in near future in becoming a truly reliable predictive tool in chemistry.